POLITECNICO
MILANO 1863

DIPARTIMENTO DI
INGEGNERIA CIVILE E AMBIENTALE

Driveability Analysis of Offshore Piles: a Generalised Friction Fatigue-based SRD Implementation

TESI DI LAUREA MAGISTRALE IN
CIVIL ENGINEERING - GEOTECHNICS
INGEGNERIA CIVILE - GEOTECNICA

Author: **Nicola Trento**

Student ID: 10938083
Advisor: Prof.ssa Donatella Valeria Sterpi
Co-advisor: Dr. Giovanni Piunno
Project Director: Davide Spinelli
Academic Year: 2023-24

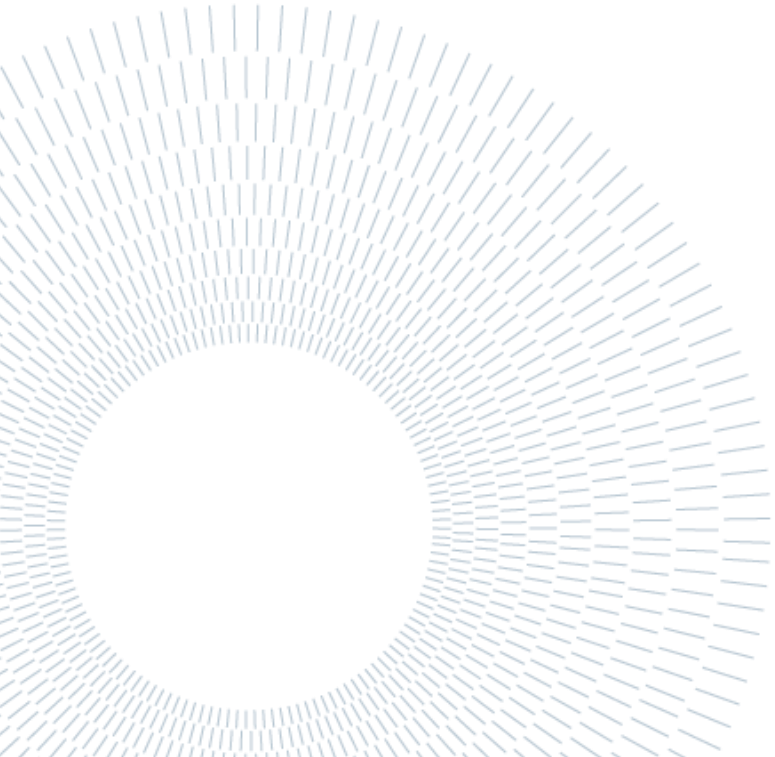

Abstract

The driveability analysis is a key step in the design of offshore foundations for structures such as wind turbines and oil platforms. This analysis involves checking whether the piles can be driven to the required depth, guiding the selection of the most suitable hammers and minimising installation risks and costs.

Currently, the most widely used software for driveability analysis is GRLWEAP, which uses the wave equation to predict the number of blows exerted by the hammer and the stresses on the piles during driving. The accuracy of such analyses is highly dependent on the correct estimation of the soil resistance to driving (SRD). Many existing methods incorporate the concept of friction fatigue to improve SRD predictions, however, there is no standardised approach to effectively replicate these formulations in analysis software, as the latter implements its own specific method to account for this.

This thesis aims to find a general procedure to convert any model that estimates SRD into a form that can be replicated in GRLWEAP. The research begins with a review of the main analytical models used to calculate SRD, with a focus on the effects of friction fatigue. Next, the internal calculation structure of the GRLWEAP software is examined. A methodology is then developed to integrate SRD estimation techniques not originally included in the software, aligning analytical approaches with numerical simulations. This procedure is implemented by means of an optimisation, which allows the software's input parameters to be calibrated to better fit the theoretical models.

Finally, through the analysis of a real case, a standardised procedure was found to back-estimate the SRD, once in possession of the driving records and some information on soil at site. This process makes it possible to obtain a deeper understanding of soil behaviour during pile installation and to validate the design methods used.

This study contributes to the advancement of offshore geotechnical engineering by enhancing the practical applicability of numerical tools.

Key-words: driveability analysis; GRLWEAP; SRD; offshore piles; friction fatigue; back analysis.

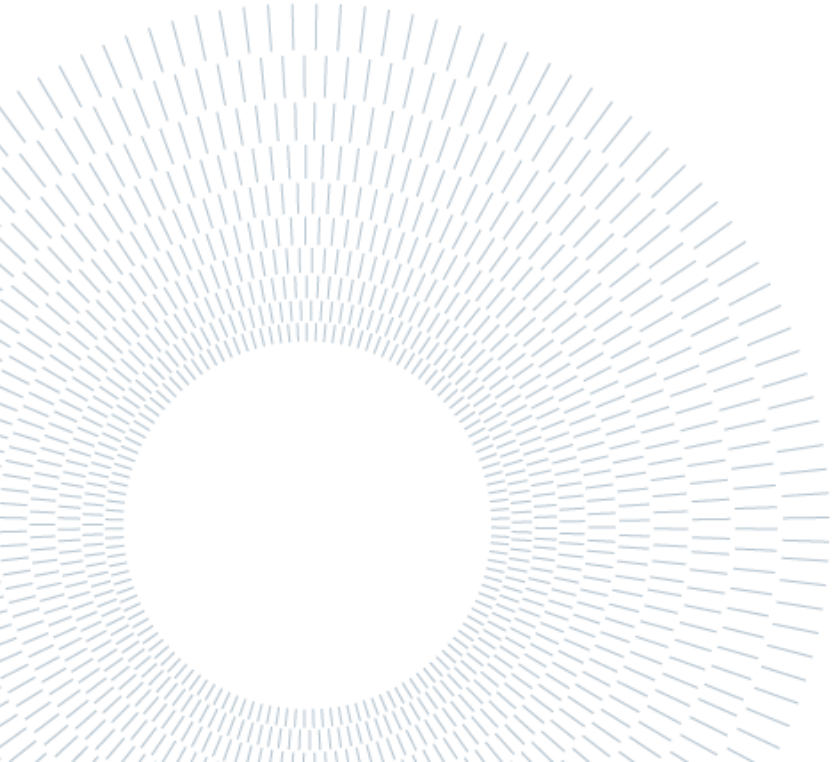

Abstract in italiano

L'analisi di battitura è una fase fondamentale nella progettazione delle fondazioni offshore per strutture come turbine eoliche e piattaforme petrolifere. Questa analisi prevede di verificare se i pali possono essere infissi alla profondità richiesta, guidando la scelta dei martelli più adatti e riducendo al minimo i rischi ed i costi di installazione.

Attualmente, il software più utilizzato per l'analisi di battitura è GRLWEAP, il quale impiega l'equazione delle onde per prevedere il numero di colpi esercitati dal martello e le sollecitazioni sui pali durante l'infissione. L'accuratezza di tali analisi dipende fortemente dalla corretta stima della resistenza del terreno all'infissione (SRD). Molti metodi esistenti incorporano il concetto di friction fatigue per migliorare le previsioni della SRD; tuttavia, non esiste un approccio standardizzato per replicare efficacemente queste formulazioni nel software di analisi, in quanto quest'ultimo implementa un proprio specifico metodo per tenerne conto.

Questa tesi si propone di trovare una procedura generale per convertire qualsiasi modello che stimi la SRD in una forma che possa essere riprodotta in GRLWEAP. La ricerca inizia con una revisione dei principali modelli analitici utilizzati per calcolare la SRD, con particolare attenzione agli effetti della friction fatigue. Successivamente, viene esaminata la struttura di calcolo interna del software GRLWEAP. Viene quindi sviluppata una metodologia per integrare tecniche di stima della SRD non originariamente incluse nel software, allineando gli approcci analitici con le simulazioni numeriche. Questa procedura viene attuata per mezzo di una ottimizzazione, la quale consente di calibrare i parametri di input del software al fine di riprodurre al meglio i modelli teorici.

Infine, mediante l'analisi di un caso reale, è stata trovata una procedura standardizzata volta a stimare a ritroso la SRD, una volta in possesso dei dati di battitura e di alcune informazioni sul terreno in situ. Questo processo permette di ottenere una comprensione più approfondita del comportamento del suolo durante l'installazione dei pali ed a validare i metodi di progettazione utilizzati.

Questa ricerca contribuisce all'avanzamento dell'ingegneria geotecnica offshore, rafforzando l'applicabilità pratica degli strumenti numerici.

Parole chiave: analisi di battitura; GRLWEAP; SRD; pali offshore; friction fatigue; back analysis.

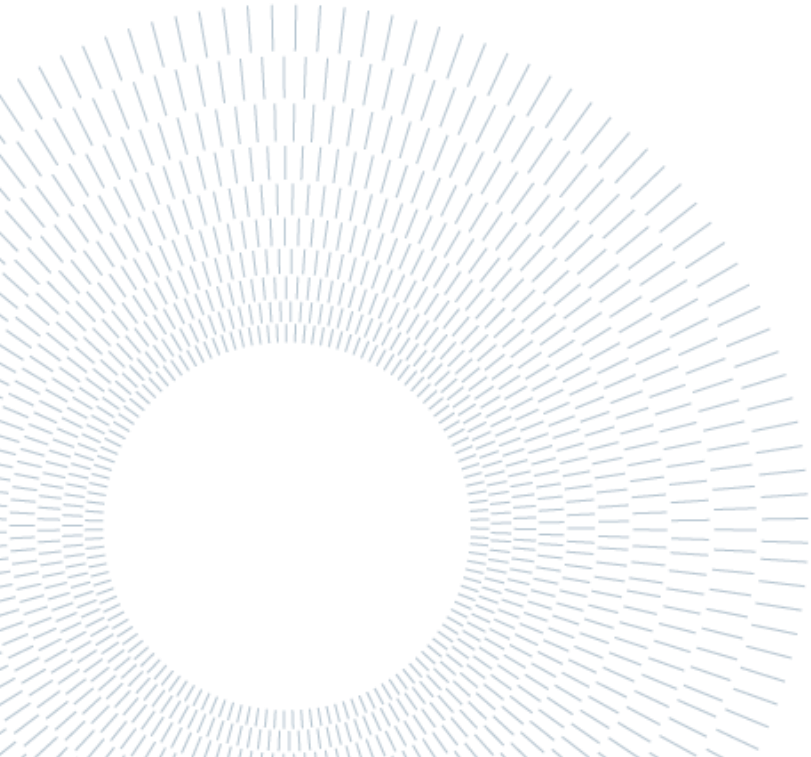

Contents

List of Figures

List of Tables

1 Introduction

In this chapter, the objectives of the study are established together with the structure for the manuscript, providing the reader with an initial understanding of the work. Additionally, the aim of the research and its expected contributions to the offshore field are highlighted.

1.1. Objectives of the Thesis

Driveability analysis is particularly important in offshore application because it helps ensure the safe, efficient and economical installation of foundation piles for structures such as offshore wind turbines, oil and gas platforms and subsea structures. It provides the designer important information on pile installation by predicting whether the piles can be driven to the required depth without refusal (premature stop) or excessive blow counts that could damage the equipment.

The driveability analysis then helps to select the most suitable hammer size, driving system and pile material, avoiding damage of the pile from buckling or fatigue, reducing unnecessary costs and avoiding delays due to inadequate equipment.

In addition, offshore pile driving generates noise and underwater vibrations that can affect marine life. Proper analysis ensures compliance with environmental regulations by selecting methods that minimise impact.

Currently, the most spread software used to perform driveability analysis is GRLWEAP ([13]), which implements Smith's theory ([20]). The theory of driveability analysis relies on wave equation analysis and is heavily affected by the soil resistance to driving (SRD). This input is a measure of the resistance offered by the soil during the installation process. Many models in literature include the concept of friction fatigue in the computation of SRD, a phenomenon according to which soil resistance for a considered depth decreases as the pile penetrates further. GRLWEAP includes a friction fatigue module, based on its own formulation. However, there is no formal procedure to reproduce an existing published analytical model exploiting the software-based formulation.

Thus, the main objective of the thesis is to find a generalised method able to compute inputs parameters for the software, in order to reproduce different analytical methodologies proposed in literature.

1.2. Organization of the Thesis

The first part of this work begins with an overview of the offshore driven piles' installation process, setting the stage for the study by explaining the various steps involved in the process and their significance in the context of pile driving. The focus is then shifted to a detailed examination of some analytical methods used in the literature to calculate the soil resistance to driving, which is a crucial parameter in the driveability analysis of piles. This section emphasizes the importance of accurately predicting soil resistance as it directly affects the expected behaviour of piles during installation. In particular, the concept of friction fatigue is explored in depth, as it plays a significant role in how the pile interacts with the soil during driving. Another significant component of this section is an in-depth analysis of Smith's theory, which uses wave equation analysis to calculate the stresses along the pile during installation. This theoretical framework is essential for understanding the entire driveability analysis procedure.

In the second part of the work, the focus shifts toward understanding the functionality of GRLWEAP module designed for driveability analysis, which includes the ability to account for friction fatigue in its calculations. The analysis is based on the documentation provided by the software developer, which details the theoretical foundation, mathematical models, and algorithms integrated into the software. A primary objective of this phase was to develop a personal implemented version of the software's calculations, ensuring that it could replicate the results generated by the software in terms of soil resistance to driving.

The third part of the work focused on implementing a technique that would allow for the replication of the analytical theories not integrated into the software yet. The aim here was to compute the necessary input parameters for the software in a manner that reflected the soil resistance driveability results for specific literature methods. This procedure, originally proposed in the literature for a specific method, was carefully studied and examined to fully understand its functionality and accuracy. During this phase, particular attention was given to analysing potential numerical issues and discrepancies in the results to determine the reliability of the method. One of the critical tasks during this stage was assessing whether the technique could be extended beyond the specific soil resistance method initially considered, and whether it could be adapted to accommodate other methods and variations described in the literature. The procedure showed to be limited to the initially considered method, thus the focus of the work moved towards finding a new procedure able to generalise the conversion.

The fourth part of the research introduced an optimization procedure designed to determine the optimal input parameters for the software to reproduce any given theoretical friction fatigue-based method. By integrating this optimization method, the study established a systematic and adaptable framework that aligns software simulations with theoretical models, a capability that was not previously available as

a standard option in the software. The optimization procedure ensures that designers can refine the input parameters, enhancing the accuracy of the soil resistance calculations and improving the overall reliability of the driveability analysis.

Finally, the last stage of the work was concentrated on the analysis of a real case. This was the input for developing an approach for back-estimating soil resistance during installation. The methodology leverages the optimization procedure developed in the earlier stages to enhance the accuracy of back analyses.

2 Offshore Pile Driving

In the past decades, offshore wind energy has undergone a large improvement and expansion. Nowadays offshore wind turbine (OWT) technologies have reached a great level of innovation but, compared to onshore renewable energy production, the cost of energy production is still significantly higher. To boost the competitiveness of offshore wind energy, it is fundamental to assess the most relevant costly factors in the life cycle of the OWT, focusing research on innovation and optimisation of these factors.

The life cycle of an OWT consist mostly in 5 phases, as illustrated in Figure 2.1 ([8]):

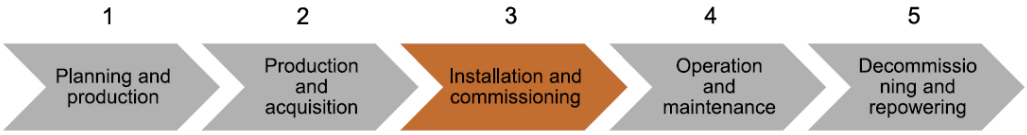

Figure 2.1: Five stages typical of an offshore wind farm.

The first stage focuses on selecting a suitable site and preparing a formal consent application. This process involves evaluating factors such as water depth, and seabed conditions during site assessments. The application includes specifications for wind turbines, an environmental impact assessment, and other critical considerations.

Stage 2 is dedicated to the manufacturing and production of components such as turbines, moorings, and cables. Historically, turbine costs have represented a substantial portion of the budget.

Stage 3 involves the installation of various components of offshore wind turbines, including cables, foundations, towers, nacelles, and blades. This phase requires specialized vessels and equipment tailored to the chosen installation methods. To ensure the smooth operation of the wind farm after commissioning, numerous marine activities are performed, such as transporting components from the port to the site, lifting turbine parts, and assembling them on location.

Stage 4 refers to ongoing operation and maintenance. This includes activities such as online condition monitoring, routine inspections, and repairs to key turbine components like blades and gearboxes.

Finally, Stage 5 addresses the end-of-life decisions for an OWF. Developers must choose between decommissioning and repowering. Decommissioning involves

completely removing the wind farm, whereas repowering upgrades the site with newer technologies. This could mean replacing entire turbines or refurbishing existing ones with updated, more efficient components.

This work will focus mainly on stage 3, in particular on the installation of driven piles, and the next sections of the current chapter will try to address the main features of this process from an operational point of view.

Because of the complexity of the site, every offshore installation requires particular nonstandard operations, which usually turn in elevated costs. The installation method strongly depends on the foundation types, site conditions and availability of the equipment. While broad studies have been carried out concerning aerodynamics, hydrodynamics, structural loads and foundation mooring, the research about installation methods is lacking. Section 2.2 aims to summarise the state of the art of the installation methods used in common practice.

2.1. Historical Background

Pile driving, the process of installing piles into the ground without prior excavation, has been an essential construction technique for millennia, [12]. Driven piles, the oldest type of deep foundation, allow structures to be built in areas with unsuitable subsurface conditions. Despite significant technological advancements, the fundamental principle of driving piles remains unchanged.

Historically, pile driving dates back to early humans who used driven piles to elevate shelters for protection. The Romans advanced this technique, employing wooden piles to stabilize infrastructure like bridges and military works.

The 19th century saw major advancements with the introduction of steam power. James Naysmith's steam hammer revolutionized pile driving, drastically reducing installation time. The use of materials also evolved, transitioning from timber to concrete and steel.

Technological innovations continued into the 20th century. Diesel hammers, developed in Germany, became popular for their portability and efficiency. Vibratory hammers, initially developed in the Soviet Union, provided an alternative method by combining vibration and impact. The development of stress-wave theory and numerical models like E.A.L. Smith's wave equation improved understanding of pile dynamics, enabling precise calculations of pile stresses, soil interactions, and capacity.

Concerning offshore foundation type, two main families can be distinguished: bottom-fixed and floating. The latter will not be discussed as it is beyond the scope of the work.

The three most common bottom-fixed foundations are illustrated in Figure 2.2 ([8]).

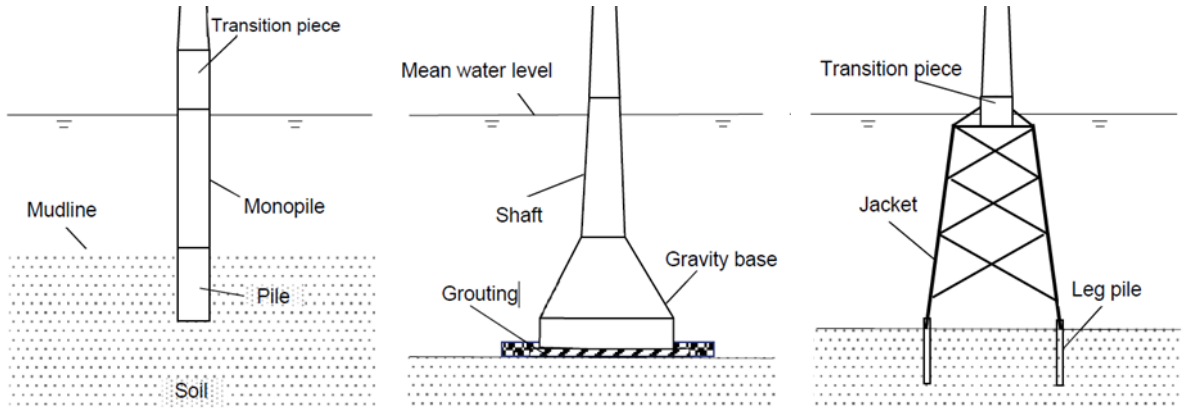

Figure 2.2: Schematic of monopile (a), gravity-based (b) and jacket (c) offshore wind turbines.

Figure 2.2 (a) show a schematic example of monopile foundation, composed of a single steel tube pile. These piles have usually large diameters, ranging in different spans depending on the use: for oil and gas platforms the range spans over 1 to 3 metres and usually serve as anchors for jacket foundations, while for wind turbine the diameter varies from 3 to 12 metres depending on turbine size and water depth. In recent years, tanks to technological innovations in the components and materials of wind turbines, it has been possible to increase more and more the diameter of these piles, resulting in very large piles. One of the open questions about these latest installations is whether the design formulations developed at the time of smaller diameters are still valid.

The length of the piles depends on the water depth and soil conditions, but for shallow to medium sea level (up to 20-30 metres), monopiles are considered in general more economic.

Gravity base foundations, Figure 2.2 (b), are usually made of concrete and use their self-weight to resist overturning moments. These structures are suitable for specific seabed conditions as long as the water depth is less than 20 metres.

Jacket foundations are frame structures welded from steel elements (generally tubular). Those structures are diffused for intermediate water depths (50 to 70 metres) up to more than 200 metres.

Following this general introduction of bottom-fixed foundations, the focus for the next sections will be on the monopiles.

2.1.1. Overview of offshore monopiles installation

During installation procedure different parts of an offshore structure are assembled. Since this activity occurs offshore, the operations must take into account many factors as weather window and safety risk in lifting operations.

(a) Tugboat

(b) Crane barge

(c) Heavy lift vessel

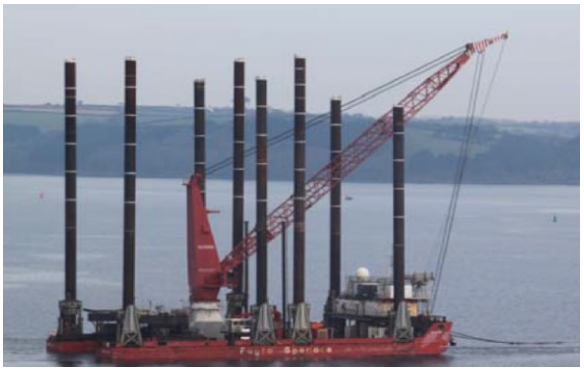

(d) Jackup barge

(e) Purpose-built jackup vessel

(f) Semisubmersible construction vessel

Figure 2.3: Common vessels used in offshore installation (photo courtesy of Damen Shipyards Group, Spanopoulos Group and Fred Olsen ASA).

To install monopiles, installation vessels are involved. These vessels differ in price, size and functionality. The most economical ones are the tugboats, Figure 2.3 (a), used to manoeuvres other vessels or barges by pushing or pulling them either by direct contact or by means of a tow line.

Heavy lift cargo vessels, Figure 2.3 (c), are designed with expansive cargo spaces that enable them to transport heavy modular components, accommodating the unique

demands of specific projects. They usually feature a pair of cranes to achieve greater lifting capacity.

As lifting operations require cranes with good capacities, crane barges, Figure 2.3 (b), and jackup barges, Figure 2.3 (d), are widely used to lift pre-assembled wind turbines or support structures during installations. Older generations of jackup barges relied on mooring systems, requiring accurate forecasts of wind and wave directions before installation to safely position the vessel relative to the location of the installation. However, these vessels had limitations, including insufficient crane height and capacity. To compensate these shortcomings, purpose-built jackup vessels have been developed over the past decade, as illustrated in Figure 2.3 (e). These modern vessels, often exceeding 100 meters in hull length, are less affected by adverse weather conditions and feature dynamic positioning systems for enhanced stability.

Semi-submersible crane vessels, Figure 2.3 (f), feature very high lifting capacities, reaching up to 20,000 tons, making them ideal for handling heavy components and to operate in challenging installation scenarios. However, their high day rates impose significant economic constraints, limiting their usage to projects where such capabilities are indispensable.

2.2. State of the Art of Installation Procedures

For the installation of monopiles, which are typically employed in stiff to semihard seabed conditions, it is necessary the use of transportation barges to bring the monopiles to the site. For the following stages of installation, either a jackup vessel or heavy lift crane can be used. The monopile is lifted from the barge using an upending frame, Figure 2.4 (a), which helps transition the monopile from a horizontal to a vertical position, preparing it for installation. Proper alignment is critical, as monopiles rely on side friction with the seabed to remain upright.

Various methods are available for the installation of monopiles, each suited to specific conditions and requirements: drilling consists in creating a hole into which the pile is gradually lowered. This approach is beneficial in scenarios where noise or weight restrictions are critical, or when soil resistance is particularly high, such as in chalk or rock formations. However, drilling generally requires more time and involves the use of complex and costly equipment, with additional processes such as grouting.

Jacking is a static technique in which a hydraulic jack is used to press the pile to the desired depth. This method is only suitable for weak soils and is rarely applied in offshore contexts due to the impracticality of providing the substantial counterweight required.

Hammer driving is the most widely used technique, employing various types of impact hammers such as drop hammers or power-assisted drop hammers powered by

steam, gas, diesel, or hydraulic pressure. Initially, the pile is lifted into position, and its own weight drives it a short distance into the soil until equilibrium with soil resistance is reached. Ramming is then initiated, typically at a frequency of 0.5–1.0 Hz. Each impact generates a stress wave that propagates through the pile at the speed of sound in steel, creating a strain that is partially transferred to the surrounding soil. This strain overcomes the soil's shear strength along the pile sides and induces a zone of yielding at the pile tip. The inertial force from the accelerated pile exceeds the soil's plastic limit, causing further penetration until a new equilibrium is established.

The two most widely used types of hammers are the hydraulic drop hammers and diesel hammers. Both types operate by allowing a ram weight to fall onto the top of the pile, effectively driving it into the ground.

Hydraulic hammers use hydraulic fluid to move the ram via a piston mechanism. These hammers are typically equipped with an electric valve, which provides precise and flexible control over the output energy, making them highly adaptable for different pile-driving requirements.

Diesel hammers, on the other hand, are available in two main configurations: open-end and closed-end designs. An open-end diesel hammer features a slender piston, known as the ram, which moves within a cylinder open at the top. As the ram falls under the force of gravity, it strikes the pile cap, driving the pile downward. Upon impact, the ram separates from the impact block almost immediately. The air-fuel mixture inside the cylinder ignites, creating combustion pressure that propels the ram upward for the next cycle.

In a closed-end diesel hammer, the cylinder is sealed at the top, causing the descending ram to compress the air trapped inside. This compressed air generates additional pressure in the bounce chamber, which, combined with gravity, drives the ram downward with greater force. This dual mechanism, involving both gravitational and pneumatic action, is referred to as double-acting operation.

Nowadays hydraulic hammers, as for example those in Figure 2.4 (c), are mostly used. These tools can operate underwater, although previously steam and diesel hammers were common, which were restricted to operating above water. While in shallow water, the piles can be driven using above-water hammers mounted on pile extensions (so-called 'followers'), in deep water, extensions are impractical, and underwater hammers are used in case of jacket structures. Modern underwater driving hammers are designed to follow the pile down through guiding sleeves on the jacket structure.

This process involves high-impact forces to achieve the required penetration depth. In some designs, grouting equipment is used to cast the transition piece to the monopile.

During pile driving, tools such as gripper devices, Figure 2.4 (b), are employed to hold and maintain the monopile's vertical orientation. These devices, mounted on installation vessels, ensure precision and stability throughout the process.

Transition pieces, Figure 2.4 (d), are meant to level out the horizontal inaccuracies after the foundation is installed and are quite common in OWT. These pieces are not in contact with the seabed even though they pass through the majority of water column. The gap between the monopile and the transition piece is normally filled with cement grout.

However, newer monopile foundations may eliminate the need for a transition piece, simplifying the installation process.

(a) Lifting of a monopile. (credits: IQIP)

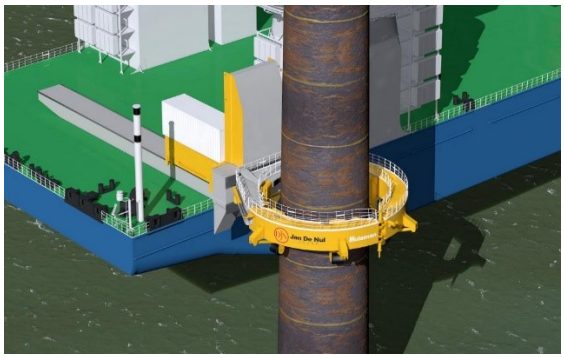

(b) Gripper device. (credits: Huisman)

(c) Hydraulic hammer (credits: Acteon)

(d) Transition piece (cswoffshore)

Figure 2.4: Installation components.

The pile-driving process generates significant underwater noise, with sound exposure levels reaching up to 210 dB, as reported by Kikuchi ([10]) in his paper about for the effect of offshore wind farm noise on fish. This might be harmful to marine life, including porpoises and seals, prompting regulatory and environmental concerns.

Various methods have been developed to reduce noise, including bubble curtains, isolation casting and cofferdam. These solutions considerably increase the installation costs. An alternative is provided by vibratory technologies, able to achieve quieter pile installation by means of low amplitude axial vibrations. This technique is also more efficient than impact driving in certain soil conditions, as dense sands.

As Tsouvalas et al, [22], explain in their papers about vibro-hammers, the input excitation is induced through the harmonic rotation of eccentric masses, usually at a frequency no larger than 40 Hz.

Another advantage of this technology compared to impact driving is the reduction of both damage and radial expansion of the pile during installation. The latter is due to Poisson effect, and plays a role in increasing the soil resistance, leading to the necessity of larger amount of energy input for the hammers in the driving process.

However, vibratory pile hammers use is impeded by a number of factors, including the incompleteness of available field observations and the impacts on pile axial capacity. Specifically, open research questions need to be addressed concerning the energy efficiency during driving, the post-installation stiffness and response to lateral loading as well as the installation process itself. Major knowledge gaps are also associated with soil's dynamic behaviour during vibro-driving and the effects of vibroinstallation on the operational performance of the pile.

The research of Tsouvalas et al. proposes a cutting-edge technology, inspired by observing that torsional vibrations do not induce radial pile expansion during driving, one of the major responsible for noise emission. This new technology is called "gentle driving of piles" (GDP).

The GDP shaker is designed to install monopiles using a combination of low-frequency axial motion and high-frequency torsional motion, offering an efficient and environmentally considerate approach to pile driving.

High-frequency torsional motion plays a crucial role in reducing the axial frictional resistance along the pile shaft. By mobilizing soil shear resistance in the circumferential direction, torsional vibration diminishes the soil's resistance to axial penetration, facilitating smoother pile advancement. This reduction in friction lowers the axial vibratory load needed to drive the pile, which, in turn, reduces the amplitude of stress waves generated during installation. The decrease in stress wave intensity also minimizes the radial motion of the pile, an effect influenced by the Poisson ratio.

This reduction in radial pile expansion during installation offers two key advantages. Firstly, it accelerates pile penetration by decreasing soil confinement around the pile. Secondly, it significantly reduces underwater noise emissions, addressing critical environmental concerns associated with offshore construction.

Under axisymmetric loading conditions, such as those involving torque, the circumferential motion of a cylindrical pile remains independent of its axial and radial movements. This decoupling ensures that torsional vibrations in the pile transmit only shear waves to the surrounding soil. These waves do not propagate through seawater and therefore do not contribute to underwater noise pollution.

The use of high-frequency torsional vibrations is particularly beneficial due to the short wavelengths they generate in the soil. These wavelengths attenuate rapidly,

meaning their amplitude diminishes within a short distance from the pile. This characteristic further enhances the environmental benefits of the technique and ensures an efficient installation process.

2.3. Geotechnical Behaviour of Soil During Pile Driving

In the present section, a purely geotechnical framework about pile driving is provided.

During installation (driving) as the pile penetrates the soil, its state of stress changes from the in situ one. To better discuss how soil resistance changes during driving process, a subdivision into different cases is needed.

2.3.1. Capacity of driven piles in clay

According to Randolph, [14], the notation in Figure 2.5 is introduced in order to differentiate different stages:

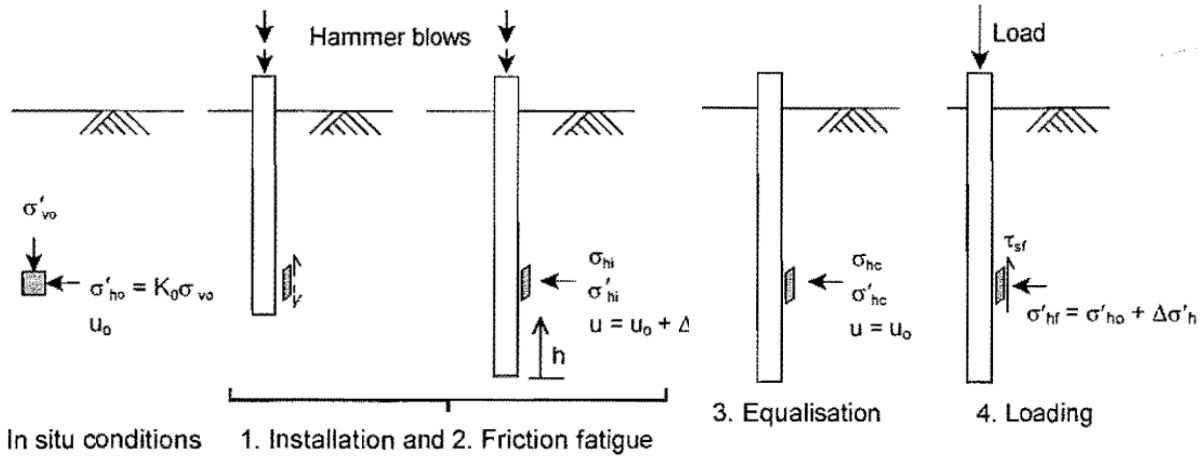

Figure 2.5: Stages in the installation and loading of a driven pile in clay.

The subscripts in Figure 2.5 correspond to:

- 0: in situ conditions;
- i: immediately post-installation;
- c: post-equalisation, meaning when any excess pore water pressure around the pile has dissipated;
- f: failure, referring to the ultimate resistance of the soil.

The quantities instead refers to:

- σ'_v is the effective vertical stress;
- σ'_h is the effective horizontal stress;
- K_0 is the lateral coefficient at rest;

- τ_s is the shear stress;
- u_0 is the hydrostatic pore pressure;
- Δu is the excess pore water pressure;
- u is the water pressure;
- h is the distance between the position of a point above the pile tip.

When a pile is driven into clay, the soil near the pile experiences significant shear deformation as the pile tip advances. This leads to remoulding of the soil, and a residual shear plane may develop along the pile shaft. The installation is generally considered as an undrained process, meaning there is no change in the soil volume, even though for very permeable clays (especially if the driving is interrupted) some drainage may occur.

As the soil is displaced, the total stress increases ($\sigma_{hi} > \sigma_{h0}$) depending on the soil's undrained shear strength and is typically around 4 to 6 times the soil's initial undrained strength, s_u.

Due to undrained shearing and increase in total stress, pore pressure also changes. Among the two, the greatest contribution is the one due to the increase of stress, that, for soft clay, generate a positive Δu, since contractile, while for stiff clay the opposite. This results in low horizontal effective stress (usually < σ'_{h0}) acting on a pile in soft clay, whereas a higher value (usually > σ'_{h0}) acting in stiff clay during and immediately after installation.

Moreover, the cyclic shearing of soil close to the pile shaft due to hammer blows is another important component to take into account in the stress state: cyclic shearing induces contraction of the soil and a reduction in effective stresses. Consequently, the horizontal effective stress after installation decreases with increasing distance (h) from the pile tip. This is because points farther from the pile tip undergo more loading cycles during the driving process. This phenomenon, where the shaft resistance decreases with distance due to these effects, is referred to as "friction fatigue", a term introduced by Heerema in 1980, [6], deepened in the following chapters.

When the driving process stops, equalization (or "set-up") takes place. During this process the excess pore pressures dissipate, effective stresses change and therefore shaft resistance.

Noteworthy to underline that equalization involves simultaneous changes in both total stress and pore pressure. While in a one-dimensional consolidation test, the total applied stress is constant and as pore pressure dissipates, any decrease in Δu directly corresponds to an equal increase in effective stress, causing the soil sample to contract, during pile equalization, the scenario differs. The pile remains fixed in size and does not expand to maintain a constant total stress on the surrounding soil as the soil

contracts due to outward water flow. As a result, the total stress acting on the pile typically decreases, alongside the reduction in excess pore pressure.

Despite these changes, as equalization progresses, the shaft resistance of the pile is influenced only by the effective horizontal stress rather than by variations in total stress or pore pressure individually.

Axial capacity in clays is generally computed by means of API method ([2]), but this doesn't include friction fatigue effect nor the influence of overconsolidation ratio (OCR). API method, also called α-method, is still widely used but particular attention must be taken in case of:

- Long piles: The database used to calibrate the method generally comprised short piles. Friction fatigue and progressive failure become more important for longer piles.
- Sensitive low-plasticity soft clays: The drop in strength and loss of effective stress when these clays are sheared can lead to very low α-values.
- Interrupted installation in permeable silty clays: Re-shearing of soft clays partway through equalisation leads to reduced α-values.
- Low friction angle clays: The correlations do not explicitly include the interface friction angle. Clays with a mineralogy that forms residual shear surfaces may show lower shaft resistance.

To better describe these effects, more complex methods should be employed.

2.3.2. Capacity of driven piles in sands

The stages encountered during a driven pile installation in sands are depicted in Figure 2.6, where the notation is the same as in Figure 2.5.

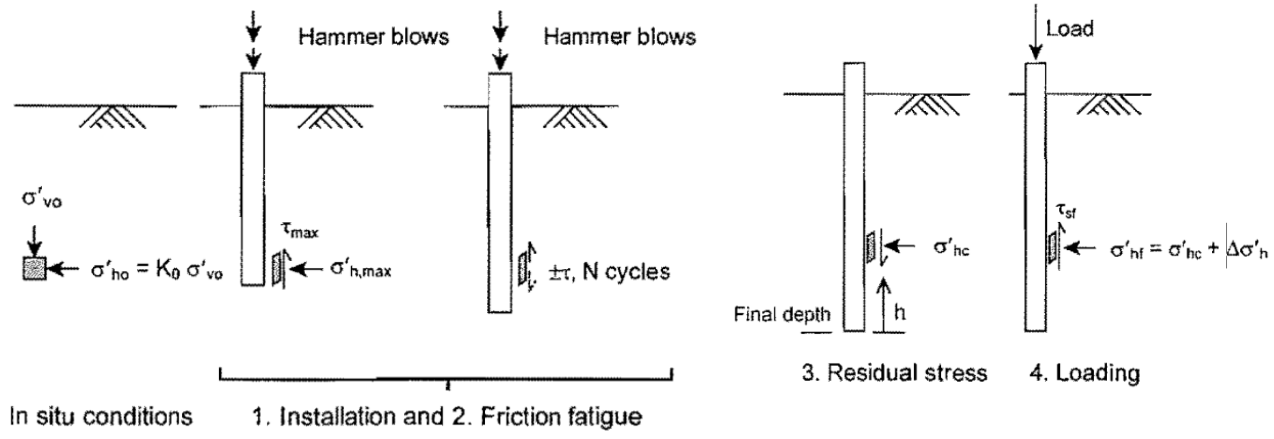

Figure 2.6: Stages in the installation and loading of a driven pile in sand.

In sands shaft resistance is governed by Coulomb's Law and τ_{sf} is estimated from the horizontal effective stress at failure, σ'_{hf} and the pile-soil interface friction angle, δ. From an initial value of $K_0 \cdot \sigma'_{v0}$ the horizontal effective stress changes during installation, friction fatigue, and finally loading, to the value at failure, σ'_{hf}. Moreover, no equalisation occur since pore excess pore pressure dissipates in a short amount of time.

During installation, as the pile tip penetrates and approaches a given element of sand, the stress level increases significantly to push the sand radially away from the pile tip and allow the advancement. The stress level at tip is comparable to the CPT cone resistance q_c, which is usually two orders of magnitude greater than the in-situ stress.

As the sand passes around the pile tip and reaches the shaft, the stresses drop since the penetration is no longer acting on the sand which has been displaced laterally. The reduced stress acting on the shaft can be compared to CPT sleeve friction f_s, which is usually 2 orders of magnitude lower than q_c.

As for clay soil, the process of friction fatigue leads to a reduction in unit shaft resistance with increasing distance behind the pile tip since the sand adjacent to the pile is sheared back and forth. This cyclic shearing leads to contraction of the sand since the permeability is high enough for volume change to occur. The contraction adjacent to the pile allows relaxation to occur in the surrounding cylinder of soil, causing a reduction in the horizontal stress acting on the pile shaft: a process known as friction fatigue. As h increases, σ'_h decreases, and hence the available shaft resistance decreases.

Friction fatigue in sands can be schematised as in Figure 2.7, where the confinement provided by the far field soil is equivalent to a spring stiffness of $k = 4G/D$, where G is the sand's shear modulus.

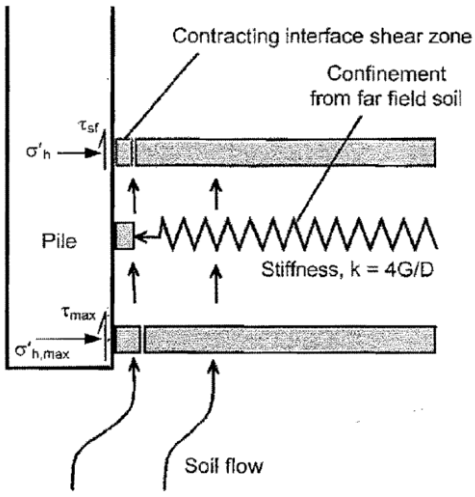

Figure 2.7: Schematic diagram of friction fatigue mechanism.

3 Driveability Analysis

One of the fundamental assessments conducted during the design of offshore piles is driveability analysis. This analysis evaluates the feasibility of driving piles into the seabed and helps ensure that the installation process can be completed efficiently and without damaging the pile or surrounding structures.

Driveability studies allow one to decide on a number of key parameters for the installation process, such as, the appropriate size of the hydraulic hammer, the number of hammer's blows and energy input needed to reach the final penetration depth, and the induced stresses in the system. The latter is important for the prediction of the fatigue life of the pile. Indication on whether refusal is encountered is also provided (refusal is practically achieved when the penetration rate is slower than 250 blows per quarter meter; when refusal is achieved it is no longer practical to drive the pile).

Driveability analyses are nowadays a major topic in offshore engineering due to the necessity to optimise and reduce installation costs. In the last years the diameter of foundation piles for offshore structures as oil and gas jackets and wind turbines increased consistently, leading to the needs of new test and research concerning the behaviour of previous theory based on the assumption of smaller diameters.

A driveability analysis involves two stages. First, the soil resistance to driving is assessed for short increments of pile penetration until the target embedment. Second, the dynamic driving process is simulated by a numerical method, using the adopted profiles of soil resistance to driving.

The dynamic driving process is usually simulated using wave analysis programs (such as GRLWEAP), which are based on the one-dimensional wave equation analysis (WEA) model developed by Smith in the 1950s [20]. To improve the predictions of original model by Smith, several additional models have been introduced over the years. In parallel, more advanced models have also been developed through the years which are primarily based on the use of the Finite Element Method (FEM) to describe the soil together with a three-dimensional description of the structure. Even though such models are expected to increase the accuracy of the predictions, they are computationally expensive, hence, they never actually replaced the original model by Smith.

Differently from bearing capacity analyses, which focus on assessing that the ultimate capacity of the pile is able to sustain axial and lateral forces without experiencing

excessive settlement or structural failure after installation, driveability analysis primarily focuses on evaluating the feasibility of installing a pile into the soil using pile-driving equipment such as hammers or vibratory drivers.

A crucial distinction between driveability and bearing capacity analysis lies in the temporal scope of each analysis. The first one is concerned with the transient, dynamic conditions during the pile installation phase. It ensures that the pile can be successfully driven to the required depth without exceeding equipment or material limitations.

The latter, on the other hand, mostly focuses on the pile's long-term, static performance. It ensures that the foundation can support the structure's loads over its operational lifespan without compromising safety or functionality.

In particular, driveability analyses, like the one carried out by solution of the wave equation, only predict the resistance to penetration at the time of driving and they do not take into account for soil set up, group effect, negative friction, and other time effects which usually influence the long-term bearing capacity. In general, soil resistance during driving is lower than the final bearing capacity due to phenomena like friction fatigue, where resistance at a given distance from the pile tip decreases as penetration progresses. However, once pore pressure equalization occurs, soil resistance can recover to a value that may be higher, lower, or equal to its initial one. For that reason, only the use of engineering soil mechanics can transform the resistance to penetration at the time of driving into the long-term bearing capacity.

3.1. Components of the Driveability Analysis

Above-mentioned wave equation analysis programs, according to Smith's theory [20], model the pile in a series of interconnected structural elements supported by non-linear springs and dashpots representing the soil stiffness and damping respectively. These two elements represent and model the soil resistance. Further, the hammer properties including ram, hammer assembly, helmet, cushion, and follower can also be modelled. In the following sections, Smith's theory will be explored in order to illustrate how driveability analysis is carried out in WEA software.

Before Smith theory dynamic pile driving formulas were employed. These formulas were applicable only for specific site/material conditions, carried out by empirical research. Moreover, they were not able to compute tensile stresses and with the advent of precast concrete piles, it turned out to be a huge limitation, since field evidence proved pile tensile failure consequent to installation.

Smith in 1960 proposed a solution for the problem of longitudinal impact driving. The idealization of the model is schematised in Figure 3.1.

Smith's solution involves modelling the continuous pile (Figure 3.1 (left)) as a series of weights and spring (Figure 3.1 (right)): the distributed mass of the pile is divided into a number of concentrated weights connected by weightless springs.

Weights are denoted by WAM and internal springs (cushions and pile springs) are denoted by $XKAM$. Soil springs (external springs) are denoted by $XKIM$ and soil dashpots are represented by SJ. The "top" weight of the system is denoted as $WAM(1)$, and the adjacent masses are numbered sequentially to the point of the pile. Since there is no pile spring beneath the last pile weight, there will always be one less internal spring than the number of weights. The external springs are numbered according to the weight upon which they act. Time is also divided into small increments.

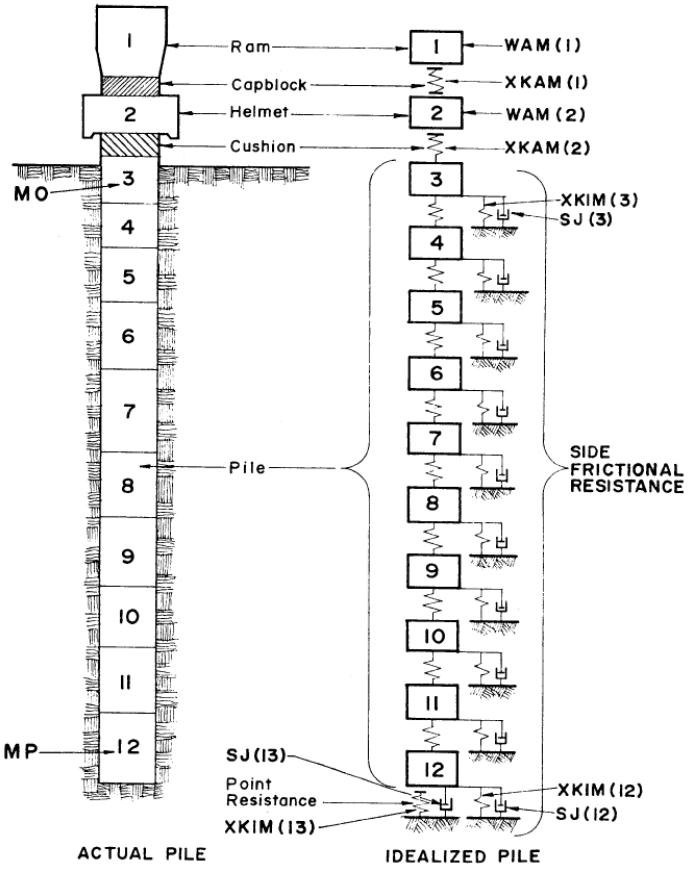

Figure 3.1: Model of the soil-pile system proposed by Smith.

3.1.1. Soil Model

According to Smith's idealisation, soil/supporting medium to the pile system is modelled as:

- Series of side springs for the frictional resistance;
- Single point spring for the base resistance.

These springs are named "external springs" and represent the resistance to dynamic loading provided by the soil.

Smith assumed load-deformation characteristics as in Figure 3.2: the path OABCDEFG represents a two-way loading and unloading cycle in side friction. Considering only compressive loading (and unloading) the path results in OABCF.

Diagram like the one in Figure 3.2 may be defined separately for each spring. The fundamental quantities are:

- Q, named soil quake, which represents the maximum deformation which may occur elastically;
- R_u, the ultimate ground resistance or, equivalently, the load beyond which the soil springs start behaving purely plastically, meaning the maximum soil resistance on a pile segment;
- $K'(m)$, the spring constant during elastic deformation for spring m, defined as $\frac{R_u(m)}{Q(m)}$.

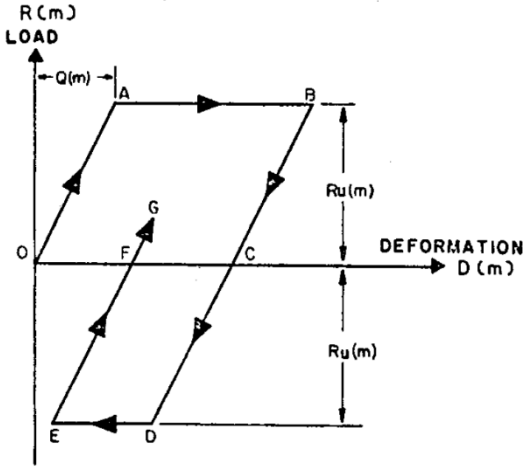

Figure 3.2: Load-deformation characteristics assumed for soil spring m.

The equation to model soil resistance at element m and time instant t, $R(m,t)$ (expressed in [lb]), proposed initially by Smith is the following:

$$R(m,t) = [D(m,t) - D'(m,t)] \cdot K'(m) \cdot [1 + J(m) \cdot V(m,t-1)], \qquad (3.1)$$

where:

- $D(m,t)$ is the displacement of element m in time interval t $[in.]$;
- $D'(m,t)$ is the plastic displacement of external soil spring m in time interval t [in.];
- $J(m)$ is the damping constant of the soil at element m $\left[\frac{s}{ft}\right]$;
- $V(m,t)$ is the velocity of element m in time interval t $\left[\frac{ft}{s}\right]$;

In Eq. 3.1, the plastic deformation $D'(m,t)$ for a given external spring behave accordingly to Figure 3.2 and may be determined by personalised routines. For example, when $D(m,t)$ is less than $Q(m)$, $D'(m,t)$ is zero; when $D(m,t)$ is greater than $Q(m)$ along line AB, $D'(m,t)$ is equal to $D(m,t) - Q(m)$. In that way $D'(m,t)$ represent only the plastic portion of the deformation.

It is noteworthy to underline that Eq. 3.1 is basically a Kelvin-Voigt rheological model (spring and dashpot in parallel) that can be represented as in Figure 3.3. The model describes an elastic behaviour of the spring until the deformation $D(m,t)$ equals $Q(m)$. At that point the spring yields plastically, with a load-deformation behaviour as depicted in Figure 3.2. The dashpot J provides a resisting force directly proportional to the velocity V of the element (that corresponds to the velocity of loading).

The damping force, given by the second term of the equation,

$$R_J(m,t) = [D(m,t) - D'(m,t)] \cdot K'(m) \cdot [J(m) \cdot V(m,t-1)], \tag{3.2}$$

is independent of pile size or total soil resistance. This force is hence constant for a given soil under a given condition (e.g. static shear strength of the soil for which R_u is determined).

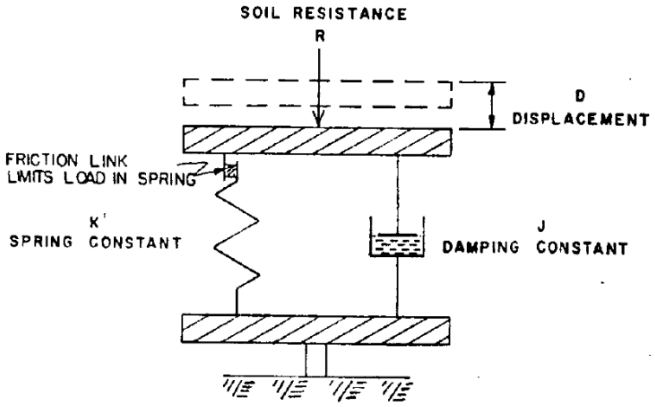

Figure 3.3 Model used by Smith to describe soil resistance on pile.

Further improvement by Smith modified the Eq. 3.1 to be used when $D(m,t)$ first becomes equal to $Q(m)$ (and so $D(m,t) - D'(m,t) = 0$, since for that time increment the deformation is purely plastic, hence the two quantities coincide):

$$R(m,t) = [D(m,t) - D'(m,t)] \cdot K'(m) + J(m) \cdot R_u(m) \cdot V(m,t-1). \tag{3.3}$$

This equation reproduces a dynamic load-deformation behaviour as the one in Figure 3.4. Path OABCDEFG represents the load-deformation that occurs for a soil particle on the side of the pile as the pile moves through the soil. For the soil at the point instead, only compressive loading can occur, since the point of the pile is free to rebound, and the load deformation path is OABCO.

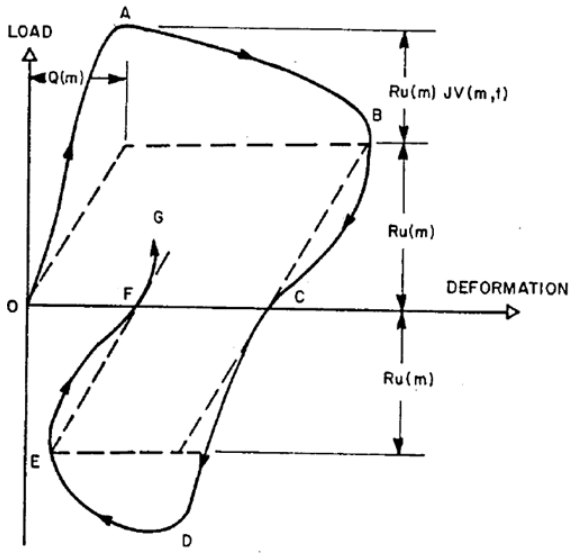

Figure 3.4 Dynamic load deformation characteristics of soil.

The fundamental quantities to describe soil resistance in the wave equation are R_u, Q and J. Smith's paper provides a way to compute them all.

The side friction parameter $R_u(m)$ is obtained by the maximum static soil adhesion or friction against the side of a given pile segment by:

$$R_u(m) = f_s \cdot \Sigma_0 \cdot \Delta L, \tag{3.4}$$

where:

- f_s is the maximum soil adhesion or friction $\left[\frac{lb}{ft^2}\right]$;
- Σ_0 is the perimeter of pile segment $[ft]$;
- ΔL is the length of pile segment $[ft]$.

In cohesionless materials (sands and gravels)

$$f_s = \sigma'_n \tan\delta, \tag{3.5}$$

where:

- σ'_n is the effective normal stress acting on the shaft of the pile $\left[\frac{lb}{ft^2}\right]$;
- δ is the interface friction angle $[deg]$.

In cohesive soils (clay) f_s during driving is the remoulded adhesion, s_{ur}, between the soil and pile.

At the tip/head of the pile (called "point" by the author) $R_u(p)$, the point resistance, is determined by the maximum static bearing strength of the soil:

$$R_u(p) = Q_u \cdot A_p, \tag{3.6}$$

where:

Q_u is the ultimate bearing strength of soil $\left[\frac{lb}{ft^2}\right]$;

A_p is the area of pile point $[ft^2]$.

The value of Q, the elastic deformation of the soil, is difficult to determine for various types of soils conditions. Many sources indicate reasonable values of Q in both friction and point bearing ranging from 0.05 in. to 0.15 in (1.27 to 3.81 mm).

The value of J, the damping constant, according to Smith suggestion varies in the range from 0.1 to 0.4 second per feet for sands and from 0.5 to 1.0 second per feet for clays. Texas Transportation Institute made some research on Ottawa sand to investigate the value of $J(p)$, finding out a range wider than Smith's one; then the original guess can be considered in reasonable agreement.

For the value of $J(m)$ no data were available at the time the paper was written, but Smith believes it is smaller than $J(p)$ and suggest a value of 1/3.

Further studies after Smith initial work suggested to write the total resistance R_{tot} provided by the soil in the form of:

$$R_{tot} = R_u \cdot [1 + J \cdot V^n], \tag{3.7}$$

where:

- R_u is the static resistance computed according to Eq. 3.4 and Eq. 3.6
- n is the damping factor, a value always less than 1, meant to employ a constant value of J (as Smith suggested initially) for the full range of velocities. Indeed, during laboratory tests, J has shown to change as the velocity changed, but the introduction of this exponent allows a single value of damping to be used anyway.

Eq. 3.7 represents the total resistance provided by the soil to the driving process and includes two contributions: one static and one dynamic, related to damping.

The first contribution is also called soil Static Resistance to Driving (SRD) and will be dealt with in more detail in the following chapters.

It can also be noted that very slowly moving pile only encounters static resistance, since the second contribution is negligible, while a rapidly moving pile also encounters dynamic resistance.

3.1.2. Pile Model

The idealisation of the pile suggested by Smith is illustrated in Figure 3.1 (left). The system includes:

- A ram, to which an initial velocity is imparted by the pile driver;
- A capblock (cushioning material);

- A pile cap;
- A cushion block (cushioning material);

These elements are idealised as discrete weights and springs, named "internal springs". For many practical cases (and as represented in the figure), ram and pile cap are assumed to be rigid. For non-rigid springs, different load-deformation characteristics can be represented, for example considering internal damping or not in the material as depicted in Figure 3.5.

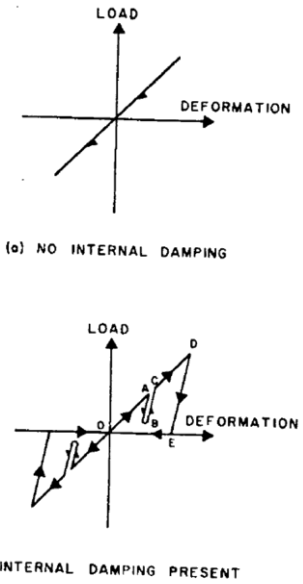

Figure 3.5: Load-deformation relationship assumed for internal spring m.

The pile itself is also modelled as a discrete element of lumped mass corresponding to a series of weights and springs. It consists in breaking the continuous pile into discrete segments, each one represented by its weight and spring contributing to the total segment stiffness. Usually, the weight representing the segment is assumed to be concentrated at the end of the segment away from the point of impact. This places the spring on top of the weight whose stiffness it represents.

Piles should be discretised into segments not to exceed approximately 10 feet in lengths, but into not less than five segments. A slight increase in solution accuracy is achieved by using shorter segment lengths, however, this usually is not convenient because of the increase in solution time and the relative accuracy of the input data. Further, it is preferable that the lengths of all the segments in the hammer-pile system be approximately equal.

The stiffness of each pile segment spring is calculated by:

$$K(m-1) = \frac{A(m) \cdot E(m)}{\Delta L(m)}, \tag{3.8}$$

where:

- $K(m-1)$ is the spring stiffness for segment m in $\left[\frac{lb}{in.}\right]$;
- $A(m)$ is the cross-sectional area of segment m in $[in.^2]$;
- $E(m)$ is the modulus of elasticity of the material of the segment m in $[psi]$;
- $\Delta L(m)$ is the length of segment m in $[in.]$.

The weight of each pile segment is calculated by:

$$W(m) = A(m) \cdot \Delta L(m) \cdot \gamma, \tag{3.9}$$

where γ is the unit weight of pile material expressed in $\left[\frac{lb}{in.}\right]$.

While for the pile's springs a linear elastic relation is sufficient, studies by Smith indicate that the stress-strain behaviour of cushion materials does not follow a linear relationship during compression. Instead, the loading phase exhibits a nearly parabolic curve. While using the precise load-deformation curve for the cushion provides accuracy, it is often impractical due to the time and complexity involved. To simplify, the load-deformation behaviour can be approximated with a straight line, using the secant modulus of elasticity as the slope.

Additionally, the dynamic coefficient of restitution for the cushion materials tested generally aligns with commonly recommended values.

It has also been shown that the effect of internal damping in the concrete and steel piles will usually have a negligible effect on the driving stresses.

3.1.3. Driveability Theory

Smith developed the following equations:

$$D(m,t) = D(m,t-1) + 12\Delta t \cdot V(m,t-1), \tag{3.10}$$

$$C(m,t) = D(m,t) - D(m+1,t), \tag{3.11}$$

$$F(m,t) = C(m,t) \cdot K(m), \tag{3.12}$$

$$R(m,t) = [D(m,t) - D'(m,t)] \cdot K'(m) \cdot [1 + J(m) \cdot V(m,t-1)], \tag{3.13}$$

$$V(m,t) = V(m,t-1) + [F(m-1,t) - F(m,t) - R(m,t)]\frac{g\Delta t}{W(m)}, \tag{3.14}$$

where:

- ( ) is the functional designation;
- m the element number;
- t the number of time interval;

- Δt the size of the time interval $[s]$;
- $C(m,t)$ is the compression of internal spring m in time interval t $[in.]$;
- $D(m,t)$ is the displacement of element m in time interval t $[in.]$;
- $D'(m,t)$ is the plastic displacement of external soil spring m in time interval t [in.];
- $F(m,t)$ is the force in internal spring m in the time interval t $[lb]$;
- g is the acceleration due to gravity $\left[\frac{ft}{s^2}\right]$;
- $J(m)$ is the damping constant of the soil at element m $\left[\frac{s}{ft}\right]$;
- $K(m)$ is the spring constant associated with external soil spring m $\left[\frac{lb}{in.}\right]$;
- $K'(m)$ is the spring constant associated with external soil spring m $\left[\frac{lb}{in.}\right]$;
- $R(m,t)$ is the force exerted by external spring m on element m in time interval t $[lb]$;
- $V(m,t)$ is the velocity of element m in time interval t $\left[\frac{ft}{s}\right]$;
- $W(m)$ is the weight of element m $[lb]$.

According to this notation, a value of J is given for every element m, but it must be underlined that the choice was made only for the sake of generality; indeed, Smith considers only two values, one for the point of the pile in bearing and one for the side of the pile in friction.

Moreover, the use of $K(m)$ as spring constant implies a linear load deformation relationship. To introduce internal damping in the cap block and cushion block, Smith proposed the following equation instead of Eq. 3.12:

$$F(m,t) = \frac{K(m)}{[e(m)]^2} C(m,t) - \left[\frac{1}{[e(m)]^2} - 1\right] \tag{3.15}$$

where $e(m)$ is the coefficient of restitution of internal spring m and defines the slope of the load-deformation relationship, while $C(m,t)_{max}$ is the temporary maximum value of $C(m,t)$. This equation reproduces the relationship illustrated in Figure 3.5 (b).

The procedure to compute the quantities of the analysis is the following:

1. From the input properties of the pile driver, the initial velocity of the ram $V(1,0)$ is determined: the velocity of the top weight is set equal to the one ram, obtained from the energy output of the hammer. Other time dependent quantities are initialised to zero or to satisfy the static equilibrium conditions;
2. Displacements $D(m,1)$ are calculated by Eq. 3.10;
3. Compressions $C(m,1)$ are calculated by Eq. 3.11;

4. Internal spring forces $F(m,1)$ are calculated by Eq. 3.12 or 3.15;
5. External spring forces $R(m,1)$ are calculated by Eq. 3.13;
6. Velocities $V(m,1)$ are calculated by Eq. 3.14;
7. The cycle is repeated for successive time intervals until maximum stresses and displacements has been found. It should be emphasized that the results of this procedure are for a single blow of the ram with the pile at a specified embedment in the soil.

In order to run Smith's solution to the wave equation, the following inputs are required:

1. The initial velocity and weight of the ram;
2. The actual dynamic stress-strain curve for the cushion;
3. The area and length of the pile;
4. The density and modulus of elasticity of the pile.

Smith also introduced a critical time interval: since the method makes use of discrete element, if the time discretization is too wide, then the solver diverges leading to non-valid results.

Following studies related the critical value also to the segment length ΔL, in order to have a sufficiently accurate solution finding out that the discrete-element numerical solution is an exact solution of the one-dimensional wave equation when:

$$\Delta t_{crit} = \frac{\Delta L}{\sqrt{\frac{E}{\rho}}} \tag{3.16}$$

where:

- ρ is the density of the pile material in $\left[\frac{lb}{in.^3}\right]$;
- E is the modulus of elasticity of the material in $[psi]$;
- ΔL is the length of segment in $[in.]$.

For practical problems, a choice of $\Delta t_{crit}/2$ (order of 1/5000 seconds) is commonly used since inelastic springs, materials of different densities, and elastic moduli are usually involved.

3.2. Results of the Driveability Analysis

The results of the analysis conducted by Smith include:

- The number of blow counts (number of hammer's blows necessary to penetrate the soil of a certain depth);
- The load bearing capacity at the time of driving, meaning the resistance to penetration afforded by the soil (above-mentioned R_u or equivalently SRD);
- The driving stresses induced in the pile;
- The resulting motion of the pile during the impact.

The results are valid for a given configuration of the system, which include hammer specification, pile and soil modelling, and for a given energy output for the pile driving hammer.

The wave equation can be employed to predict the permanent set per blow of a given hammer, which can then be used to relate the ultimate static soil resistance at the time of driving to the number of blows required to advance the pile one foot.

Consideration on the driving stresses revealed that the stress amplitude at the pile head, induced by the impact of a falling ram, is primarily governed by an equation that is directly proportional to the ram's velocity upon impact. Additionally, the stiffness of both the cushion and the pile significantly influences the magnitude of the generated stress. Furthermore, the soil resistance acting along the pile's shaft and at its tip also plays a crucial role in determining the stress levels within the pile.

The wave equation is quite often used as an aid in design. For example, it is commonly used to optimize the cushion, i.e., to determine which cushion will effectively limit the driving stresses induced in the hammer and pile, and yet will still produce the maximum possible permanent set per blow of the hammer, and to determine the influence of the other driving accessories. Indeed, it has been shown that in many cases the driving accessories absorb a major portion of the total energy output of the hammer. In some cases, these accessories account for a 50% reduction in the energy output of the hammer. The use of the wave equation enables the selection of optimum driving accessories required to minimize these losses.

It is also used to determine the correct size of the driving hammer reducing the chance of picking a very large and expensive hammer whose capacity is not needed, as well as the situation of picking a small hammer unable to drive the pile to the required penetration.

Despite having been one of the most used and accepted methods, Smith's model is not without limitations. In a driveability analysis, the modelling of the soil performance is one of the most important issues in order to get reliable results. Consequently, Smith´s model is only as good as the certainty of the values used for soil parameters. The soil factors used in the model cannot be associated with soil properties; moreover, they cannot be measured using common geotechnical investigation methods. Thus, extensive research has been carried out in the recent years to provide accurate quake and damping values to develop a better representation of the soil reaction.

4 SRD and Friction Fatigue Concept

4.1. Soil Resistance to Driving

One of the most important factors in the driveability analysis is the soil resistance to driving. Indeed, while the mathematical framework of the wave equation approach based on Smith's work is solid, its predictive capability is very sensitive to the soil resistance driveability input (see 3.1.1).

This parameter is composed of two contributions: a static part (static resistance to driving, SRD) and a dynamic one which is related to damping and is usually expressed as in Eq. 3.7.

The concept of soil resistance to driving refers to the resistance that soil provides against the installation and penetration of a driven pile, which means how easily a pile can be driven into the ground without refusal or excessive damage.

In general, two different parts contribute to the computation of SRD, one from the pile shaft, one from the pile tip (which, for open end, pipe piles, corresponds to the cross section of the pile, so an annular area).

The behaviour of open end is classified in two families: coring piles and plugged piles.

Coring piles are hollow piles that allow soil to pass through the pile as it is driven into the ground. This results in less soil displacement, and the pile may partially "core" the soil, leaving an open section inside. They rely mainly on skin friction along both the outer and inner pile's surface.

On the other hand, plugged piles are also hollow but behave like solid piles once soil or rock fills the interior during driving, forming a "plug." This plug significantly increases resistance at the pile's tip, making the pile act as a closed-ended system. Plugged piles typically displace more soil compared to coring piles and provide higher end-bearing capacity.

For large diameter piles, as the case of offshore foundation piles, the dominant behaviour is coring.

The SRD can be written in a general form that highlights the contribution of each part.

For coring piles, the shaft resistance is given by the contribution of two different components, one provided by internal friction, one by the external one. In this case the SRD can be written as:

$$SRD = F^{ext} + F^{int} + Q_{bA}, \tag{4.1}$$

where F^{ext} is the contribution of the external soil-pile friction that formally is obtained by:

$$F^{ext} = \int_0^{z=L} f_s^{ext} \cdot \pi \cdot D_{ext} \cdot dz, \tag{4.2}$$

so the integral of the mobilised tangential stresses, f_s^{ext}, along the embedded length of the pile, considering D_{ext} the external diameter of the pile.

F^{int} is the contribution of the internal soil-pile friction that formally is obtained by:

$$F^{int} = \int_0^{z=L} f_s^{int} \cdot \pi \cdot D_{int} \cdot dz, \tag{4.3}$$

so the integral of the unit shaft resistance, f_s^{int}, along the length of the embedded pile, considering D_{int} the internal diameter of the pile.

The total friction can be written in an incremental way, useful for implementation, according to the following formula:

$$F_s = F_{s,e} + F_{s,i} = \pi D_e \sum_{z=0}^{z=L} f_s \cdot \Delta z + \pi D_i \sum_{z=0}^{z=L} f_s \cdot \Delta z. \tag{4.4}$$

Q_{bA} is the contribution of the tip, given by the annular cross section in case of coring pile:

$$Q_{bA} = \frac{\pi\left({D_e}^2 - {D_i}^2\right)}{4} \cdot q_b \tag{4.5}$$

where q_b is the unit end bearing resistance of the soil at the tip of the pile.

In the case of fully plugged conditions F_s and Q_{bA} are calculated as:

$$F_s = F^{ext} = \int_0^{z=L} f_s^{ext} \cdot \pi \cdot D_{ext} \cdot dz, \tag{4.6}$$

$$Q_{bA} = \frac{\pi {D_e}^2}{4} \cdot q_b. \tag{4.7}$$

It must be underlined that, in the formulation depicted above, q_b is assumed to be equal across the pile tip annulus and across the soil plug.

In literature many different analytical methods are proposed to compute the SRD. Some of these, such as Stevens 1982, [21], Alm and Hamre 2001, [1], and Jones et al. 2020, [9], are discussed in more detail in later chapters. Usually, these methods provide an upper and lower bound value, based on the best estimates of the soil parameters. In general, the upper bound is chosen for design purposes in order to be on the safe side for a possible refusal during driving.

4.2. The Friction Fatigue Concept

In the computation of the shaft resistance of the total SRD, in the last decades, it has been observed that the shaft friction, for a certain horizontal, reduces as the pile penetrates deeper layers. Regarding this topic, referred as "friction fatigue", more and more studies has been conducted to investigate the behaviour of this phenomenon.

Currently there is no consensus as to which is the most suitable method for assessment of friction fatigue. Some designs relate the friction fatigue to the height of a soil layer above the pile tip, as Alm and Hamre 2001, [1]. Others relate the phenomenon to the height of the pile normalized by its diameter, such as the ICP formulation, [7]. Other authors, like White and Lehane (2004), [23], reinforce the notion that the primary mechanism controlling the friction fatigue is the cyclic loading that the pile suffers during installation.

Despite this debate all methods agree that friction fatigue can be defined by a reduction of the maximum friction up to a residual value, as the penetration increases.

Among the research conducted in the recent years, two particularly significant studies are presented in the following section to provide the reader a deeper understanding of the friction fatigue phenomenon.

4.2.1. Heerema 1980: predicting pile driveability, Heater as an illustration of the "friction fatigue" theory

Among the 6 papers published by the company Heerema about the Heater Platform piling, the fifth, [6], is about the friction fatigue as part of the background in the prediction of the driveability.

The outcomes of this fifth paper are based on a laboratory test, and a mathematical model is provided for the shape of the horizontal stress distribution along the pile shaft. The analysis has been conducted in stiff and hard clays.

The analysis had been started since the site of Heater Field initially showed clays' undrained shear strength of 800 kN/m^2, while at depths near to design penetration of

the pile, it was found to be half of it. Such a high value of S_u sounded quite challenging, but the research group was nevertheless optimistic about the possibility of reaching design penetration.

The optimism was based on the outcomes of another work in Kontich (Belgium) stiff clays finished just few years earlier, in 1974. In that occasion it was noted that although the clay's shear strength gradually increased with depth and therefore the cumulative driving resistance should be expected to increase progressively, the blow count indicated through computer post-analysis that the total driving resistance increased only less-than-linearly with depth of penetration.

Given that, if the shear strength of the clay remained constant, total wall friction would be expected to increase linearly with depth, the observed less-than-linear increase in total driving resistance suggests that the unit skin friction actually decreased with depth, even though the clay's shear strength increased, but this would be illogical. A more plausible interpretation is that skin friction was somehow reduced as the pile advanced.

If friction is being lost during driving, this likely results from wear along the slip surface. Thus, in authors mind, it is reasonable to assume that the clay exerts its maximum frictional resistance on the pile wall near the tip, where the soil is least disturbed. As the pile continues downward, the soil around it is gradually affected by movement, leading to a progressive reduction in the soil's frictional effect on the pile wall.

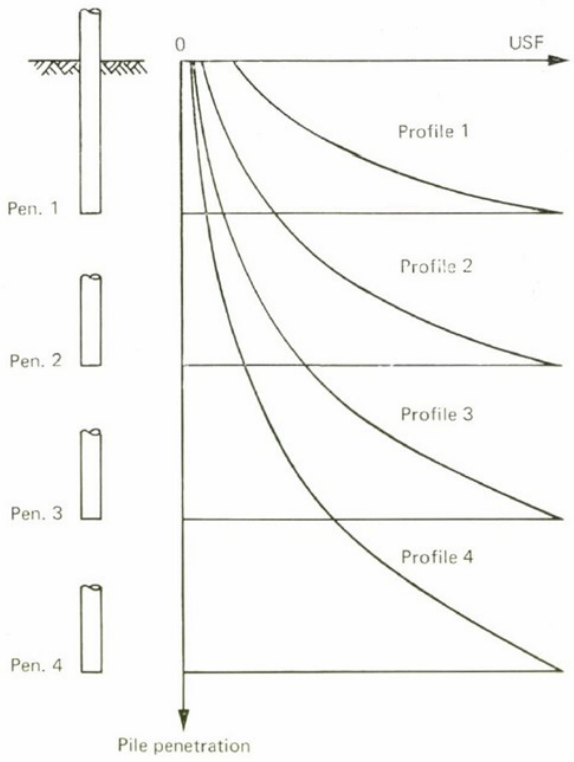

Figure 4.1: Suggested schematic unit skin friction profiles at four penetrations in a soil with constant shear strength.

Figure 4.1 illustrates four schematic profiles of unit skin friction with depth based on this concept. These profiles show that cumulative side friction increases in a less-than-linear manner, consistent with the results observed in Belgium. Traditional methods for estimating friction resistance during pile driving assumed that the friction gained by the pile wall at the tip remains constant as the pile penetrates further.

The authors have introduced the term "friction fatigue" to describe the phenomenon where friction decreases during driving. Following the Kontich tests, it was suggested that developing a mathematical model for friction fatigue could be a valuable advancement for improving the accuracy of pile driving predictions.

To gain a deeper understanding of the friction fatigue phenomenon, a simple laboratory test was designed to simulate the behaviour of a pile wall moving through soil. The setup allowed for controlled observation of how friction between the pile wall and soil might diminish as movement progresses, thereby providing valuable insights into the mechanics of friction fatigue in pile driving.

A typical result is showed in Figure 4.2: it can be noted that, for a given depth (29 m), as the number of cycle increases, due to the installation and penetration of the pile, the friction decreases sharply.

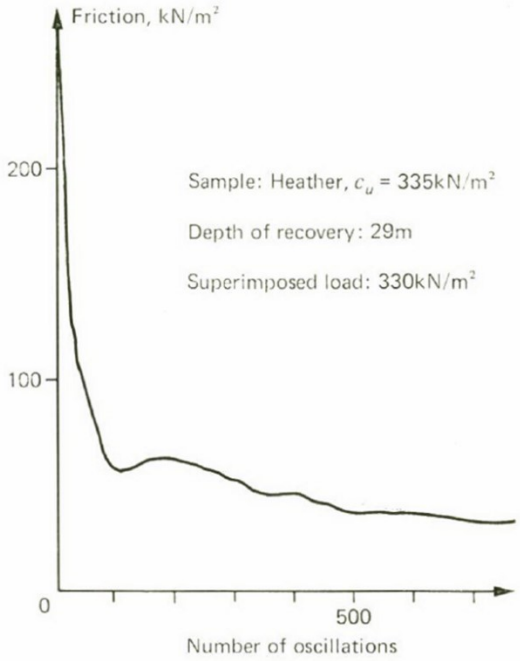

Figure 4.2: Typical test measurements of shaft friction for a given horizontal.

The research group asserted that the friction decrease along the pile wall cannot be caused by remoulding only but must be a consequence of a decrease in horizontal stresses. The decrease could be related to pile wall irregularities that push the soil outward, take some soil downward and to elastic expansion and transverse vibration of the pile, creating a horizontal arch effect around the pile. Nevertheless, they also

underlined the impossibility of determining the in situ horizontal stress acting on the pile shaft.

By means of wave equation computer post-analysis, from the recorded blow count, it is possible to determine the total driving resistance, but still, not the distribution of friction along the pile. The authors therefore assumed an exponential function for the unit skin friction profile, with peak value at the pile tip, where no oscillations have occurred yet. Considering $\sigma_{h_d}^{0.7}$ (horizontal stress at depth d to the power of 0.7) as the unit skin friction, the general law can be written as:

$$\sigma_{h_d}^{0.7} = \sigma_{h_i}^{0.7} \cdot e^{n(d-p)}, \tag{4.8}$$

where:

- n is the shape/fatigue factor and can be chosen solely dependent on clay's undrained shear strength and the pile's penetration depth, which relationship must be determined by post-analysis pile driving field data;
- p is the tip depth;
- d is the actual depth;
- $\sigma_{h_i}^{0.7}$ the initial value of horizontal stress before fatigue.

From experimental evidence, $\sigma_{h_i}^{0.7}$, appeared to be dependent only on s_u in a linear way:

$$\sigma_{h_i}^{0.7} = 0.25 \cdot s_u, \tag{4.9}$$

Where both quantities are expressed in kN/m^2.

In order to find the total driving friction resistance, it is sufficient to integrate the stress equation (Eq. 4.8) along the depths of clay layers, which, if considered a representative value of shear strength valid for all layers, results in:

$$A = \int_0^d \sigma_{h_d}^{0.7} \cdot dz = \frac{\sigma_{h_i}^{0.7}}{n} \cdot e^{n(d-p)} \Big]_0^d \tag{4.10}$$

Where A is the area obtained consequent to integration.

In case the relationship $n = f(s_u, p)$ is known, then A must be calculated by considering as many intervals as the complexity of shear strength profile requires and each interval has its own n value.

The paper then provides a methodology to develop the relationship between the shape factor n and undrained shear strength and depth.

This was obtained by post-analysis of many significant penetration data, which provided the value A from which, once the representative s_u value was selected, it was possible to define n. The procedure led to the formulation of the following relationship:

$$n = 0.33 + (0.057 - 1.02 \cdot p^{-0.65}) \cdot \ln\left(\frac{s_{u_d}}{790}\right) \tag{4.11}$$

valid in the (experience) range:

$$70 < s_u < 750 \quad [\text{kN/m}^2]$$

$$6 < p < 80 \quad [\text{m}]$$

According to the results obtained in the calibration and computation of the shape factor, some considerations can be done. First, for larger undrained shear strength, the value of n is smaller, and so the rate of friction fatigue: so, for stiffer clays, the rate of friction reduction is smaller. Second, for larger pile penetration, the value of n decreases, resulting in a smaller friction reduction rate. Both considerations were in agreement with the laboratory tests.

An important thing to underline is that the friction fatigue does not affect the bearing capacity, since the phenomenon is caused by a loss of horizontal stress along the shaft, but this occurs only temporary ("setup" phenomenon).

In conclusion, the main outcomes of the research concern friction fatigue phenomenon in clays: it is showed that the friction resistance experienced by the pile wall is initially large (i.e. at the pile tip), but decrease gradually along the pile shaft while the pile proceeds downward. This decrease cannot be attributed to clay remoulding only and must be a consequence of horizontal stress decrease of the surrounding soil, which result in forming a temporary horizontal arch around the pile during the setup time.

Since it is not possible to quantify stress state along the shaft in an analytical way during driving, to quantitatively use the friction fatigue theory for driveability predictions, the researchers came up with a model, validated on numerous piles driving cases in the North Sea.

4.2.2. Lehane and White 2004: friction fatigue on displacement piles in sands

The paper by Lehane and White 2004, [23], aims to investigate the behaviour of displacement piles in sands, which have shown that the ultimate shaft friction for a given horizon decreases as the pile tip penetrates, phenomenon known as friction fatigue.

In the last decades, the earth pressure approach for displacement piles has been replaced in the onshore environment by methods that relate shaft resistance to in situ

test parameters such as CPT cone resistance. After Heerema 1980, [6], design methods started taking into account also friction fatigue using relationships that relate the maximum available shaft friction to the degradation due to pile penetration.

Results from field and laboratory tests showed that friction fatigue does not occur in absence of loading cycles and that for a greater number of cycles imposed during the installation, the reduction of shaft resistance at a given soil horizon is larger. For that reason, it sounds more reasonable to link friction fatigue to the loading cycles induced by the installation method rather than employing empirical relationships related to the distance from the pile tip.

The aim of the further experiments is then to investigate the effect of the installation method on shaft capacity of displacement piles in sands by means of scaled models of instrumented piles in a geotechnical drum centrifuge, focusing on the distribution of lateral stresses acting during installation and subsequent cyclic load tests.

After the description of the experimental set, the model pile, the soil profile characterization and test programme, the paper illustrates the results of head load measurements and horizontal stresses. In particular, the horizontal stresses are measured for three different situations: monotonic installation, jacked installation and pseudo-dynamic installation. Those three methods differ mainly in the type of loading: monotonic installation result in monotonic loading, jacked installation in one-way cyclic loading, and pseudo-dynamic in two-way cyclic loading.

The measurements recorded during monotonic installation resulted mirroring the CPT q_c profile. The horizontal stress acting on the pile shaft σ'_{hm} had been normalised by the corresponding q_c values and plotted against depth in Figure 4.3, where h is the height above the pile tip and B the pile width, so the three curves represent three different sensors at different positions in the pile.

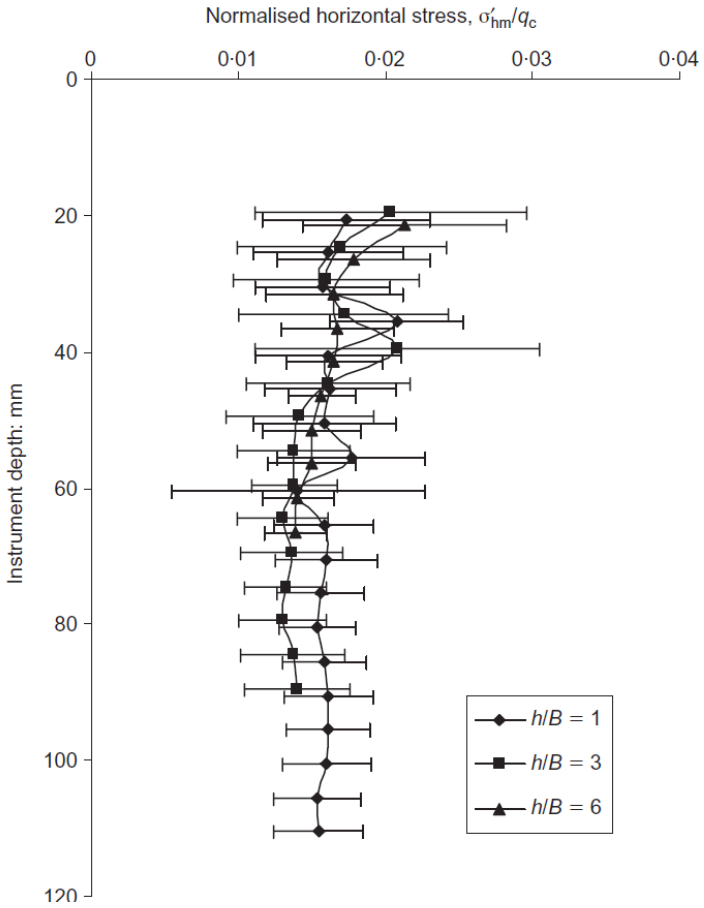

Figure 4.3: Normalised horizontal stress during monotonic installation (mean of all four tests, error bars 1 std dev.).

From the obtained results it can be noted that the normalised horizontal stress remains approximately constant throughout installation, and they are independent of the distance behind the pile tip, so, for a given horizon, almost the same horizontal stress is recorded by each instrument as it passes that point. That means that no friction fatigue is evident.

During cyclic installation the jack stroke length was insufficient to mobilise full friction therefore the σ'_{hm} data cannot be compared directly with the measurement recorded during monotonic installation. The influence of installation method on shaft friction can be instead estimated by considering the stationary horizontal stress σ'_{hc}, which is the stress when the pile is unloaded to zero head load, recorded during each installation cycle. In the monotonic installation this happens only at half of the installation depth and at the end, due to the installation setup (the authors decided to stop and unload monotonic installation at half of the depth of the pile final penetration). In case of pseudo-dynamic installation, this value is the minimum value recorded during each cycle, that means at zero pile head load, so when the load changes sign.

Figure 4.4 shows the profiles of σ'_{hc} with depth for each installation method, grouped by instrument position and averaged over the tests. In this case, differently from monotonic installation, friction fatigue is evident, indeed one can note that σ'_{hc}, at a given depth, decreases as each instrument passes: the first instrument, Figure 4.4 (a), closer to the tip, recorded a higher resistance than the second, Figure 4.4 (b), and way higher than the third one, Figure 4.4 (c).

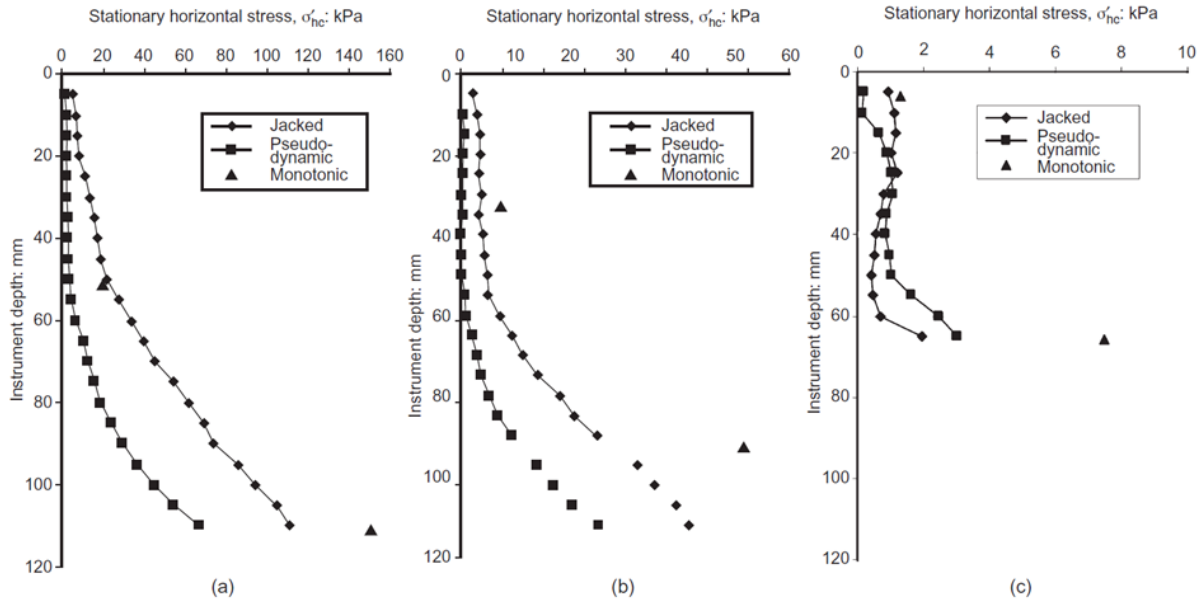

Figure 4.4: Variation of stationary horizontal stress with installation method: (a) h/B = 1; (b) h/B = 3; (c) h/B = 6.

Comparing the horizontal stress recorded on the pseudo-dynamic piles with the monotonic, this results in a way smaller value: the first 60 metres installed by pseudo-dynamic methods has typically only the 10% of the stationary horizontal stress of the monotonic case. The one way cyclic induced by jacking, leads instead to values in the between of the two.

The normalised value of horizontal stress, σ'_{hc}/q_c, at a given depth has also been plotted against distance above pile tip, Figure 4.5 (a), and number of cycles, Figure 4.5 (b): a better agreement between the two sets of data is achieved in the second case.

For a given soil horizon, the number of cycles (N) experienced at each lateral stress sensor position is simply $2h$ for the pseudo-dynamic installation since the net penetration is 0.5 mm per cycle. For jacked installation, the value of N required to bring a given sensor to a specific soil horizon increases slightly with depth since the rebound during unloading increases as the pile head load increases.

Comparing the two plots it can be noted that the change in normalized horizontal stress along the pile shaft correlates more strongly with the number of cycles (N) than with the distance from the pile tip (h) or its ratio to pile diameter (h/B). A direct comparison can be made between the instrument placed at h/B = 3 during jacked installation and at h/B = 1 during pseudo-dynamic installation, as shown in Figure 4.5

(b). In this case, each instrument experiences approximately 18 and 20 cycles, respectively, and records similar normalized stationary horizontal stresses.

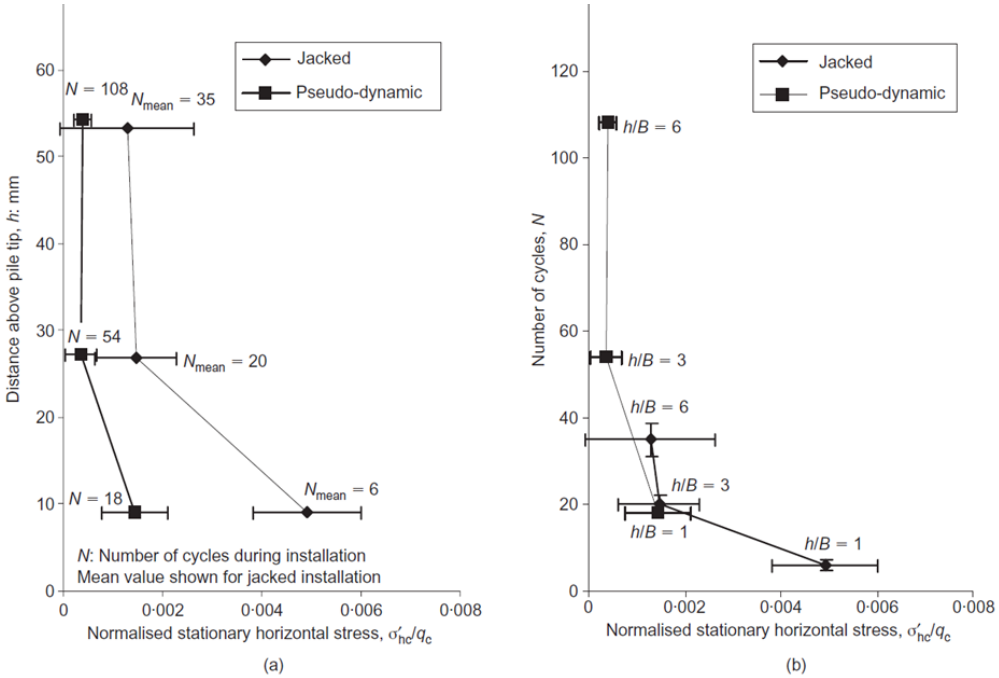

Figure 4.5: Influence of loading cycles during installation on stationary horizontal stress: (a) normalised horizontal stress against distance above pile tip; (b) normalised horizontal stress against number of cycles.

Although jacked installation involves one-way loading of the pile head and pseudo-dynamic installation involves two-way loading, both methods exhibited similar stress degradation after around 20 cycles. Cyclic load tests, discussed later, showed that with a higher number of cycles, two-way loading at the pile head leads to more pronounced degradation. It is also noted that while one-way pile head loading is applied during jacked installation, some degree of two-way loading occurs along the pile shaft due to rebound effects.

The effects on shaft friction of cyclic loading during installation and a cyclic 'working load' may be compared by examining the horizontal stress measurements during the cyclic load tests.

What came out is that for one-way load cycling, σ'_{hc} reaches a stable, limiting value after 30 cycles, whereas under more intense two-way cycling, the stress progressively declines toward zero, as can be seen in Figure 4.6, which shows the degradation of normalized horizontal stress observed in each cyclic load test, once adjusted, in order to take into consideration also the cycles introduced during installation (for different installation techniques, different initial number of cycles are required).

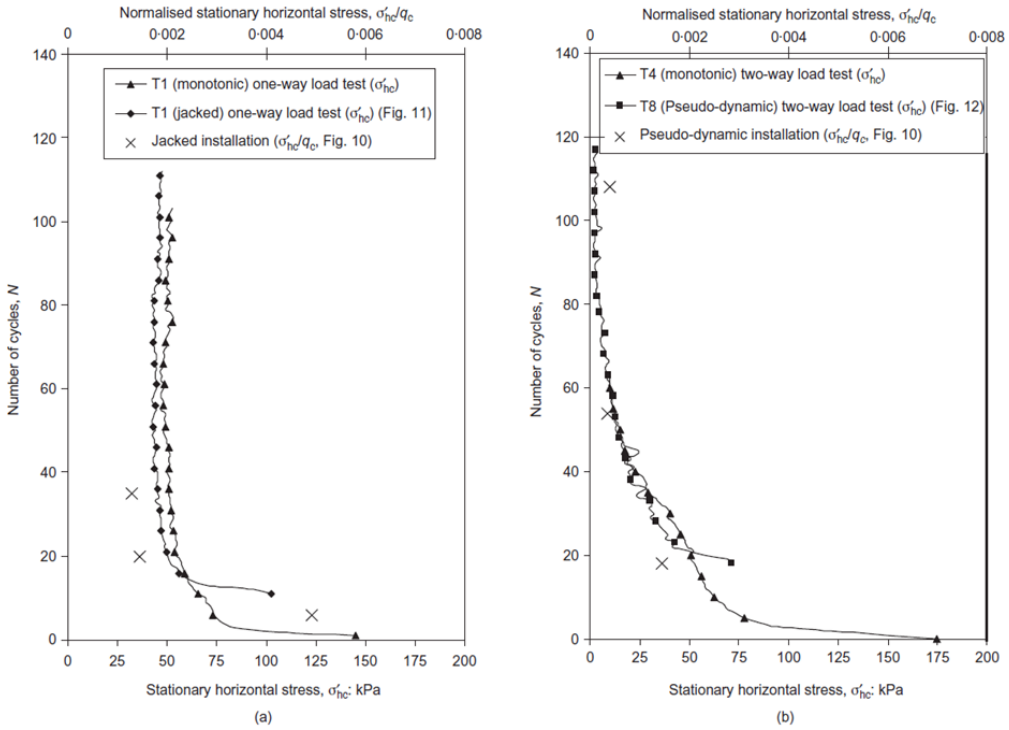

Figure 4.6: Degradation of stationary horizontal stress with cycling at h/B = 1 during load tests: (a) one-way compression load test; (b) two-way compression-tension load test.

What is evident, therefore, is that there is a reducing trend of σ'_{hc} with increase in the number of cycles. Outcomes of the different tests suggest hence that cyclic loading is the only mechanism leading to degradation of side friction.

Moreover, a discrepancy can be noted between the cyclic load test amplitude and the one of installation cycles in jacked installations. This is possibly explained due to the fact that jacking procedure involves larger cycles of displacement than that induced in the one-way cyclic test. This discrepancy highlights the influence of both the number of cycles and their amplitude on friction fatigue.

This reasoning leads to the conclusion that friction fatigue depends for sure on the number of cycles but also on the mode and amplitude of cycling: two-way cycling leads to greater degradation than one-way and, as just mentioned, the larger the cycle, the larger the degradation.

5 SRD Models

The computation of SRD depends on the way the shaft friction and base resistance are modelled. These quantities can be computed in different ways according to different theories. In particular, in the following sections, different methods to compute unit skin friction and unit base capacity are illustrated. Some of the methods rely on CPT quantities to model the soil behaviour, some on physical properties; some includes also the friction fatigue concept, while other (the older ones) are based only on the static analysis.

5.1. Stevens 1982

The SRD formulation proposed by Stevens et al. (1982, [21]) was derived through back-calculation of soil resistance using wave equation analysis, which bases are theorized by the Smith theory, [20].

The two main uncertainties of Stevens' theory are:

- The energy transmitted by the hammer to the pile-soil.
- Soil-pile interaction during driving.

In Smith's theory, soil-pile interaction is represented by soil quake and damping coefficients. These parameters were required in the back analysis conducted to obtain the method, but it must be underlined that they are not intrinsic properties of the soil but used just as a correction to take into account all the uncertainties. Nevertheless, when applying this method to calculate the total SRD, it is preferable to use the same coefficients as those originally used in its development.

The author adopted side and point quake values of 0.1 [in] for stiff to hard clay, silt and sand. Side damping in hard clay was taken as 0.03 [sec/ft] and point damping to 0.15 [sec/ft], while for sands 0.08 [sec/ft] and 0.15 [sec/ft] for side and tip damping respectively.

The estimation of soil resistance is different depending on the type of soil:

5.1.1. Cohesive Soils

The unit skin friction during continuous driving is computed using the stress history approach presented by Semple and Gemeinhardt, [19]: skin friction is first computed

by the API RP 2A (January 1981) Method [2], then adjusted incrementally using a pile capacity factor F_p determined empirically from wave equation analyses:

$$f_s = F_p \cdot \alpha s_u, \tag{5.1}$$

where s_u is the actual undrained shear strength, α can be found in [2], and

$$F_p = 0.5 \cdot OCR^{0.3}. \tag{5.2}$$

The overconsolidation ratio (OCR) is computed as:

$$\frac{s_u}{s_{unc}} = (OCR)^{0.85}, \tag{5.3}$$

where s_{unc} is the undrained shear strength of the clay if normally consolidated.

According to Skempton, s_{unc} is computed as:

$$s_{unc} = \sigma_{v0}' \, (0.11 + 0.0037 \, PI), \tag{5.4}$$

where σ_{v0}' is the effective overburden pressure and PI is the plasticity index.

Unit tip bearing capacity is computed as:

$$q_b = s_u \cdot N_c, \tag{5.5}$$

where N_c is the dimensionless bearing capacity factor assumed equal to 9.

5.1.2. Granular Soils

The unit skin friction is computed using static pile capacity procedures:

$$f_s = K \cdot \sigma_{v0}' \cdot \tan \delta, \tag{5.6}$$

where K is the lateral earth pressure coefficient, taken as 0.7 and δ is the angle of friction between soil and pile and can be found in tables.

In the paper, in the same table where the value of δ are presented, values for limiting unit skin friction f_{max} are included.

Table 5.1: Soil-pile friction angle and limiting skin friction in function of soil type, [21].

Soil Type	Soil-Pile Friction Angle, δ, [°]	Limiting Unit Skin Friction, f_{max} , [ksf]
Sand	30	2.0
Silty Sand	25	1.7
Sandy Silt	20	1.4
Silt	15	1.0

The unit end bearing capacity is computed as:

$$q_b = \sigma_{v0}' \cdot N_q', \tag{5.7}$$

where N_q' is the dimensionless bearing capacity factor.

In this case a table is also included, providing values of N_q' and the limiting unit end bearing q_{max}.

Table 5.2: Bearing capacity factors and limiting end bearing in function of soil type, [21].

Soil Type	Dimensionless Bearing Capacity Factors, N_q'	Limiting Unit End Bearing, q_{max} , [ksf]
Sand	40	200
Silty Sand	20	100
Sandy Silt	12	60
Silt	8	40

5.1.3. Rocks

In case the rock is severely fractured then driving piles into it would reduce it to granular material, hence unit skin friction is computed assuming sand parameters.

For more competent rock, unit end bearing capacity is computed as:

$$q_b = u \cdot N_u, \tag{5.8}$$

where u is the compressive strength of the rock and N_u is the dimensionless bearing capacity factor, assumed equal to 3.

Stevens then provides a lower and upper bound for both coring and plugged piles conditions.

For a coring pile, the lower bound is computed assuming that the skin friction developed on the inside of the pile is 50% of that on the outside of the pile, while the upper bound is assumed equal (so 100%) to the external friction.

For plugged piles the lower bound is the one presented already. For the upper bound instead, in the case of granular soil only, the value of skin friction is increased by 30% and the unit end area by 50%.

A corresponding increase in limiting values for unit skin friction and unit end bearing is assumed. For cohesive soils end bearing is computed assuming $N_c = 15$ instead of 9 (so an increase of 67%).

The paper then presents several case histories:

In case of very dense sand the number of blow increase with depth. In case of hard clay, the number of blows is constant with penetration and plugged and coring piles provides similar results. In case of mixed profile coring and plugged give very similar results in terms of number of blows per foot. In case of weak rocks, the blow counts are exceeding the 250 blows per foot. If the rock is stronger, then the driving is not working.

The author then suggests evaluating the pile drivability according to RQD: if RQD is greater than 50%, the recovery greater than 85% and the uniaxial compression strength (UCS) greater than 100 ksf, then the installation will probably fail.

The method can be expressed in an effective way considering the following notation:

$$f_s^{tot} = (1 + k_f) f_s, \tag{5.9}$$

and

$$q_b^{tot} = (1 + k_q) q_b, \tag{5.10}$$

where k_f and k_q are coefficients added to the external shaft resistance (the value of one) to consider the internal contribution of friction.

The value of the coefficients can be summarised in the table below:

Table 5.3: Summary of the shaft coefficient.

k_f	Lower Bound		Upper Bound	
	Cohesive Soil	Granular Soil	Cohesive Soil	Granular Soil
Coring pile	0.5	0.5	1	1
Plugged pile	0	0	0	0.3

Table 5.4: Summary of the tip bearing coefficient.

k_q	Lower Bound		Upper Bound	
	Cohesive Soil	Granular Soil	Cohesive Soil	Granular Soil
Coring pile	0	0	0	0
Plugged pile	0	0	0.667	0.5

5.2. Alm and Hamre 2001

The paper by Alm et Hamre (2001), [1], aims to present an improved version of the model already introduced by the same authors in 1998 for soil driveability, directly correlated to CPT measurements in order to avoid error due to interpretation of measured data. Indeed, in 1998, the concept of friction fatigue had been already introduced but the individual interpretations of soil properties were a significant source of variability in the predictions.

The Alm and Hamre method, developed through back analysis of pile installation data from the North Sea, suggests side and point quake values of 2.5 mm, a side damping factor of 0.25 $\frac{s}{m}$, and a point damping factor of 0.5 $\frac{s}{m}$. This method incorporates friction fatigue into the calculation of side friction using the following formulation:

$$f_s = f_{sres} + (f_{si} - f_{sres}) \cdot e^{k(d-p)}, \tag{5.11}$$

where:

- f_s is pile the side friction $\left[\frac{kN}{m^2}\right]$;
- f_{sres} is the residual pile side friction $\left[\frac{kN}{m^2}\right]$;
- f_{si} is the initial pile side friction $\left[\frac{kN}{m^2}\right]$;
- d is the actual depth in the layer $[m]$;
- p is the pile tip penetration $[m]$;
- k is the shape factor for degradation [-] and can be computed for both sands and clays as:

$$k = \frac{\left(\frac{q_T}{\sigma_{\mathrm{v0}}'}\right)^{0.5}}{80}, \tag{5.12}$$

and:

- q_T is the cone tip resistance from CPT $\left[\frac{kN}{m^2}\right]$
- σ_{v0}' is the effective overburden pressure $\left[\frac{kN}{m^2}\right]$

According to this formulation of the degradation factor, dense sands degrade quickly, while soft clays degrade more slowly. This is because sands typically have higher base resistance, and a higher exponent results in faster degradation.

As in Stevens's formulation, the estimation of soil resistance is different depending on the type of soil:

5.2.1. Cohesive Soils

In the case of clays, the initial friction f_{si} is taken as the recorded CPT sleeve friction, while the residual is computed as:

$$f_{res} = 0.004 \cdot q_T \left(1 - 0.0025 \cdot \frac{q_T}{\sigma_{\mathrm{v0}}'}\right). \tag{5.13}$$

Unit tip resistance is taken as 60% of the total cone resistance:

$$q_{TIP} = 0.6 \cdot q_T. \tag{5.14}$$

5.2.2. Granular Soils

For sands, the initial friction is taken as the basic static friction formulation, i.e.:

$$f_{si} = K \cdot {\sigma_{v0}}' \cdot \tan \delta, \tag{5.15}$$

where δ is the constant volume friction angle [°] and K is the horizontal stress ratio after driving [-], which is directly linked to cone resistance by the correlation suggested by Jardine & Chow (1996):

$$K \cdot {\sigma_{v0}}' = 0.0132 \cdot q_T \cdot \left(\frac{{\sigma_{v0}}'}{p_a}\right)^{0.13}, \tag{5.16}$$

where p_a is the reference pressure assumed to be 100 $\frac{kN}{m^2}$.

For the sake of clarity, it must be underlined that the computation of f_{si} already includes the effect of coring piles: in particular, as can be seen in his paper, Jones (see [9]) assumes that the contribution of internal and external soil-pile friction is the same. This can be assumed since his reference to the formula employed in Alm & Hamre paper is the following:

$$K = 0.0066 \cdot \frac{q_c}{{\sigma_{v0}}'} \cdot \left(\frac{{\sigma_{v0}}'}{p_a}\right)^{0.13}. \tag{5.17}$$

What can be noted is that the two formulas used to find the lateral stress coefficient are one twice the other. This confirms the fact that Jones assumed that the two contributions are the same.

It is also noteworthy that Jones assumes q_T as the normalised cone tip resistance with $n = 1$, as it is usually done for sands.

In this case no upper limit on unit friction is included, while the best fit for residual values was found to be 20% of the initial friction:

$$f_{sres} = 0.2 \cdot f_{si}. \tag{5.18}$$

Unit tip resistance is computed as:

$$q_{TIP} = 0.15 \cdot q_T \cdot \left(\frac{q_t}{{\sigma_{v0}}'}\right)^{0.2}. \tag{5.19}$$

For all the cases, unplugged piles have been assumed during driving.

Moreover, comparing results with back-calculations, a factor of 1.25 in the prediction of the upper bound is suggested.

Table 5.5 summarises the computations of relevant quantities.

Table 5.5: Summary of Alm & Hamre formulas for the computation of SRD.

	Best Estimate		Upper Bound
	Cohesive Soil	**Granular Soil**	**All Soils**
Coring pile	$f_{s,tot} = f_s^{ext} + f_s^{int} = 2 \cdot f_s$	$f_{s,tot} = f_s^{ext} + f_s^{int} = 2 \cdot f_s$	$SRD = 1.25 \cdot SRD_{LB}$
Plugged pile	-	-	-

5.3. Jones 2020

A more recent CPT-based method for the computation of SRD including the concept of friction fatigue is proposed by Jones et al.. This method appears to perform at least as well as Alm and Hamre but more accurately in heavily overconsolidated (OC) clays.

To model the SRD-blow count relationship, a value of quake and damping parameters is also necessary. Jones recalls the value employed in previous studies (Fenske and Hirsh, Alm and Hamre) and decides to adopt for both the shaft quake Q_s and the tip/point quake Q_t a value of 2.5 mm in case of large diameter piles.

Regarding soil tip damping J_t a value of 0.50 $\frac{s}{m}$ is considered, while 0.25 $\frac{s}{m}$ for the shaft damping J_s in case of non-cohesive soils and 0.65 $\frac{s}{m}$ in case of cohesive soils, in agreement with Schneider and Harmon.

In case of multilayered soils, the value of J_s is taken as the average across the embedded length. Those coefficients hold for continuous driving of the piles.

The author then underlines that in general, in offshore conditions, piles usually don't plug and, in case of doubts (e.g. where D_i is smaller than 1 m), the method should be based on a dynamic criterion.

As previously stated by Alm and Hamre, characteristic soil properties should be input to calculate the best estimate SRD with the high estimate SRD equal to 125% of the best estimate.

Jones et al. then present the degraded shaft resistance relation according to Alm and Hamre model:

$$f_s = f_{s,res} + \left(f_{s,i} - f_{s,res}\right) \cdot e^{k\left(z - z_{tip}\right)}. \tag{5.20}$$

The shape factor for degradation k is computed in a slightly different way:

$$k = \frac{\left(\frac{q_T}{\sigma_{v0}'}\right)^{0.5}}{100 \cdot \tan(\delta)} \quad , \tag{5.21}$$

where q_T is the CPT cone tip resistance, σ_{v0}' is the in situ vertical effective stress, and δ is the interface friction angle.

In this updated model the denominator had been changed such that the shaft resistance degrades more rapidly in soils with lower δ.

The estimation of soil resistance differs depending on the type of soil:

5.3.1. Granular Soils

The unit skin friction is computed in the same way as already described in section 5.2.2 by Alm and Hamre:

$$f_{s,i} = K \cdot \sigma'_{v0} \cdot \tan(\delta), \tag{5.22}$$

where:

$$K = 0.0066 \cdot \frac{q_c}{\sigma_{v0}'} \cdot \left(\frac{\sigma_{v0}'}{p_a}\right)^{0.13}, \tag{5.23}$$

and:

$$f_{sres} = 0.2 \cdot f_{si} \tag{5.24}$$

The only changes introduced are:

- The upper limit for the coefficient K, which must be smaller than the passive earth pressure limit that, according to Rankine's theory is:

$$K_p = \tan^2\left(45° + \frac{\phi'}{2}\right), \tag{5.25}$$

  where ϕ' is the internal friction angle.

- $\tan(\delta)$ is limited to a value of 0.55 (i.e. $\delta \leq 28.8°$)

5.3.2. Cohesive Soils

Since Alm and Hamre tend to overpredict the SRD for heavily OC clays, the approach proposed by Jones is the following:

$$f_s = \min\{ f_{s,TSA} , f_{s,ESA} \}, \tag{5.26}$$

where $f_{s,TSA}$ is the unit skin friction computed according to the total stress approach (TSA), as in Alm and Hamre formulation, which considers:

$$f_{s,i} = f_{s,CPT}, \tag{5.27}$$

$$f_{s,res} = 0.004 \cdot q_T \left(1 - 0.0025 \cdot \frac{q_T}{\sigma_{\mathrm{v0}}'}\right) \geq 0. \tag{5.28}$$

$f_{s,ESA}$ is instead the unit skin friction computed according to the effective stress approach (ESA).

The ESA uses Eq. 5.15, with K calculated as:

$$K = 0.00844 \cdot YSR^{0.42} \cdot \left(137.5 + YSR - 54.375 \cdot \Delta I_{vy}\right). \tag{5.29}$$

The yield stress ratio (YSR) is a parameter used to determine the value of preconsolidation stress resulting from mechanical overburden that can be changed by many post-depositional processes like secondary and tertiary compressibility, cementation, aging temperature changes and others. The YSR is defined as the relationship between vertical yield stress (σ_{yv}') to the effective vertical stress (σ_{v0}'). The most used YSR is the overconsolidation ratio OCR.

$\Delta I_{vy}$is a measure of sensitivity on the oedometer test, generally computed as:

$$\Delta I_{vy} = \log_{10}(S_t), \tag{5.30}$$

where S_t is the sensitivity defined as the ratio of the undisturbed undrained shear strength s_u and the remoulded undrained shear strength s_{ur}:

$$S_t = \frac{s_u}{s_{ur}}. \tag{5.31}$$

In case of $S_t \approx 1$ Shonberg et al. observed a CPT sleeve friction degrading to 58% of its original value. Therefore, for the effective stress approach:

$$f_{s,res} = 0.58 \cdot f_{s,i}. \tag{5.32}$$

The end bearing capacity for any type of soil is computed as:

$$q_b = 0.6 \cdot q_T. \tag{5.33}$$

The method can be summarised as in Table 5.6:

Table 5.6: Summary of Jones formulas for the computation of SRD.

	Best Estimate		Upper Bound
	Cohesive Soil	**Granular Soil**	**All Soils**
Coring pile	$f_{s,tot} = f_s^{ext} + f_s^{int} = (1 + 0.8) \cdot f_s$	$f_{s,tot} = f_s^{ext} + f_s^{int} = 2 \cdot f_s$	$SRD = 1.25 \cdot SRD_{LB}$
Plugged pile	-	-	-

6 Driveability Analysis in GRLWEAP

GRLWEAP is one of the most diffused software for driveability analysis. It is used to select and optimize pile driving equipment and it is also capable to compute the pile static capacity. The software is a powerful tool that is able to accurately simulate motions and forces in a foundation pile when driven by either an impact hammer or a vibratory hammer. In general, the software is able to generate essential information regarding the pile driveability, such as:

- the blow count of a pile under one or more assumed ultimate resistance values and other dynamic soil resistance parameters given a hammer and driving system, or from a static analysis;
- the axial stresses in a pile, both tension and compression, average over the cross section for a certain pile penetration and associated ultimate capacity values. Consideration of bending stresses is also possible;
- energy transferred by the hammer to the pile for certain pile penetration and associated capacity values;
- the pile velocity and displacements along the pile for certain pile penetration and associated capacity values;
- residual stresses remaining in the pile between hammer blows.

GRLWEAP make use of a finite difference scheme to solve the basic wave equation analysis (WEA) to calculate:

- the displacement of any point along a slender, elastic rod at any time during and after impact/dynamic loading;
- from the differences of displacements between neighbouring segments one obtains stresses and forces;
- from the differences of displacements over time one obtains velocities and accelerations.

The theory implemented to solve the WEA is the one proposed by Smith [20] and illustrated in chapter 3.1.3.

The software's driveability option allows the user to compute these above-mentioned quantities up to 100 different depths, simulating the process of pile penetration. In

order to perform such driving analysis, the user needs to input some information. As with the other options, input consists of unit shaft resistance and end bearing, usually estimated by the means of a static analysis or by using the software different tools to access soil resistance. In a general way these values are a means of calculating the final resistance value, SRD.

6.1. SRD Models

In "*GRLWEAP14 Background Report Part 2: Static Soil Resistance Models*", the software documentation ([13]) basic models to compute the static resistance are first described: in the first 6 chapters right after the introduction, methods like CPT or SPT based, or API procedures are summarised. These models are implemented in the software and can be chosen to drive the analysis.

In 2016 GRLWEAP added two new methods to take into account friction fatigue.

The first is the Alm and Hamre (AH) method, the second is the GRLWEAP Friction Fatigue (GWFF) approach. In the AH procedure, the initial and residual resistance are calculated internally from CPT data. Moreover, the method requires that the soil is classified as either clay or sand. GW14 performs the soil classification automatically, according to Robertson et al. (1986), [15].

The formulation of Alm and Hamre method in the software is analogous to the one already depicted in section 5.2. The only difference is that the software needs also as an input a setup factor. This factor is a measure of how much resistance is gained or lost after the driving and will be better described in the following sections.

A third option to simulate the degradation of friction encountered through driving, employed before the implementation of friction fatigue, is the standard set-up method, performed assuming an empirical soil setup factor for each layer. The method assumes that during driving, regardless of the number of load cycles, the soil resistance would be the long-term static resistance divided by the soil setup factor.

For example, if the soil setup factor was 2, then the resistance during driving was assumed to be 50% of the long-term resistance. The setup factor in this case is defined as the ratio of the initial to the residual resistance for each soil layer. The inverse of the highest setup factor is then, again, the shaft Gain/Loss factor.

Note, however, that Alm and Hamre does not claim that the initial resistance would be the Long-Term Static Resistance (LTSR) of the pile.

One main difference between the two methods is that AH computes all the internal parameters based only on the CPT recorded data, while GWFF method does not calculate Shape Factors or Limit Lengths internally. Selections should be made by

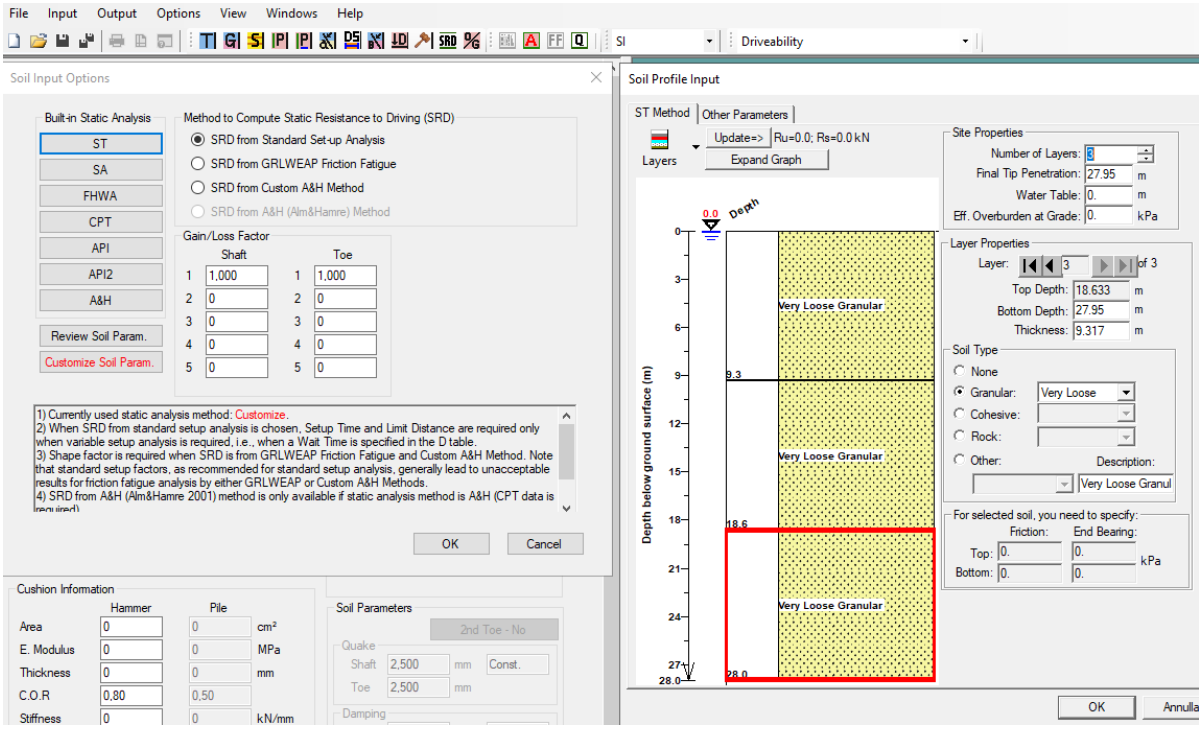

Figure 6.1 : "S window" and soil profile input parameters for static analysis.

matching existing, comparable driving records and setting them as inputs in the software.

To perform an analysis using the methods mentioned above, it is necessary to enter an input stratigraphy into the software, as illustrated in Figure 6.1, which requires a long time to set all the parameters.

Nowadays common practice in GRLWEAP to speed up the process is to use the "customized soil parameters" section, which allows the user to enter a table containing fundamental quantities obtained from the static analysis, such as shaft and base resistance. In such a manner the software skips the static analysis (which has to be performed manually) and directly proceed with the driveability analysis, using user inputs. This allows greater control over the process and the feature will be extensively used in the remainder of this work.

6.1.1. Standard Setup Approach: Calculating the SRD from LTSR

In the following the setup factor will be discussed helping the reader to have a clearer picture of how the code works.

The setup phenomenon is a process which occur when the pile installation stops: during driving process, the shear strength of the soil decreases and the pore pressure builds up. Over time, the shear strength of the soil surrounding a driven pile tends to increase as the disturbed or remoulded soil along the pile's shaft reconsolidates and excess pore water pressure dissipates, returning to equilibrium. This phenomenon, commonly referred to as "setup," is particularly significant in cohesive soils.

As the disturbed or remoulded clay consolidates and regains its strength, the bearing capacity of the pile improves. This is because the adhesion or friction strength of the clay typically recovers over time. Loading tests conducted at progressively longer intervals post-driving indicate that the ultimate adhesion strength of the clay approaches its original, undisturbed cohesion.

The magnitude of the increase in bearing capacity over time is influenced by the sensitivity of the clay and its ability to reconsolidate. In cohesive soils with higher sensitivity, the enhancement in shear strength and, consequently, bearing capacity, can be substantial.

6.1.1.1. Fixed Loss of Setup

By means of static analysis methods as the ones described in the first chapters of the documentation, the long term static resistance (LTSR) is obtained. This parameter is enough to lead bearing capacity analyses. However, in case of driveability analyses this is only the first step in calculating SRD.

In Alm and Hamre, there is no need to compute LTSR by static approaches since it is already included in the method if one considers the initial resistance as LTSR.

Moreover, differently from GRLWEAP approach, Alm and Hamre do not claim that after a period of time the SRD will return to the full initial resistance. Meanwhile, the standard setup approach assumes that the full LTSR is regained some time after pile driving (i.e. after setup time).

Two different factors are defined: the Gain/Loss factors, G/L, and the setup factors, f_{su}.

The first one control the absolute change of static soil resistance, the latter controls the relative change of soil resistance among various soil layers.

For a particular soil type:

$$LTSR = f_{su}\, SRD. \tag{6.1}$$

SRD in this case is the unit shaft resistance, f_s in Alm and Hamre, so the value of skin friction after the pile is driven at a certain depth. After some time t_s (setup time), the resistance will be gained again to LTSR.

As stated above the Gain/Loss factor controls the distribution and evolution of resistance. This factor allows the user to model total or partial loss of soil setup, relaxation effects or the long-term resistance. GRLWEAP gives the option to analyse up to five different Gain/Loss factors, thus providing up to five different capacity values at every analysed depth.

Essentially Gain/Loss factor is an analysis option for the user to simulate resistance gains or losses:

- $G/L = 1$ No change in soil strength during driving and thus no resistance gain/loss will be analysed. Meaning that the full LTSR is analysed;

- $G/L < 1$ Proportionally reduces the resistance values under consideration of their relative setup factors and thus reflects that the soil resistance is lower during driving and increases after pile installation (i.e. soil setup, pile gains strength after installation);

- $G/L > 1$ Proportionally increases the resistance values and thus reflects the soil relaxation scenario. Soil resistance is greater during driving (i.e. relaxation, pile loses strength after installation).

G/L is calculated based on the soil setup factor, f_{su}. In a normal analysis, G/L should be made equal to the inverse of the biggest soil setup value, $1/f_{su}$.

The Gain/Loss factor f_{GL} is then explained by means of an example.

Let us consider, for example, a single soil layer composed entirely by clay with a setup factor of $f_{su} = 2.5$. The reduction factor in this theoretical exercise, would therefore be $1/2.5$. If the user intends to evaluate the reduction of LTSR to SRD the G/L factor used should be 0.4. However, if needed, we could analyse the restrike situation with full setup, meaning that no reduction in friction was considered, hence a G/L factor of 1.0 would be required. There might also be a need to analyse incomplete setup, in that situation the friction reduction factor should be any value intended by the user as long it is between the minimum value of 0.4 and the maximum value of 1.0, e.g. 0.7.

However, in most cases, there are more than just one soil type. When using GRLWEAP to analyse multiple layers this might present a problem, since there would be several different setup factors and therefore multiple gain loss factors. When facing, for instance with a layer of sand, $f_{su} = 1.2$ and a clay layer, $f_{su} = 2.5$ and analysing full loss of resistance, there would be two different reduction factors of 0.8 and 0.4 for sand

and clay respectively (meaning the sand would lose 20% of the static resistance whilst the clay would lose 60%).

GRLWEAP solves this problem by considering only one G/L factor specified by the user to be consistent with the most sensitive layer, i.e. the maximum setup factor of the two layers. Therefore, if we were to analyse a gain loss factor of 0.4, 0.7 and 1.0 the sands reduction factor would not be the same as the clays. Instead GRLWEAP applies capacity multipliers for each layer.

Since considered a f_{GL} of 0.4, the sand one must be scaled according to the following formulation:

The scaled setup factor ${f_{su}}^*$ is computed as:

$$ {f_{su}}^* = \frac{\left(1 - \frac{1}{f_{su}}\right)}{\left(1 - \frac{1}{f_{sux}}\right)}, \tag{6.2} $$

where f_{sux} is the setup factor for the most sensitive layer (highest setup factor of all soil layers), in the present case the one of the clay, so 2.5.

Substituting the values for sand, one finds ${f_{su}}^*$ as 0.333. This makes sense since the gain loss factor for sand is a third of the one of the clay from the moment that sand loses 20% of the LTSR while clay 60%.

To compute the scaled reduction factor during driving, one can use the following formula:

$$ f_{RD} = (1 - {f_{su}}^* + {f_{su}}^* f_{GL}). \tag{6.3} $$

For example, if f_{GL} for clay is set to 0.7 (so when the resistance is 70% of the long term one), the sand will have $f_{RD} = (1 - 0.333 + 0.333 \cdot 0.7) = 0.9$, so 90% of its full capacity.

6.1.1.2. Variable Loss of Setup

To take into account the interruptions during driving, a variable loss of setup option is also offered. During this wait time, the shaft resistance increases logarithmically until the setup time is reached, or when it regains full LTSR. When driving resumes, the shaft resistances decrease linearly with driven distance and reaches SRD after a so-call "limit distance" (or Limit Length), L_{Li}. Note the limit distance can be different for each segment.

This approach works fairly well for short distances. But it does not work well when losses of resistances occur over a greater distance of driving. In such case L_{Li} needs to be much greater than the length of a few meters.

Figure 6.2 shows the trend of the setup: during driving the decrease in resistance is linear up to the residual value, which is reached once the pile has penetrated a distance higher than the limit length L_{Li}. When the driving stops, the gain follows the logarithmic trend until SRD reaches the LTSR again.

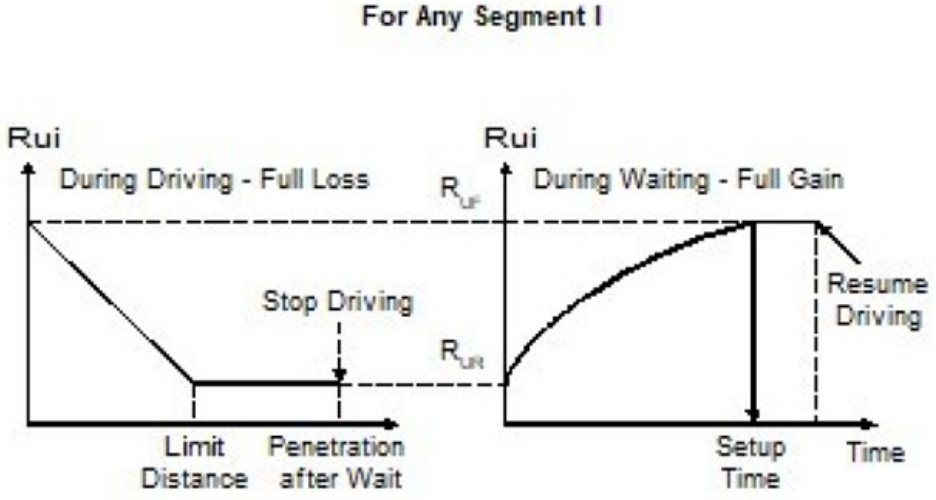

Figure 6.2: Variable setup concept.

Nevertheless, in the section of limitation and suggestions, the documentation states that the variable setup analysis cannot be performed for friction fatigue analyses. Moreover, it is said that, due to the uncertainties of limit distance, set-up time, and their variation with time, the constant loss/gain analysis is as reasonable or more reasonable than the variable analysis.

If no set-up factors are specified, GRLWEAP assumes set-up factors of 1 for all layers. Gain/loss factors then produce uniform capacity gains or losses in all soil layers along the pile.

It is also underlined that there is no point in specifying set-up time if the limit distance is unknown or vice-versa. Entering one parameter while not specifying the other leads to curious results.

6.1.2. The GRLWEAP Friction Fatigue Approach

This method aims to model that pile driving causes little loss of shaft resistance close to the pile tip but much higher loss closer to the seabed, since the pile shaft has worked

the soil more. This work leads to an exponential decrease of shaft resistance in the shallow part of the soil stratigraphy.

The GWFF Approach differs from the AH method in 2 major ways. First, the LTSR can be calculated by any static analysis method. Second, the GWFF uses the same shape factor for all layers, while in AH is computed at each depth according to the discretization and CPT values.

In addition, this method allows for a certain distance near the pile toe to have the same SRD, coinciding to the LTSR in the formulation.

The shaft resistance of a pile segment is calculated as:

$$f_s = LTSR_i \cdot f_{fi}, \tag{6.4}$$

where f_s is the shaft resistance (named SRD_i in the documentation) and f_{fi} is the friction reduction factor for layer i.

The reduction factor is computed as follows:

$$ff_i = \begin{cases} 1, & (p-d) \le f_L \cdot L_{Li} \quad (6.5) \\ \dfrac{1}{f_{sui}}, & (p-d) \ge (1+f_L) \cdot L_{Li} \quad (6.6) \\ \dfrac{1}{f_{sui}} - f_{0i} + \chi_i e^{(\alpha_i \cdot z^*)}, & f_L \cdot L_{Li} < (p-d) < (1+f_L) \cdot L_{Li} \quad (6.7) \end{cases}$$

where:

$$z^* = \big((p-d) - f_L \cdot L_{Li}\big), \tag{6.8}$$

$$\chi_i = 1 - \left[\left(\frac{1}{f_{sui}}\right) - f_{0i}\right], \tag{6.9}$$

$$\alpha_i = \frac{ln\left(\frac{f_{0i}}{\chi_i}\right)}{L_{Li}}, \tag{6.10}$$

And:

- $p - d = z$ in the original formulation, where p is the pile tip penetration and d the actual considered depth.
- $LTSR_i$ is the long term static resistance;
- f_{sui} the setup factor;
- f_L a portion of limit length of undegraded friction;
- L_{Li} the limit length for a given soil layer;

- f_{0i} the shape factor which defines the shape of the exponential function.

In case the considered depth is lower than $f_L \cdot L_{Li}$, the lateral resistance coincides with the long-term resistance, indeed the pile is not penetrated enough to reduce it. This feature is the one mentioned previously and not present in AH.

For a pile segment who penetrated more than the limit distance, L_{Li}, plus the bottom section, $f_L L_{Li}$, the reduction factor is the inverse of the setup factor in case of full loss of resistance.

In the other cases for which the selected depth is in the between of these two values, the friction reduction factor increases exponentially with increasing value of z^*(that means for depths farer from pile tip).

The limit length and setup factor can be chosen differently for the various soil layer.

The software applies the following limits:

$$f_{0i} \leq 0.9\left(\frac{1}{f_{sui}}\right), \tag{6.11}$$

$$f_{0i} \geq 0.001, \tag{6.12}$$

$$f_{sui} \geq 1, \tag{6.13}$$

6.2. Comparison with Literature Approaches

The main limitation of the software is the fact that the approach provided for the friction fatigue module has no theoretical roots, and the input parameter have to be set based on the experience of the user. While f_0 and f_L have the meaning of a shape factor and undegraded resistance and are quite easy to set, the value of L_L requires more attention since determining the penetration after which the residual value is reached and should have a physically related meaning instead of being purely an input parameter.

This procedure can lead to results with little control on it if not compared to literature benchmarks. The ideal approach would be being able to select different literature approaches such that the outcomes are based on a solid and approved by scientific community theory.

In literature few information is found related to this topic and on how to relate GRLWEAP to analytical approaches. An example is provided by Milewski and Kennedy, [11], which propose their solution for a conscious input setting.

6.2.1. Procedure by Milewski and Kennedy 2019

The authors of the paper, [11], propose an alternative method for modelling friction fatigue. The method aims to capture the shape of the side friction distribution by demonstrating how a given friction fatigue model can be adapted to align with GRLWEAP's own friction fatigue format. As an example, the Alm and Hamre (2001) model is used to illustrate this transformation, allowing for improved use of the GRLWEAP friction fatigue module and enabling consistent driveability analysis across all penetration depths. This approach is also suggested to be used and adapted for other friction fatigue models that follow similar principles.

Milewski and Kennedy suggest first to write GRLWEAP formulation in the same notation as AH: considering Alm and Hamre model and GRLWEAP variables notation one can obtain the following equivalences:

- $f_{si\ A\&H} = LTSR$
- $f_{s\ res\ A\&H} = \frac{f_{si\ A\&H}}{f_{su}}$
- $z = p - d$, where p is the pile tip penetration and d the actual considered depth.

According to this notation the AH formulation becomes:

$$f_s = \frac{LTSR}{f_{su}} + \left(LTSR - \frac{LTSR}{f_{su}}\right) e^{-kz}. \tag{6.14}$$

Equating the latter with GRLWEAP formulation, the following is found:

$$\frac{LTSR}{f_{su}} - LTSR f_0 + LTSR \chi_1 e^{\alpha_i z^*} = \frac{LTSR}{f_{su}} + \left(LTSR - \frac{LTSR}{f_{su}}\right) e^{-kz}. \tag{6.15}$$

The meaning of the terms was already explained in the previous chapters (see 6.1.2).

Among the terms in the latter equation, $LTSR$, f_{su}, k, z, are known and derived by Alm and Hamre formulation. Hence the unknown quantities are: f_0, χ_1, α_i, z^*.

Recalling the Eq. 6.8, 6.9, 6.10, the unknowns reduce to: f_L, f_0, L_{Li}, hence one single equation in 3 unknowns must be solved.

The author then considers f_L to be equal to zero since AH does not consider any undegraded part of the pile, and f_0 equal to 0.001 since, plotting different values of the shape factor, its minimum value accepted in GW formulation is the one that better fit the AH curve. In particular $f_0 = 0.001$ is smoother in approaching the residual value of side friction when the limit length is reached, as AH does.

Then the only remaining unknown is the limit length, which can be found by solving the equivalence in Eq. 6.15 for L_{Li}:

$$L_{Li} = \frac{\ln\left(\frac{0.001}{1.001 - \frac{1}{f_{su}}}\right) z}{\ln\left(\frac{\left(1 - \frac{1}{f_{su}}\right) e^{-kz} + 0.001}{\left(1.001 - \frac{1}{f_{su}}\right)}\right)}. \tag{6.16}$$

This equation depends only on known quantities provided by AH formulation f_{su}, k, and it is function of the independent variable $z = p - d$.

This dependency tells that the limit length is not constant with depth, but GRLWEAP allows the user to input only a single value of L_{Li} for each soil layer depth (d), regardless of the degree of pile penetration (p) at a given stage in the analysis.

The authors underline that a value of L_{Li} obtained at small depths provides a very good fit at all greater values of z. If the value of limit length is instead computed at larger pile penetration, the accuracy of the match decreases.

This observation is a crucial point. According to the AH formulation, both initial and residual resistance at a given depth must be continuously updated as the pile penetrates further. As a result, multiple values of limit length are computed for each depth. However, GRLWEAP allows only a single value, requiring the user to make a choice. Based on the authors' recommendations, the value computed near the pile tip when it first reaches a given depth appears to effectively reproduce the AH SRD within the GRLWEAP formulation.

7 Implementation and Validation of the Methodologies

This section aims to prove the effectiveness of the implemented analytical methods by comparing them with benchmarks found in literature.

7.1. Code Background

The code implemented to perform the computation of the SRD has been written in such a way that can be used in as many situations as possible. In order to achieve this goal, the work has been divided in three main blocks: the soil model, the pile model, and the computation of SRD.

Each section will be shortly described in the following, trying to focus on the main features that makes this code working functional and in a practical way.

7.1.1. Soil model

For a given input raw model in which at least soil layer definition is provided, the code discretises the stratigraphy according to the accuracy provided as input by the user. The refined discretization will then be used for the rest of the code and as a starting point for the analysis.

Essential soil properties per layer can also be given as input and will then be automatically discretised and, in case not constant from the top to bottom of the layer, linearised. Soil data can also be imported from external files: for example, CPT tests can be provided and will be interpolated in order to fit the refined discretisation.

If water table depth and unit weight for each layer are provided, the code computes total and effective vertical stresses at the discretised depths and then plot in order to get a clear representation of the stress state of the site. If CPT data are given, side friction and toe resistance are visualised as well.

The code also verifies the presence of essential columns and checking for inconsistencies in input data to ensure reliability. A noteworthy strength of the implementation is its comprehensive integration of tasks, from data preprocessing to visualization. By automating these steps within a single class, the code facilitates a streamlined workflow for soil analysis, reducing the potential for human error.

Furthermore, its modular design makes it extensible, allowing for future additions, such as incorporating additional data from soil testing.

7.1.2. Pile model

This block contains all the information related to the pile, including material, geometrical shape, sizes, cross section type. The essential inputs are the pile radius and, in case of open-ended pile, also the internal radius. The code then computes quantities useful for the analysis such as pile circumference and base area.

Creating a separate block for the pile allows to deal at the same time with multiple piles if different piles have to be analysed instead of having to change inputs every time.

7.1.3. SRD computation

The third block is the core of the code and contains all the analytical methodologies implemented in order to perform the computation of the static soil resistance to driving. The block allows the selection of the preferred method to calculate the SRD and offers a visualization of the results, plotting the total shaft force and base resistance during driving at any depth as well as the SRD value.

7.2. SRD Methodologies from Literature

The methods described in chapter 5 have been implemented in order to run analysis and test their performances.

7.2.1. Stevens 1982

Steven's method has been implemented according to the suggestions in section 5.1.

The code provides a total of four outcomes: lower and upper bound coring and lower and upper bound plugged. The choice of an appropriate result stands to the designer and must represent the condition of the site and project requirements.

The computation of SRD together with the other necessary quantities is straightforward: a single loop running on the discretised depths distinguishes if the considered point is either sand, clay or rock and computes unit skin friction and unit base resistance storing them in a vector at the corresponding place.

The values of base and shaft resistance are then corrected for the four cases separately according to Table 5.3 and Table 5.4.

Finally shaft resistance is computed by integrating the unit skin friction along the depths, this is easily made, assuming small discretization depths by cumulating the

product of unit skin friction and shaft area. Base resistance instead is simply the product of base area and unit end resistance.

The final value of SRD is then the summation of the two contributions.

One difference in the implementation with respect to the analytical formulation lays in the computation of the OCR. Instead of using Eq. 5.4, the following is employed:

$$s_{unc} = 0.22 \cdot \sigma'_{v0}. \tag{7.1}$$

This allows to avoid the necessity of the plasticity index as input parameter.

Moreover in Eq. 5.3 the exponent 0.85 is replaced by 0.8.

7.2.2. Alm and Hamre 2001

Alm and Hamre's formulation considers only coring piles and provides a best estimate and an upper estimate to take into account for uncertainties. The implementation requires more in-depth attention: since the method includes friction fatigue, the shaft resistance for a certain depth decrease as the pile penetrates. Hence for any pile tip penetration depth a new computation of unit skin friction (degraded shaft resistance) along the entire pile has to be done. This leads to the necessity of a nested for loop: one running along pile tip advancement (named with index ppx), one running along all the depths up to current pile penetration (name with index i).

A graphical representation is illustrated in Figure 7.1.

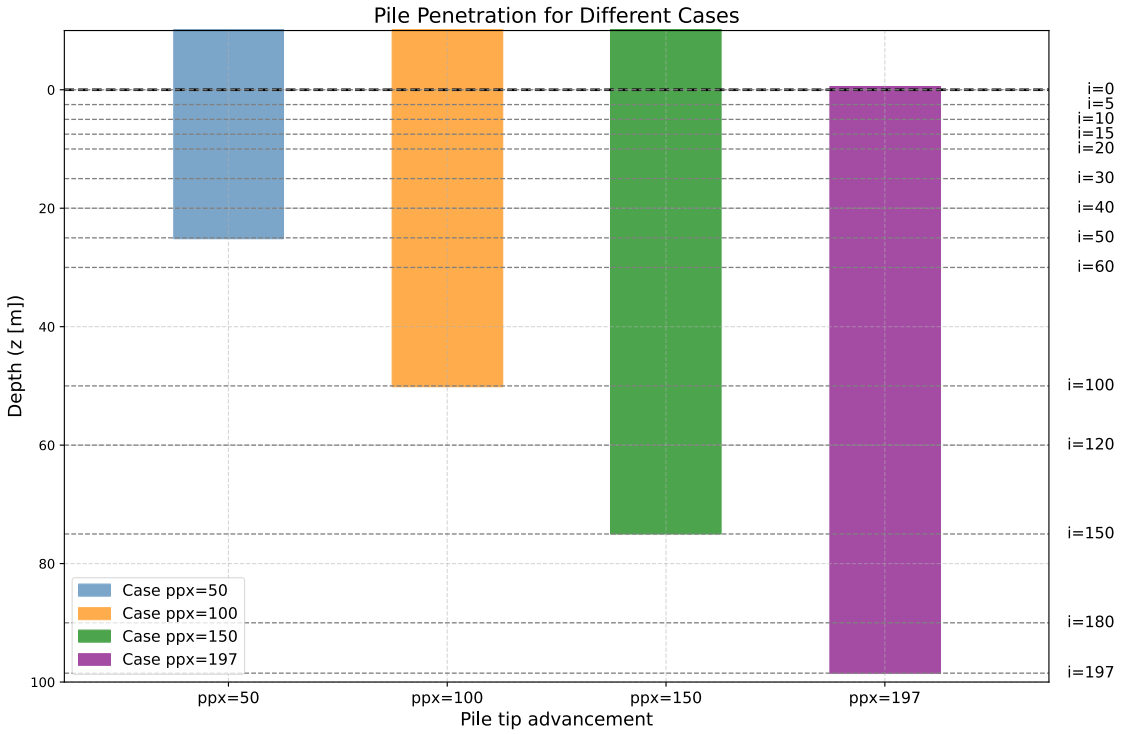

Figure 7.1: Graphical representation of the nested loop.

In Figure 7.1 four different cases of pile advancement are represented: $ppx = 50$, $ppx = 100$, $ppx = 150$, $ppx = 197$. For the first case, the index i in the nested loop can run only from zero to ppx, meaning that i runs from the first discretised depth to the 50-th discretised depth. Depending on the discretisation step (Δz or dz) the 50-th depth can be different (deeper or shallower).

In the second case, the driving process has proceeded, and the pile tip has penetrated more, up to the 100-th discretised depth. Due to cycling and friction fatigue, skin resistance will be decreased for example at the 50-th discretised depth, and this holds for any depth shallower than the current under consideration. Therefore, it is necessary to run the index i along the entire pile to compute updated shaft resistance corresponding to the 100-th discretised depth.

This procedure allows to compute shaft resistance in a correct way taking into account for friction fatigue.

A modification was introduced in the implemented formulation to ensure that the unit skin friction does not fall below the residual value (f_{res}). Specifically, when the difference between f_{si} and f_{res} becomes less than zero, indicating that the residual resistance exceeds the initial resistance, a scenario that is physically unrealistic but it might happen in the computations, the degraded skin friction is automatically set to the initial side friction value, f_{si}. This adjustment eliminates any reduction due to friction fatigue but errs on the side of safety. By assuming a higher resistance, the calculated hammer energy required for installation is increased. This approach ensures that, in cases where the actual resistance is lower, the installation will still proceed successfully. Conversely, if the actual resistance is higher and requires a more powerful hammer, this conservative assumption prevents installation failure due to insufficient hammer capacity.

7.2.3. Jones 2020

Jones's method implementation is based on the same scheme of Alm and Hamre since the main difference between the methods lays in the computation of the initial and residual skin friction, with the formula for calculating degraded skin resistance remaining unchanged. Hence, also in this case the nested for loop is employed (maintaining the same index notation).

Modification from the original formulation is the same applied for Alm and Hamre, that is the adoption of the initial shaft resistance, f_{si}, for the degraded resistance in case the residual is higher than the initial one. This is employed also in the effective stress approach comparing the initial effective resistance, which includes parameter as the sensitivity, with the residual.

For the three methods presented, the input parameter δ is always considered being 5 degrees less than the friction angle.

7.3. SRD Implementation according to GRLWEAP documentation

According to the suggestion in section 6.1.2, the software way of computing SRD has been hand-implemented to test, understand and predict its behaviour. The model requires as input, for any depth, the following quantities:

- The discretised depths;
- The long term static resistance $LTSR$;
- The tip resistance;
- The setup factor f_{su};
- The limit length L_L;
- Undegraded resistance factor f_L;
- Shape factor f_0.

The code works in a similar way compared to the method described in the previous sections, making use of the nested for loop.

The software basically computes shaft component of the SRD for a certain depth by integrating along the pile embedded length the unit shaft resistance, which is computed as the product of the $LTSR$ and a degradation factor, f_f. So, the model assumes that at any depth the value of shaft resistance is a portion of the undegraded one, depending on the distance from the pile tip.

The implementation has no option in considering whether the pile behaves as cored or plugged. The only option to obtain one of the two behaviour is to set an adequate value of $LTSR$ in a similar way to what is done in Stevens. For example, if the user knows that the analysis is to be conducted for a large diameter pile, it can increase the $LTSR$ by multiplying it for a certain factor (usually 2 or 0.8 is assumed).

7.4. Implementation of Milewski & Kennedy Procedure

Milewski and Kennedy procedure provides a way to compute the limit length L_L enabling the replication of Alm and Hamre's analytical results using the GRLWEAP approach.

This is achieved by utilizing the offshore driveability settings and GW friction fatigue command in the "S window" of the software, as illustrated in Figure 7.2.

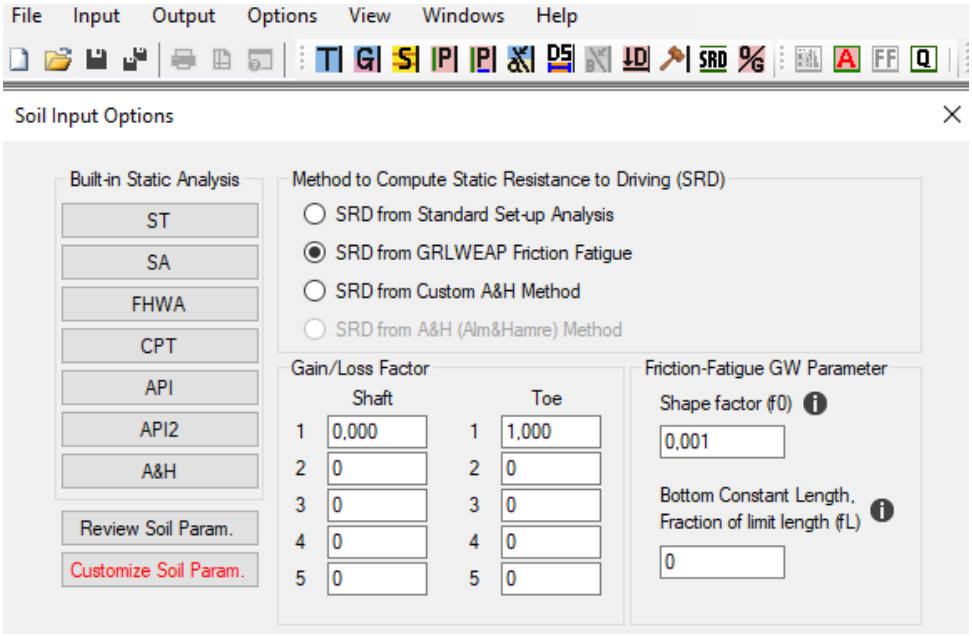

Figure 7.2 : "S window" in which customized soil parameters can be set.

By setting the customised soil parameters, users' input such as shaft and base resistance, quake and damping values and tip area can be set for every depth. Among these parameters the user can set also all the parameter related to the GWFF method, meaning L_L, f_0, f_{su}. These parameters determinates the shape and degradation rate of the shaft resistance modelled by the software. It is then crucial to provide an accurate input in order to obtain the expected values computed by the software. To achieve this, recalling that the authors suggest a constant f_0 value set to 0.001, the remaining parameters to be calculated are the limit lengths and the setup factors.

To reflect Alm and Hamre results, the computation of these parameters has decided to be included in the Alm and Hamre implementation itself.

For every calculation step of degraded shaft resistance, a value of initial and residual is computed according to the analytical method, and the ratio of the two is defined as the setup factor. These values are then stored in order to be used as input data for the software.

As discussed in section 7.2.2 and 7.2.3, if the residual resistance is found to be greater than the initial resistance, the degraded resistance is set to the initial shaft friction. This adjustment must also be reflected in the software input. Indeed, to reproduce a degraded shaft resistance equal to the initial one, the value of $f_{su} = \frac{f_{si}}{f_{res}}$ must be 1, hence also the residual value must be set to the initial resistance.

It is important to emphasize that these quantities are independent of the pile penetration and depend solely on the considered depth, as they are calculated based on effective stress and CPT properties. In other words, for two successive penetration

depths (e.g., $ppx = 50$ and $ppx = 51$), the value of f_{su} at a specific depth remains unchanged for both penetration levels ($f_{su}[ppx = 50, i = 5] = f_{su}[ppx = 51, i = 5]$).

This unfortunately is not true for the limit length, which depends on the exponential decay (e^{-kz}, referring to notation in section 6.2.1), whose value changes at every penetration advancement. Evidence is provided in Figure 7.3, which shows the dependency of the limit length with tip advancement for different AH shape factors.

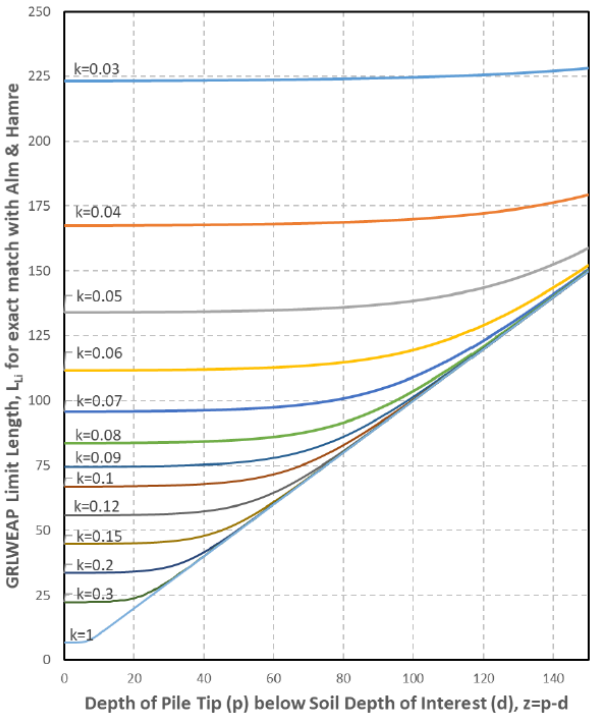

Figure 7.3 :Variation of GRLWEAP limit length with z and AH shape factor k.

For that reason, a different value of L_L is computed at every depth for every iteration, leading to many values of limit length for the same depth as much as the number of discretised depths below this point. For example, if one discretises the pile in $ppx = 50$ depths, for horizontal corresponding to the 5th depth from seabed, at the end of the analysis the user will obtain $50 - 5 = 45$ different values of limit length.

This is a great limitation since the software allows to enter only one single value for each discretised depth, but its value must be valid for the entire analysis. To address this inconsistency, the authors observed that selecting the L_L value calculated for small z (e.g., when the pile tip is just below the depth of interest, such as $z = 0.5\ m$) , not only provides an exact match for that specific z value but also delivers a very close approximation for all greater values of z. Conversely, using an L_L value derived from larger pile penetrations does not yield a good approximation for smaller z values.

Therefore, it has been decided to follow the authors' suggestion and consider the limit length corresponding to the one first computed at the pile tip, hence by storing the

limit length computed at the tip for every penetration advancement in the refined model, a data frame which contains all the relevant quantities for the analysis.

7.5. Validation of GWFF implementation

In order to validate the implementation of GRLWEAP FF module, it was chosen to replicate the examples provided in the software's documentation (appendix D.1 of the manual).

7.5.1. Example 1

The first example considers a single uniform 100 metres thick soil layer where $LTSR$ of each segment ($\Delta z = 1\,m$) is $500\,kN$ with a 10 metres circumference and $50\,kPa$ unit shaft resistance. The shape factor f_0 is set to 0.01 and the bottom section factor f_L to 0.

Limit length L_L was set to 50 metres for all depths and the setup factor f_{su} to 5, leading to a residual shaft resistance of $100\,kN$. The unit shaft resistance distribution has been calculated for pile toe depths of 25, 50, and 75 metres, which is equivalent to 0.5 L_L, L_L, and 1.5 L_L.

As it can be seen in Figure 7.4, the implementation (a) replicates in a very good way the example (b) provided by the documentation. The three curves represent the degraded resistance for different depths computed according to the formulation provided in the software's documentation. It can be noted that for the case of 25 metres depth, at the seabed the resistance is higher compared to the other two cases. This is because the limit length was set to 50 metres, meaning that, at 25 metres of penetration, the top part of the stratigraphy has not reached the residual values yet.

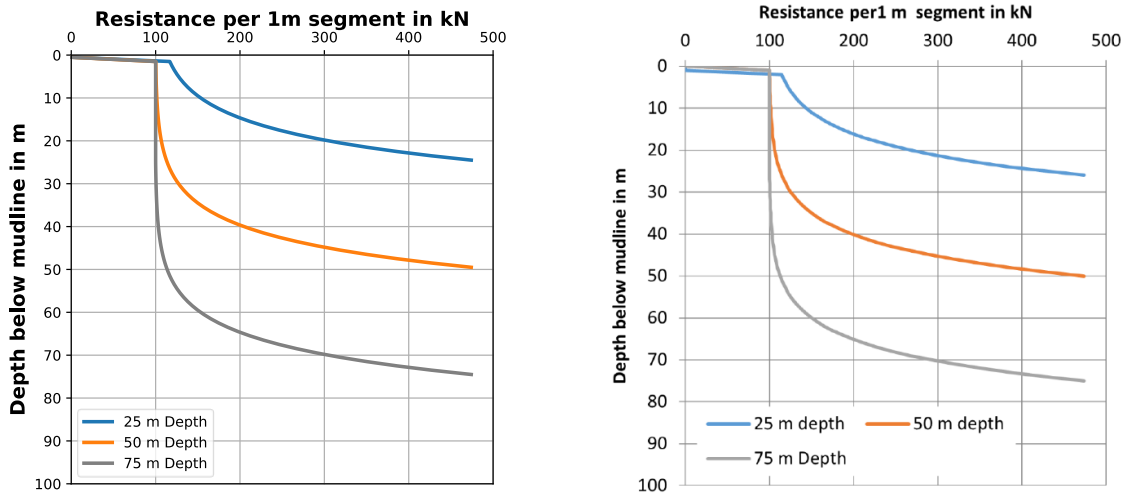

(a) (b)

Figure 7.4: Implementation of example 1 (a) and documentation results (b).

7.5.2. Example 2

The second example considers a double layer stratigraphy. The first 50 metres are a sand layer with a setup factor of $f_{su} = 1.25$ and shaft resistance ($LTSR$) of 250 kN, while the 50 metres below are a clay layer with $f_{su} = 5$ and $LTSR$ of 500 kN. In both cases the limit length, L_L, was set to 50 metres for all depths. In this example the bottom section factor f_L is set to 0.05.

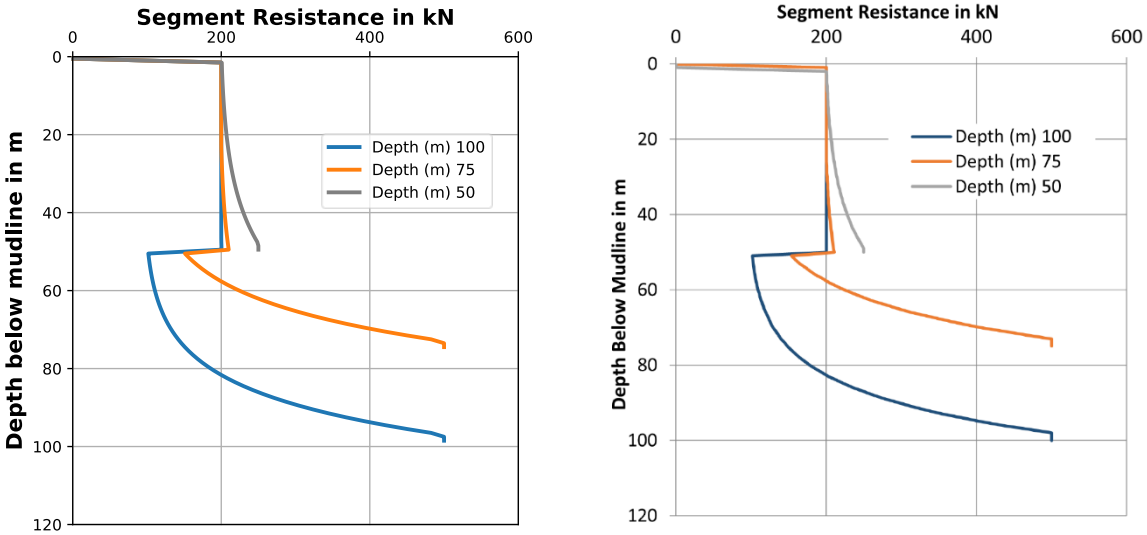

Figure 7.5: Implementation of example 2 (a) and documentation results (b).

Again, a perfect agreement is obtained between the implementation and the documentation, hence the implementation can be considered validated.

7.6. Validation of literature methods

To validate the analytical models, a case study from the literature published in 2016 was selected as a benchmark. This case study is detailed in the paper by Anusic, Eiksund, and Liingaard, [3], and aims to investigates the performance of various literature methods for computing the SRD in chalky soils. Among these methods are there is the one proposed by and Alm and Hamre. The researchers conducted a back-analysis to compare these models' predictions.

The analysis was lead in The Westermost Rough offshore wind farm, located in the North Sea, around 8 km off the Yorkshire Coast north of Hull.

The general ground conditions at the analysed sites comprise 10 to 50 meters of overconsolidated clays combined with sand layers, overlaying chalk bedrock. Results from the paper were sampled in order to be used as a comparison and validation of the methods implemented and described in the previous sections.

Soil characterization for the study was conducted using a combination of geological and geophysical surveys, as well as CPT testing, ensuring precise delineation of soil stratigraphy and accurate identification of design soil properties.

The geological setting of the site reveals quaternary soils overlying a chalk bedrock. The uppermost layer comprises Holocene Deposits (HLCN), which include sand, sandy gravels, and low to high-strength clays with thicknesses ranging from 0.2 to 3.7 meters. Below this are Channel Infill Deposits (CHF), consisting of very low to low-strength silty clays and silty sands, varying from 3 to 8 meters thick, with localized increases to 16–22 meters in the northern part of the site.

Underlying these are the Bolders Bank Formation layers. The upper layer (BSBK_U) consists of very stiff, high to extremely high-strength gravelly clay. The middle layer (BSBK_M), 1 to 10 meters thick, includes gravelly sands with occasional sandy gravel or cohesive soils. The lower layer (BSBK_L), 1 to 12 meters thick, comprises very stiff to extremely high-strength slightly sandy and slightly gravelly clay.

In local channels, Rough Formation (ROUGH) deposits occur, comprising low-plasticity, high to extremely high-strength sandy gravelly clays, with thicknesses between 1.3 and 13 meters. These may be underlain by the Swarte Bank Formation (SWBK), ranging from 1.5 to 13 meters in thickness.

The chalk bedrock, referred to as the Westermost Rough Chalk Formation (WMR), has a variable top surface depth, ranging from 28 to 40 meters below the seabed in the central and southwestern areas and 10 to 19 meters in other regions. This chalk is generally extremely weak to very weak, low-density. Key geotechnical characteristics of this chalk include its intact strength, related to porosity and density, and its fracture condition as defined by CIRIA grades. The chalk comprises three units: structureless chalk (Grade D), structured fractured chalk (Grades B and C), and structured assumed intact chalk (Grade A).

In the paper the soil properties are summarised as in Table 7.1:

Table 7.1: Soil properties at six positions, index a-f corresponds to positions P01-P06, respectively

	$\gamma' \left[\frac{kN}{m^3}\right]$	D_r [%]	s_u [kPa]	$\varphi'[deg]$
HLCN	7	15[aef], 27[c], 36[b], 46[ad]	-	35
CHF_C	11	-	(140-280)[f]	-
CHF_S	7	(27-47)[f]	-	(31-33)[f]
BSBK_U	11	-	(130-280)[a], (120-330)[b], (130-230)[c], (130-530)[e]	-
BSBK_L	11	-	(470-1500)[a], 350[e]	-
BSBK_MC	11	-	(160-240)[b], (240-390)[d]	-
BSBK_MS	10	15[c], (65-80)[de], (80-100)[de]	-	28[c], (34-40)[ade]
ROUGH	11	-	615[a]	-
SWBK	10	-	(750-930)[a]	-
WMR_D	9.3	-	125	-
WMR_B/C	9.3	-	-	-
WMR_A	9.3	-	-	-

The provided CPT tests are illustrated in Figure 7.6:

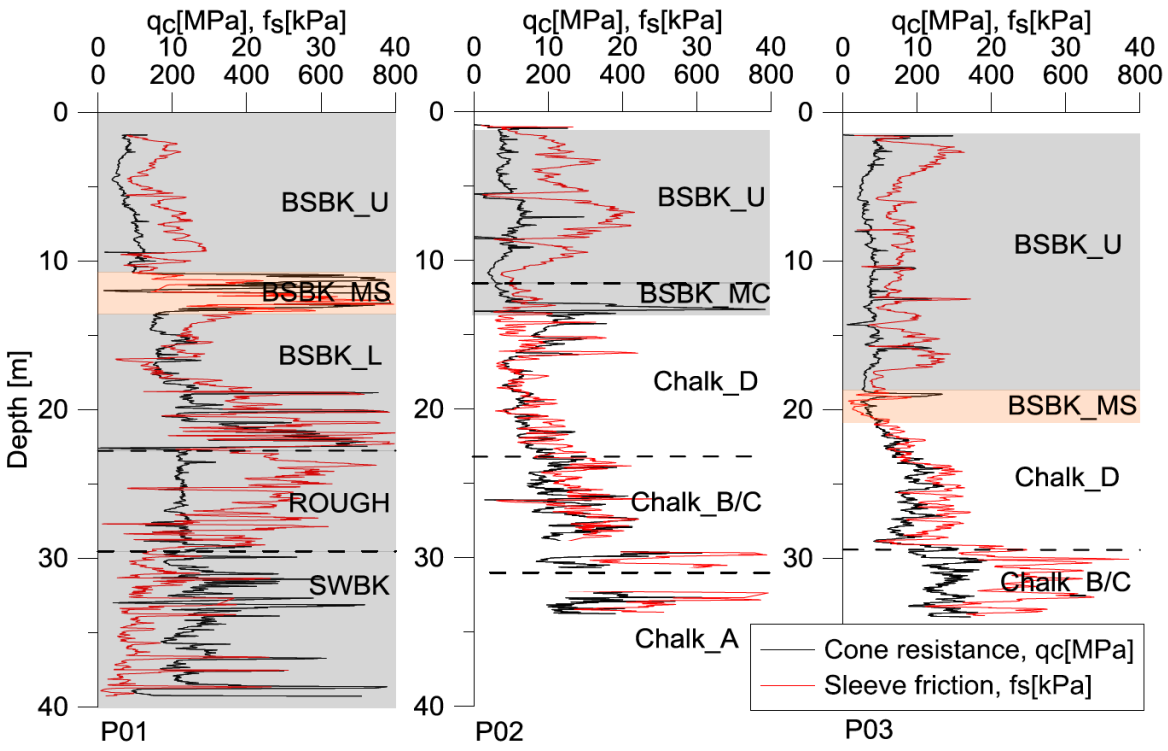

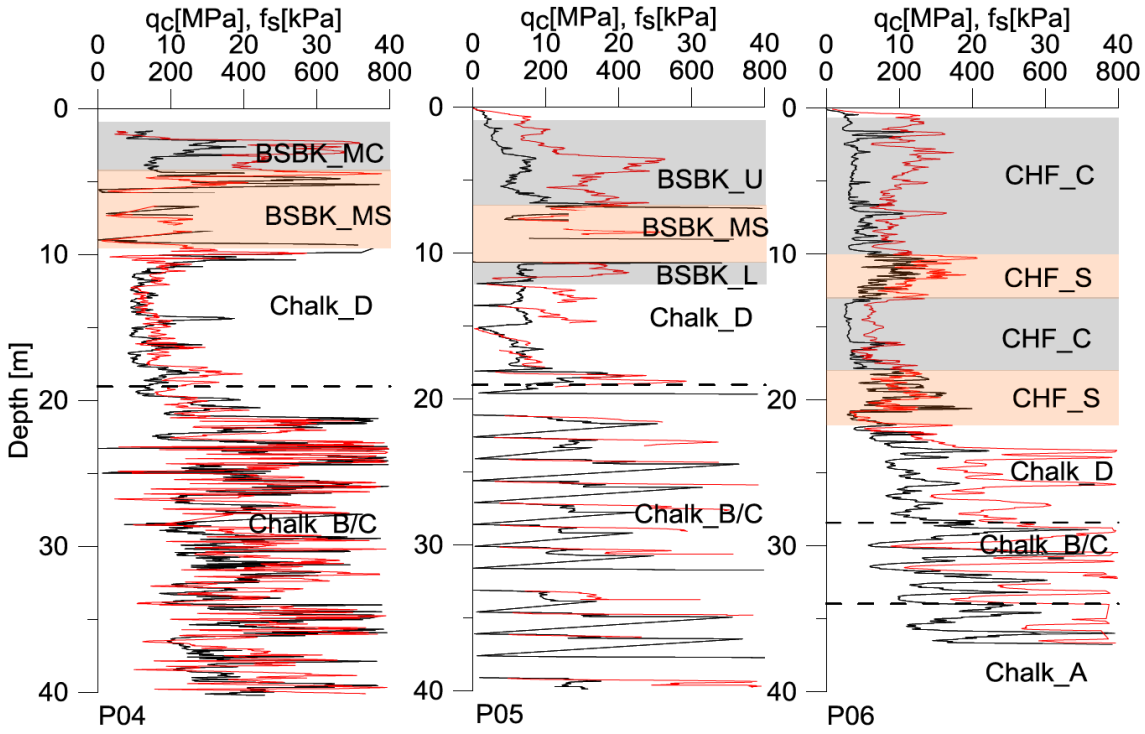

Figure 7.6: CPT profiles for location P01-P06.

For the validation it has been decided to compare the results with the two locations that better represented the behaviour of the back analysis: P03, P06.

Table 7.2, Table 7.3 summarise the choices for the inputs data according to the ones suggested in the paper for the three selected location.

Table 7.2: Input raw model for location P03.

P03	$\gamma' \left[\frac{kN}{m^3}\right]$	$z\ start\ [m]$	z end [m]	$s_u\ start\ [kPa]$	$s_u\ end\ [kPa]$	$\varphi'[deg]$
BSBK_U	11	0	19	180	180	0
BSBK_MS	10	19	21	0	0	28
WMR_D	9.3	21	29.5	125	125	0
WMR_B/C	9.3	29.5	34	0	0	0

Table 7.3: Input raw model for location P06.

P06	$\gamma' \left[\frac{kN}{m^3}\right]$	$z\ start\ [m]$	z end [m]	$s_u\ start\ [kPa]$	$s_u\ end\ [kPa]$	$\varphi'[deg]$
CHF_C	11	0	10	210	210	0
CHF_S	7	10	13	0	0	31
CHF_C	11	13	18	210	210	0
CHF_S	7	18	22	0	0	31
WMR_D	9.3	22	28	125	125	0
WMR_B/C	9.3	28	34	0	0	0
WMR_A	9.3	34	37	0	0	0

These inputs are enough for the computation of the SRD but not sufficient for a wave analysis. Indeed, during the installation of the piles, hammer energy and blow counts are logged. These data are fundamental for back analyses, which allows to compare installation results with the design prediction to check the accuracy of the methods.

The hammer blow counts record for the selected sites P03, P06, are illustrated in Figure 7.7 (a) and (b) respectively (black curve), as well as the results of the authors' back analysis using Alm and Hamre model (green curve).

The methods implemented are able to compute the SRD only, not to perform the full driveability analysis. To validate and compare results it is then necessary to run the driveability analysis in GRLWEAP by giving as input the SRD computed separately. In such a way, it is possible to compare software's results with the outcomes provided in the paper.

To simulate the actual driving conditions, the hammer stroke is adjusted according to the driving energy used during installation. Normally a driveability analysis is performed using the full hammer stroke to evaluate if the selected hammer is able to drive the pile to target depth and to evaluate the maximum stresses on piles. By adjusting the hammer stroke, the actual hammer energy recorded in the driving log at the time of installation is used to demonstrate how the predicted SRD suits soil conditions.

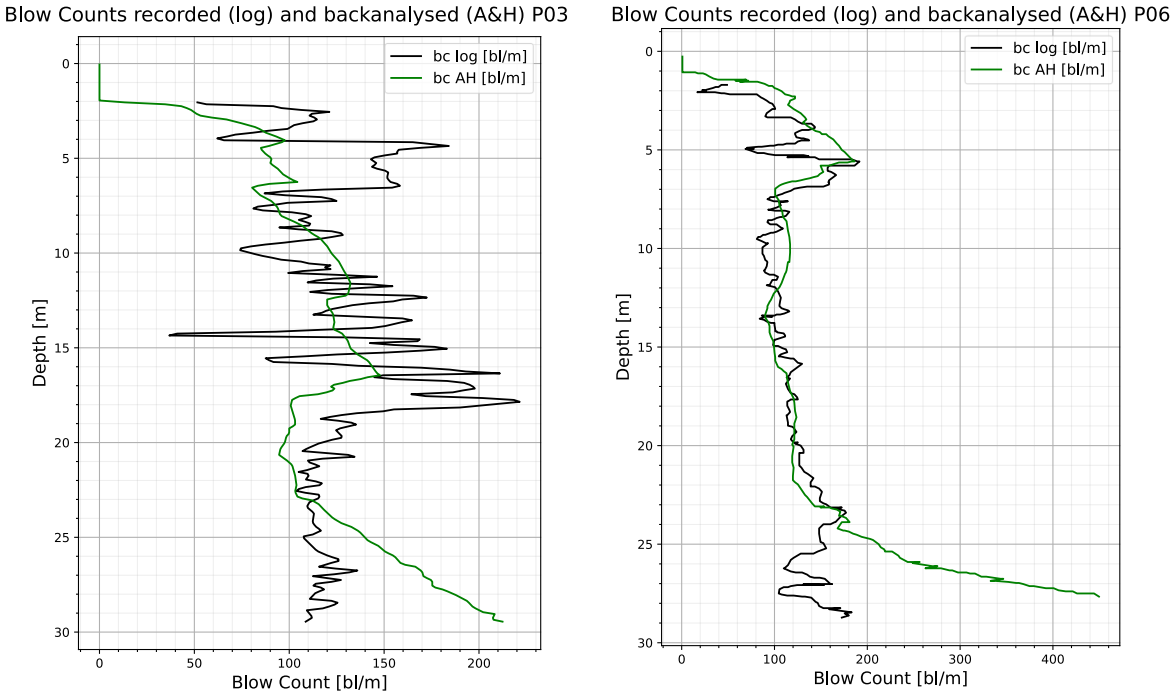

(a) (b)

Figure 7.7: Driveability prediction P03 (a), P06 (b).

For that reason, to simulate the actual driving conditions, selecting the same hammer used in field (IHC-S2000) to perform the analysis is GRLWEAP is not sufficient. The energy of the hammer must be set accordingly to the one effectively used and provided in Figure 7.9 (a).

GRLWEAP allows the user to set the hammer stroke for any analysed depth in the hammer settings ("D window", hammer information, as shown in Figure 7.8).

Given that hammer energy, according to Smith's theory, is computed as:

$$E_{tot} = W_R \cdot h, \tag{7.2}$$

where W_R is the ram weight and h the observed or actual ram stroke; the stroke can be easily obtained by dividing the energy of the hammer by its ram weight (990 kN for the IHC-S2000). The hammer energy and stroke profile for the different locations is illustrated in Figure 7.9 (a) and Figure 7.9 (b) respectively.

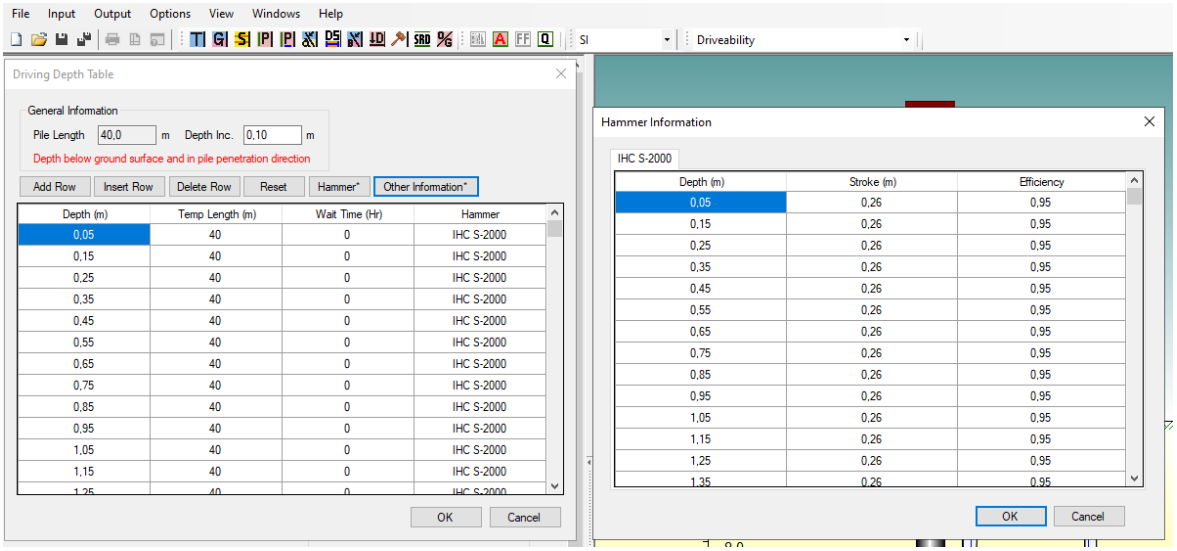

Figure 7.8 : "D window" and hammer's stroke settings.

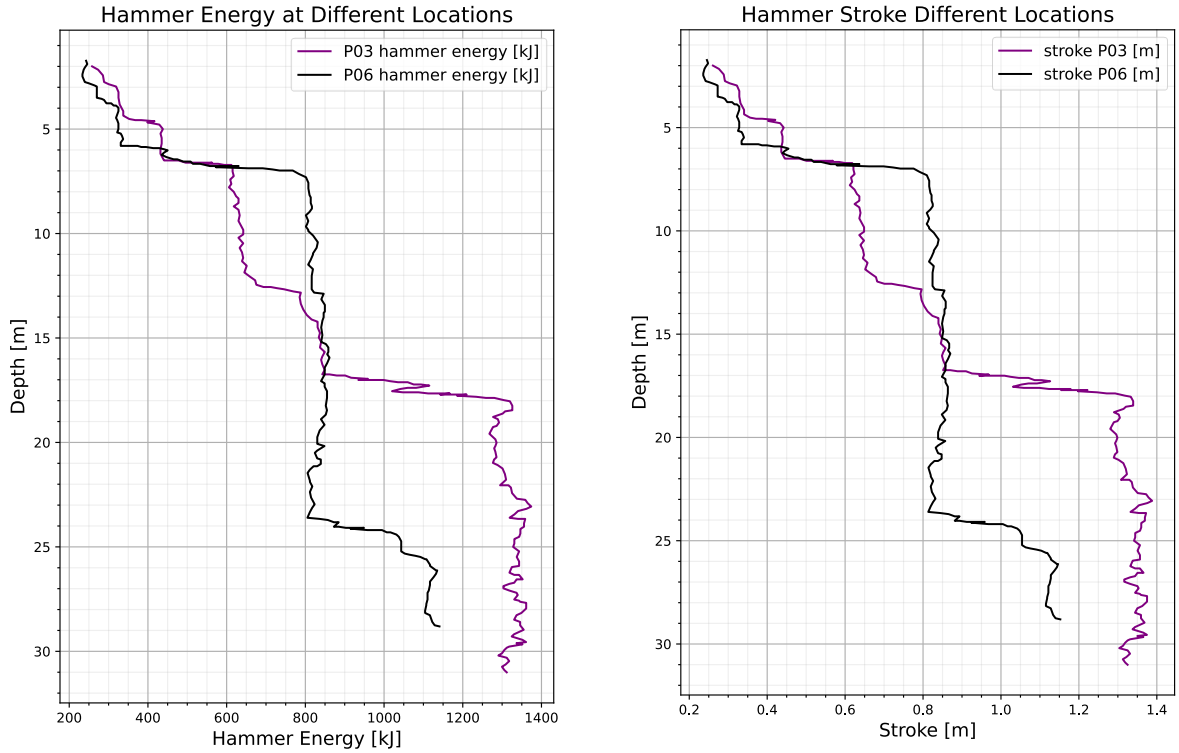

(a) (b)

Figure 7.9: Hammer energy profile (a) and hammer stroke profile (b).

The most crucial part of the analysis is the selection of input data for the "S window" in the software's inputs. In case of Alm and Hamre analysis, the built-in friction fatigue module is used. As explained in detail in section 7.4, Alm and Hamre soil inputs, include degraded shaft friction and limit lengths, and have to be attached in the section "customize soil parameters".

Concerning pile inputs, the geometry for the different locations is summarised in Table 7.4. Total pile length was not specified and for the analysis in GRLWEAP it has been assumed a value of 60 metres.

Once soil and pile inputs, hammer settings and analysed depths are set, the analysis is ready to run, and the software provides the results based on the inputs SRD. The outcomes from GRLWEAP are then compared to the data available: SRD profile with the one computed by the hand-implementation, and blow counts profile with those in Figure 7.7 (a), (b).

Table 7.4: Pile geometry for different locations.

	Pile length [m]	Penetration depth [m]	Penetration in chalk [m]	Pile diameter [m]	Wall thickness at tip [mm]
P03	60	31.06	10.26	6.5	72
P06	60	28.46	6.67	6.5	72

The first validation check was performed for location P06 in order to test the accuracy of Alm and Hamre implementation.

The results of the GRLWEAP driveability analysis provide as outcomes both SRD and blow counts profiles. If the first is in a good agreement with the one computed in the hand-implementation (already validated in section 7.5), then Milewski method is proven to work, since the limit lengths inputted were computed according to Eq. 6.16.

If the blow counts profile is comparable with the one provided in the paper, then this means that the Alm and Hamre implementation is validated, since the software uses the same SRD (being Milewski's method validated) and produce the expected blow counts.

The results are illustrated in Figure 7.10, and show a good agreement, especially in the computation of SRD, Figure 7.10 (a), meaning that Milewski's method is very accurate in predicting Alm and Hamre behaviour using GRLWEAP numerical formulation.

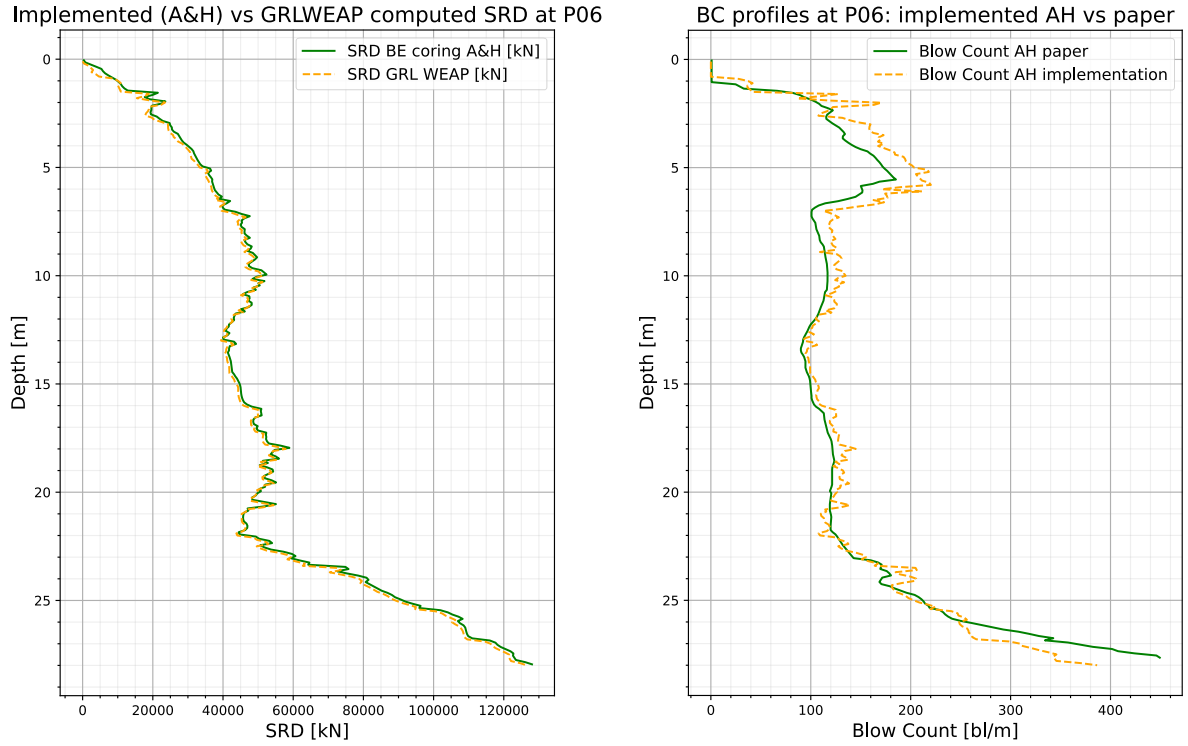

(a) (b)

Figure 7.10: SRD profile comparison (a) and blow counts profile comparison (b) at location P06, Alm and Hamre's method.

Regarding the comparison between the computed blow counts and paper's one, Figure 7.10 (b), some small discrepancies in the top and bottom part of the curve are present. This is addressed to the input data provided to the software. It might be due to the SRD or to the dynamic part of the soil resistance. Another source of uncertainty is the

length of the pile, that was assumed to be 60 metres. Concerning SRD uncertainties they might be correlated to the CPT input data, indeed the CPT provided in Figure 7.6 had to be sampled by hand in order to be given as input for Alm and Hamre implementation. The sampling comparison with the original one showed good agreement but, as the computation of SRD implies many computations, it might be that small errors led to an SRD slightly different from the one obtained by the researchers. Besides that, the biggest uncertainty is considered to be the hammer stroke that had to be first sampled, then computed and given as input manually.

The second site considered is P03, the same procedure has been applied leading to similar results and considerations. Results are shown in in Figure 7.11.

Again, a good agreement in the SRD is found, confirming Milewski's approach works properly. Concerning the blow counts the 2 curves show a slightly different behaviour in the middle part. The reasons of the discrepancy are probably the same of the one introduced for the previous location, P06. Nevertheless, considering this work is trying to reproduce a paper without having the original data, the results can be considered as sufficiently accurate for the aim of the validation of the implementation.

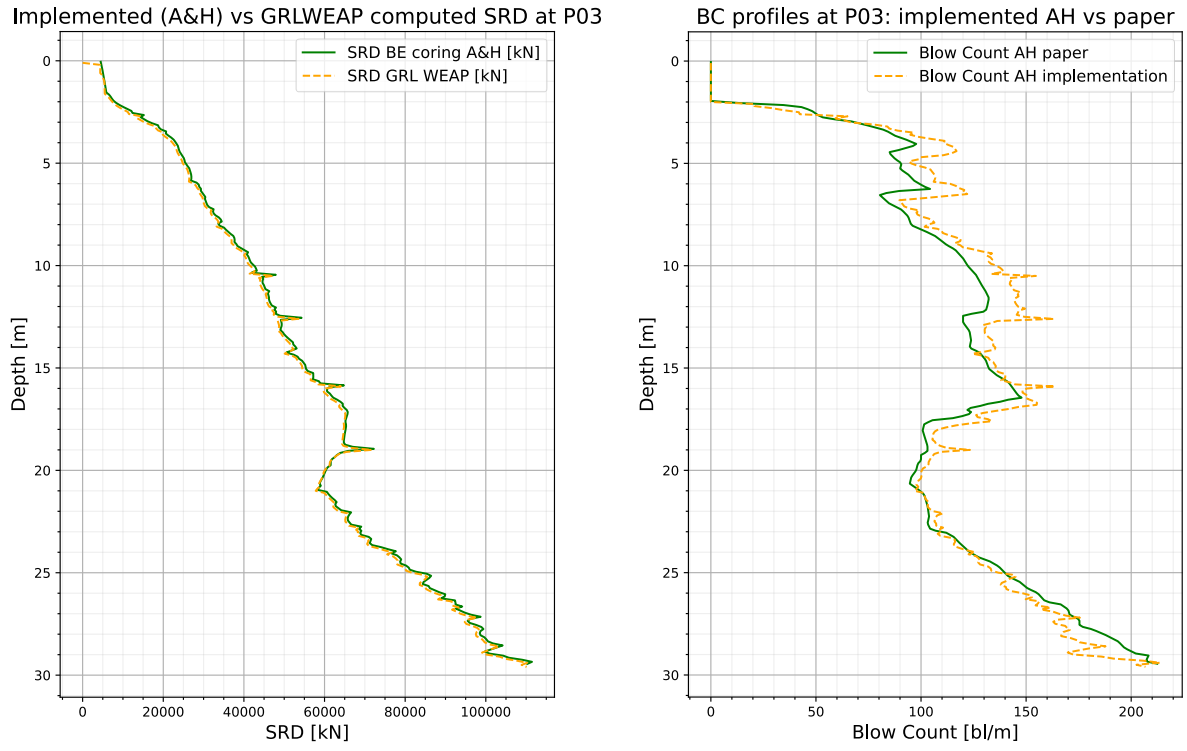

(a) (b)

Figure 7.11: SRD profile comparison (a) and blow counts profile comparison (b) at location P03, Alm and Hamre's method.

8 Proposed Approach for a General Implementation of SRD Methodologies in GRLWEAP

The approach proposed by Milewski and Kennedy had proven to work in an accurate way: the validation illustrated in the previous chapter showed a good agreement between the Alm and Hamre method modelled in GRLWEAP by user inputs (meaning that limit lengths were calculated by Milewski's approach) and the results obtained by Anusic et al.

Further aim of this research is to extend this methodology to other methods for the computation of the SRD. In particular, it was chosen to prove it on the Jones et al. approach, which is a recent method not implemented in GRLWEAP yet.

8.1. Extension of Milewski's Method for other Analytical Approaches

A considerable effort was made to try to extend the Milewski approach to Jones' method as well. The main difference between Jones's and Alm and Hamre's method is in the computation of the decay shape factor, k, and the initial and residual shaft resistance, f_{si} and f_{res}, of cohesive soils.

In fact, Jones suggests calculating these values differently, following an effective stress approach and a total stress one. Once the quantities have been calculated, using the same formula provided by Alm and Hamre for calculating the degraded lateral resistance, Eq. 5.11, two different values are obtained. The minimum of the two is assumed to be the resistance representative of the soil behaviour at a specific depth, for a specific penetration advancement.

8.1.1. Parametric Study of Jones's Method

To fully understand the behaviour of the method, a parametric study has been conducted. The idea was to start from the simplest case: the shape factor k, that in Jones depends on the interface friction angle, was set to the one Alm and Hamre suggested, and the code had been modified in order to choose the Total Stress

approach (TS) every time a clay layer is found. In this way the implementation actually coincides with the Alm and Hamre formulation.

To perform the parametric study, the input stratigraphy summarised in Table 8.1 has been used. The pile length was set to 99 metres, the inner and outer radius 1.232 m and 1.295 m respectively.

Given the input data in Table 8.1, if an analysis using AH or Jones's method is conducted, the same results are obtained, as shown in Figure 8.1.

The only differences between Jones and AH SRD profile, Figure 8.1 (b), lie in the fact that the two methods assume different base resistance contributions for sands. This proof that the implementation of Jones total stress approach is correct. Moreover the "$Fs\ GW\ documentation\ [kN]$" curve, which is the hand-implemented software formulation, also fit Jones profile, meaning that Milewski's approach is able to find representative limit lengths that can reproduce Jones' TS behaviour in the software.

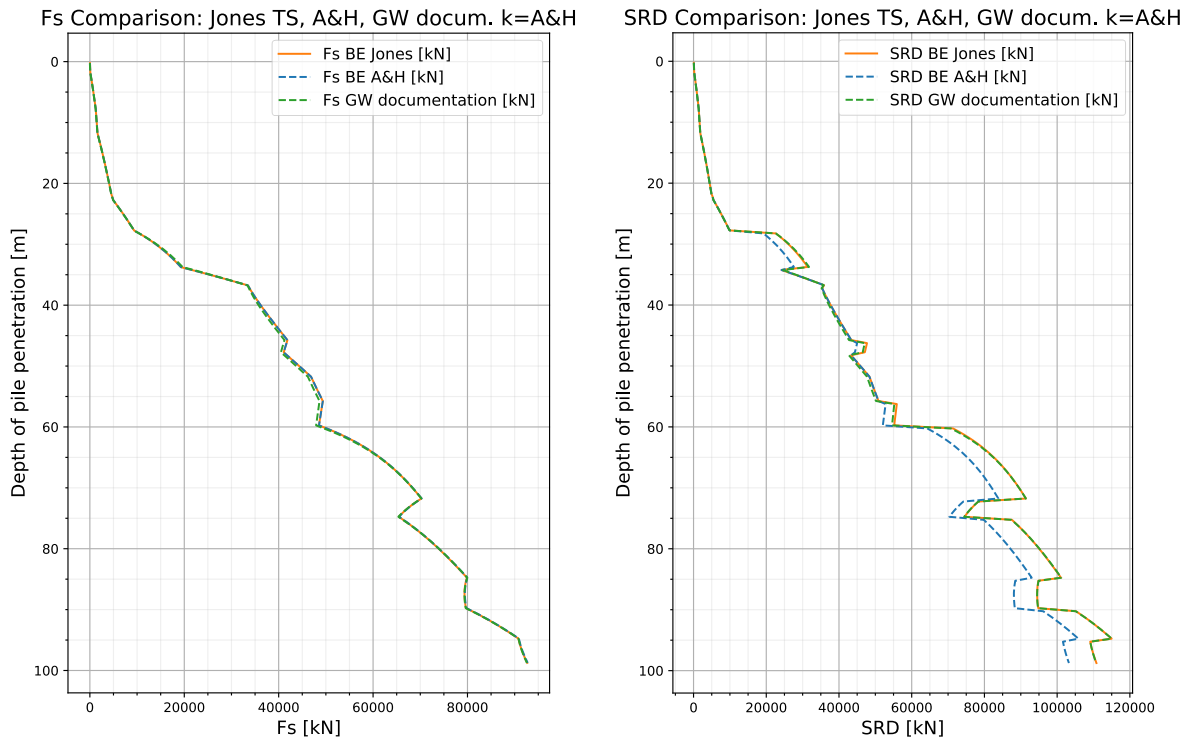

(a) (b)

Figure 8.1: Fs profile (a) and SRD profile (b) comparison of Alm and Hamre (A&H), Jones and GRLWEAP implementation, A&H shape factor, TS approach.

Table 8.1: Soil stratigraphy input data.

Behaviour Type	U. Weight $\left[\frac{kN}{m^3}\right]$	z start $[m]$	z end $[m]$	s_u start $[kPa]$	s_u end $[kPa]$	φ' $[deg]$	δ $[deg]$	f_s $[kPa]$	q_t start $[kPa]$	q_t end $[kPa]$
cohesive	16.61	0	2	13.3	17.8	0	0	3	200	300
cohesive	16.61	2	8	17.8	31.0	0	0	13.5	300	600
cohesive	16.61	8	12	31.0	39.9	0	0	9	600	800
cohesive	16.61	12	22	39.9	62.0	0	0	24	800	1300
cohesive	17.81	22	23	88.7	87.5	0	0	34	1700	1700
cohesive	18.82	23	28	87.5	81.2	0	0	68	1700	1700
granular	19.31	28	34	0.0	0.0	33.8	28.8	200	40000	40000
cohesive	20.01	34	37	489.3	489.3	0	0	400	8000	8000
cohesive	20.01	37	46	289.3	277.2	0	0	175	5000	5000
granular	20.01	46	48	0.0	0.0	33.8	28.8	160	20000	20000
cohesive	20.01	48	52	274.5	269.1	0	0	200	5000	5000
cohesive	20.01	52	56	269.1	263.7	0	0	150	5000	5000
granular	20.01	56	60	0.0	0.0	33.8	28.8	880	22000	22000
granular	19.81	60	72	0.0	0.0	33.8	28.8	1050	70000	70000
granular	19.81	72	75	0.0	0.0	33.8	28.8	450	30000	30000
granular	19.81	75	85	0.0	0.0	33.8	28.8	1050	70000	70000
granular	19.81	85	90	0.0	0.0	33.8	28.8	750	50000	50000
granular	19.81	90	95	0.0	0.0	33.8	28.8	1200	80000	80000
granular	19.81	95	99	0.0	0.0	33.8	28.8	900	60000	60000

A second step was to test the effective stress approach. Maintaining the shape factor unchanged, the implementation of Jones method was modified in order to model soil behaviour with an Effective Stress (ES) approach every time a cohesive soil is found.

Obviously, as it clear from Figure 8.2, the results of Jones implementation in this case differs from the one produced by Alm and Hamre, but still the Milewski's method is able to reproduce Jones behaviour as in the TS approach.

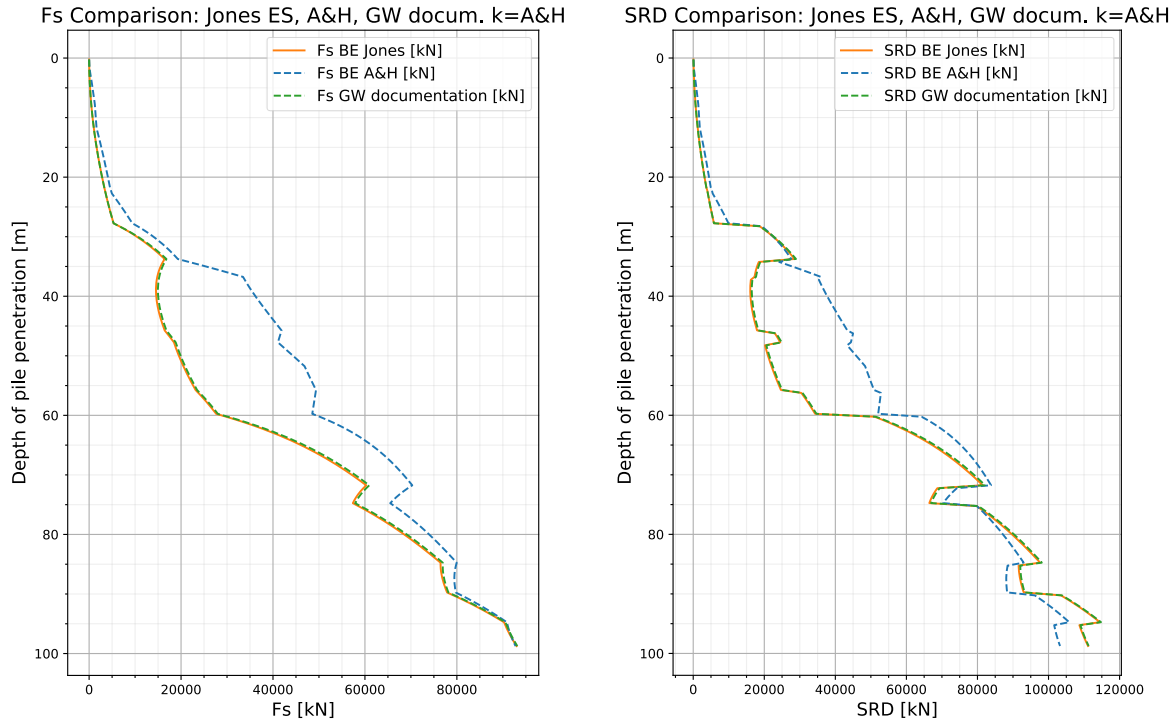

(a) (b)

Figure 8.2: Fs profile (a) and SRD profile (b) comparison of Alm and Hamre (A&H), Jones and GRLWEAP implementation, A&H shape factor, ES approach.

The outcomes in Figure 8.2 are a particular case, since, in order to reduce the number of parameters influencing the analysis, it was decided to set the remoulded shear strength equal to 1/20 the undrained shear strength. Recalling Eq. 5.29, YSR set to a constant value of 2 and δ to a value of 10 degrees, the computation of the initial shaft resistance is then reduced to:

$$f_{si} = 0.00844 \cdot 2^{0.42} \cdot (137.5 + 2 - 54.375 \cdot \log_{10} 20) \cdot \sigma'_{v0} \cdot \tan\delta$$
$$f_{si} = 1.185 \cdot \sigma'_{v0} \cdot 0.176 = 0.209 \cdot \sigma'_{v0} \quad (8.1)$$

Being $K = 1.185$ constant and lower than the passive earth coefficient $K_p = \tan(45 + \frac{15}{2})^2 = 1.699$, the value actually used for the whole analysis is K.

The final step to collect the necessary data for first part of the parametric study was to run the code as suggested by Jones, meaning that for every depth (index notation i, see section 7.2.2 and 7.2.3) at every penetration step (index notation ppx), if the considered depth is a clay, the degraded resistance is the minimum between the ES and TS approach. This approach has been named Mixed Formulation (MF).

Results of the MF are shown in Figure 8.3, where it can be noted that at the bottom of the F_s curve the software implementation is not able to reproduce Jones' SRD exactly as it did previously.

Hence the parametric study aimed to analyse the relevant quantities produced as output of the implementation (f_{si}, f_{res}, f_{su}, f_s and LL_i) for the three different cases (TS, ES, MF) in order to have a comprehensive understanding concerning why Milewski's method does not produce a perfect agreement for Jones's MF formulation.

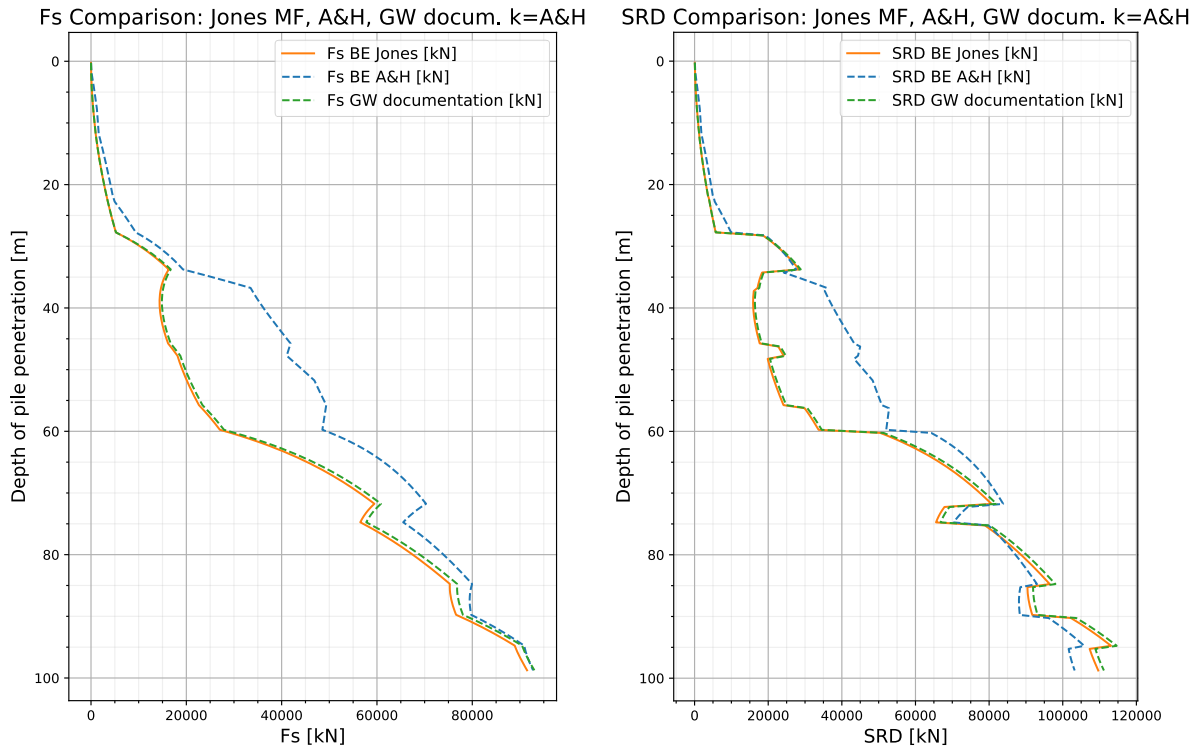

(a) (b)

Figure 8.3: Fs profile (a) and SRD profile (b) comparison of Alm and Hamre (A&H), Jones and GRLWEAP implementation, A&H shape factor, MF approach.

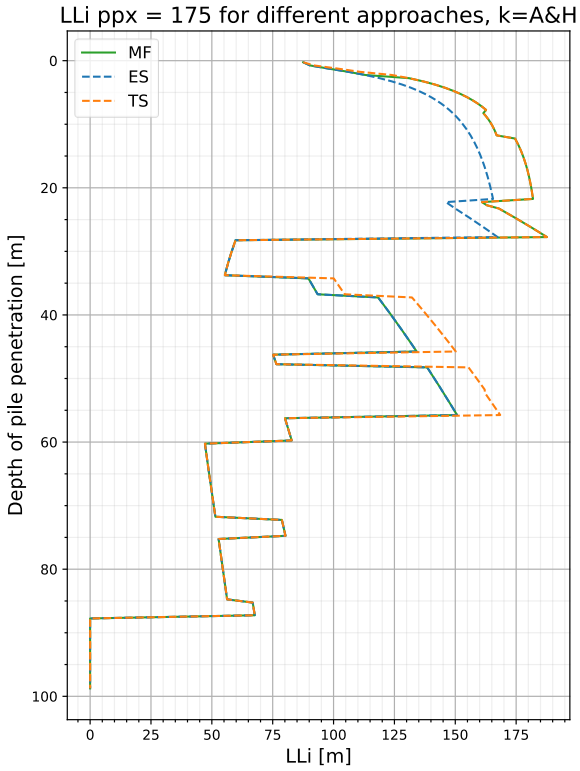

Figure 8.4 : Limit length profile with z, for the three approaches and AH shape factor k at pile penetration of 87.5 metres.

The first parameter to be checked are the limit lengths, since main character involved in the computation of SRD in the software implementation.

In Figure 8.4 it is illustrated the outcome of Jones method in the computation of limit lengths when the pile has penetrated up to a depth of $z(ppx = 175)$. Being the discretization step of 0.5 metres, the pile tip has advanced up to $z = 87.5$ metres. For that reason, limit lengths below that depth are not calculated yet and initialised to zero.

What can be noted is that in the last part of the plot the limit lengths for the three approaches coincide. This is not unexpected since the considered layer is made of sand and the formulation provides only one possible way to compute the shaft resistance, the effective stress approach. The fact that also the total stress is plotted is only because the implementation stores the limit lengths in a single vector regardless the case.

However, it is peculiar that in this part of the stratigraphy, where the limit lengths coincide, Milewski's formula fails. To gain deeper insight into this anomaly, it is helpful to examine the behaviour during the penetration process.

Figure 8.5 illustrates the results of Jones's approach for a specific depth corresponding to index $i = 50$. In the figure, the data corresponding to a depth of 25 meters (cohesive soil type) is represented, providing a closer examination of the behaviour at this depth.

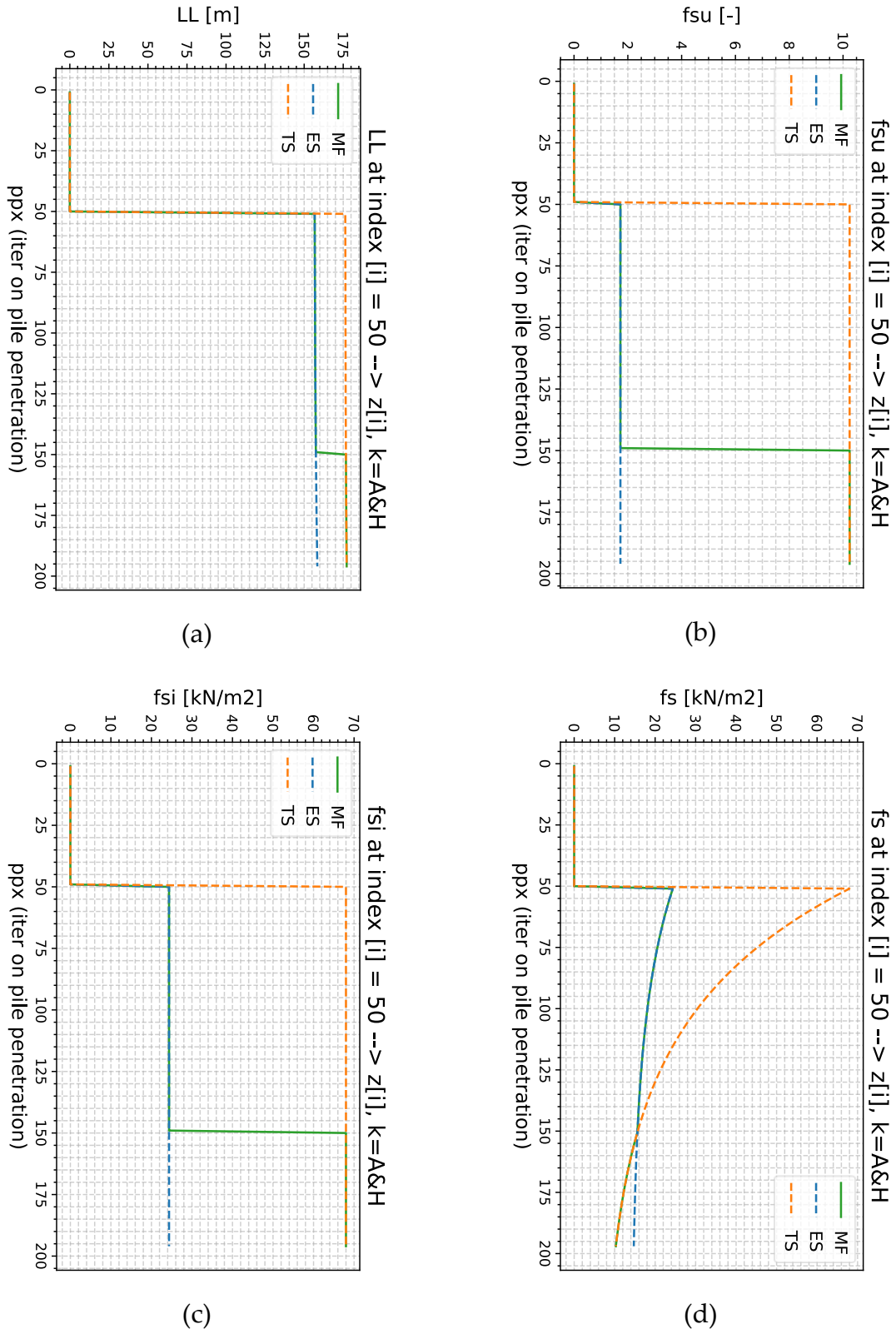

Figure 8.5: LL (a), fsu (b), fsi (c), fs (d) profiles for TS, EF, MF approaches, AH shape factor. The profiles are obtained for a fixed depth (z=25 m) and increasing pile advancement.

As highlighted in the previous sections, the quantities f_{si}, f_{res}, f_{su} remain constant at any stage of pile penetration for a fixed depth. This is because these formulations depend solely on depth-related factors, such as the soil's state of stress, and are unaffected by the pile tip's advancement.

Examining the path followed by the MF approach in the four images, at a certain point, as the penetration proceed (ppx increase), the value snaps from one approach to the other. The cause of this transition is evident in Figure 8.5 (d). Indeed, at the same ppx at which the approach changes, the curve corresponding to the degraded resistance computed according to the TS approach becomes smaller than the EF.

This behaviour presents a significant issue. Beyond a certain point of pile penetration, the approach used to represent the soil at a specific depth change; consequently, the soil layer above that depth is no longer accurately represented by the parameters previously computed. However, the software cannot account for this because it only accepts a single set of input values for initial resistance, residual resistance, and limit length for each depth. This limitation means that beyond a certain penetration depth, the degraded resistance for some specific depth is calculated incorrectly.

This behaviour is also illustrated in Figure 8.4. For a pile penetration depth of 87.5 meters, the limit length determined by the MF method, corresponding to 25 meters, is the one associated with the TS approach. However, this limit length is not the value stored in the global vector. When the pile tip reached a depth of 25 meters, the governing behaviour was determined by the ES approach, and the limit length was calculated using different parameters, as it can be seen in Figure 8.5 (a).

This discrepancy introduces errors in the integration process when computing shaft force. When the soil behaviour changes during penetration, the parameters stored earlier cannot accurately reproduce the area above the affected depth. This leads to a higher shaft force (F_s) profile when computed according to the software's implementation. Snapping from one approach to the other, due to the fact the latter is smaller, causes the software to rely on higher initial and residual resistance values. This, in turn, produces a higher resistance profile at the affected depth.

To better understand and confirm this, a second test had been made. In this case the exponent considered is the one suggested by Jones's originally, which is expected to be higher compared to the one of Alm and Hamre.

It is important to underline that, for a pure total stress approach in clays, the formulation should be independent on the friction angle. While this was ensured in Alm and Hamre, in Jones this is not true since the shape factor includes the tangent of the interface friction angle. An approach to address this issue is suggested by OPILE online documentation, [24], which simply suggest increasing the denominator from 80 to 100 for a faster degradation.

Results of the second analysis are shown in Figure 8.6, Figure 8.7 and Figure 8.8.

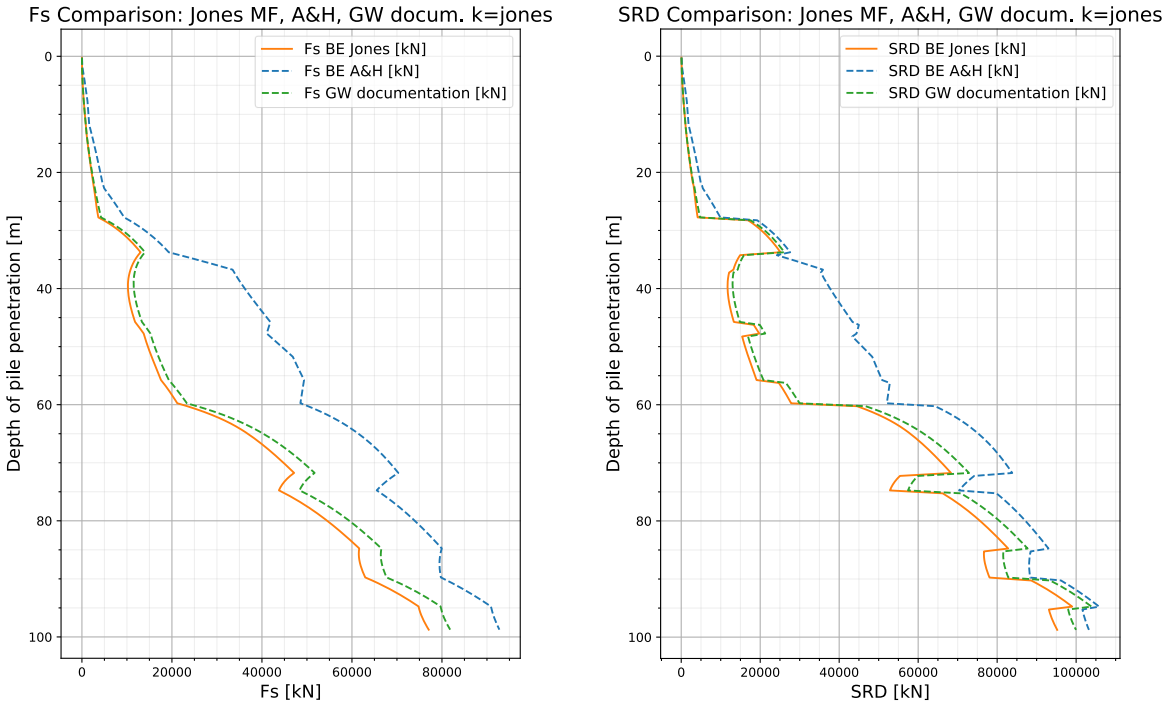

(a) (b)

Figure 8.6: Fs profile (a) and SRD profile (b) comparison of Alm and Hamre (A&H), Jones and GRLWEAP implementation, Jones's shape factor, MF approach.

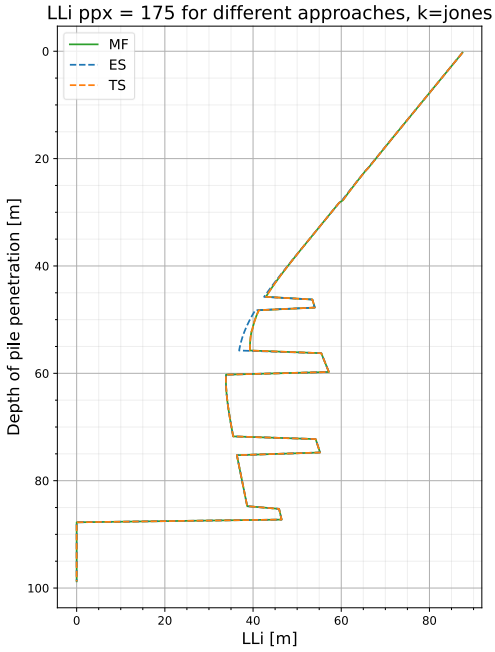

Figure 8.7 : Limit length profile with z, for the three approaches and Jones shape factor.

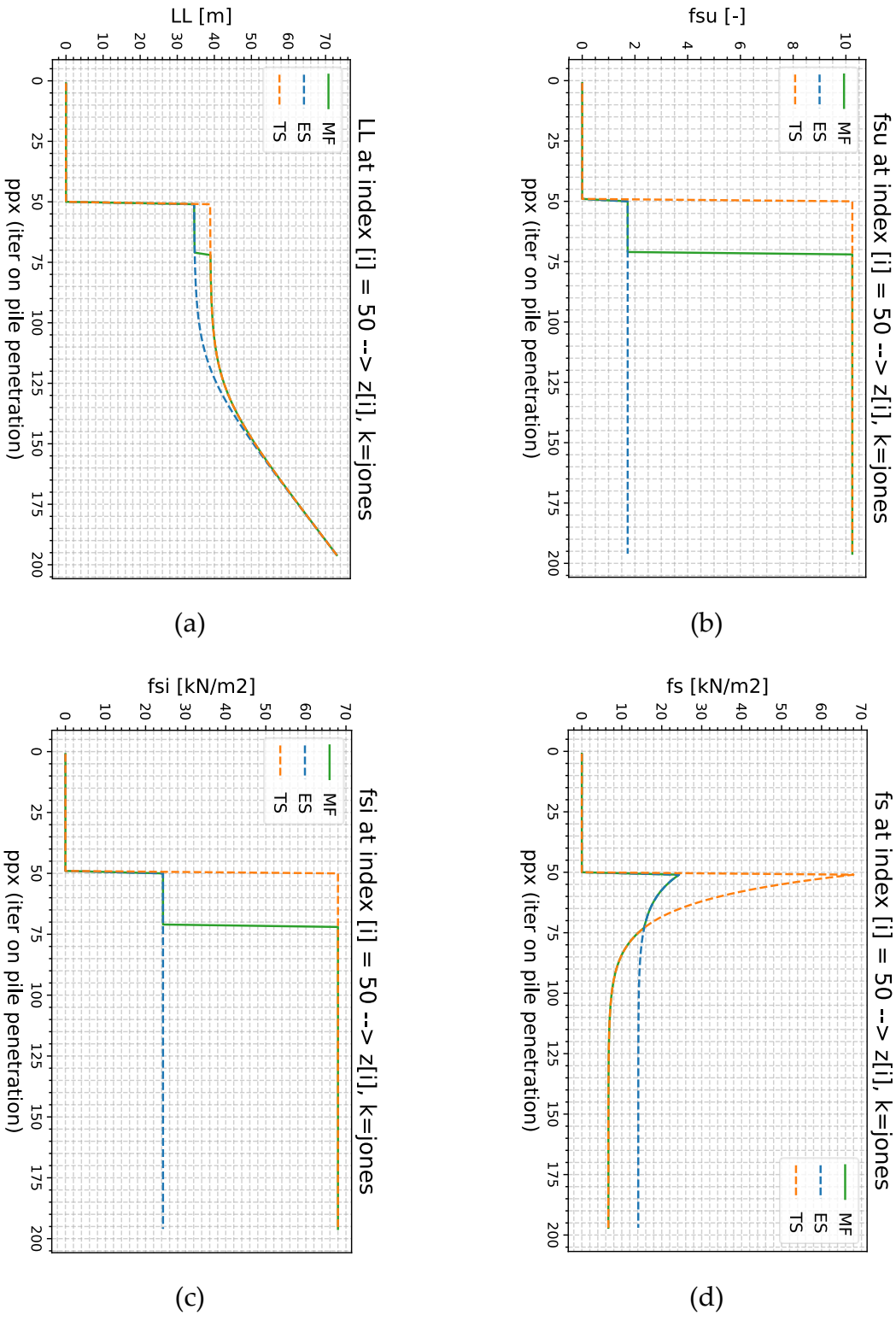

Figure 8.8: LL (a), fsu (b), fsi (c), fs (d) profiles for TS, EF, MF approaches, Jones shape factor. Profiles obtained for a fixed depth (z=25 m) and increasing pile advancement.

In Figure 8.6, comparison with Alm and Hamre has been kept only for the purpose to show that, since the shape factor k for the exponential degradation is higher in Jones, the final value of SRD is lower.

Figure 8.8 illustrates the results of the analysis. The first difference from the previous case is the trend of the limit lengths (Figure 8.8 (a)), which is more than linear. This is consistent to what explained in section 7.4, since the shape factor is higher, higher variability in the limit length is also expected. This is also reflected in the degraded resistance, which shows to degrade faster (Figure 8.5 (d), Figure 8.8 (d)).

The behaviour observed in Figure 8.7 can be explained by the fact that, as the pile penetrates, the limit length computed according to the different approaches tend to converge. This likely indicates that the influence of the exponential decay, which depends on the distance from the tip, becomes the dominant factor in the computation of the limit length. This is particularly evident since the setup factor remained unchanged. Reason behind this behaviour will be clearer examining Figure 8.8 (a): at $ppx = 175$ the value of LL at the depth of $z(i = 50)$ according to the three formulations coincide.

What can be noted in Figure 8.9 is that Jones shape factor is greater than Alm and Hamre's at every depth, leading to a faster degradation of the skin resistance. Furthermore, due to the very low input interface friction angle associated with cohesive materials, the shape factor is even higher. These considerations are in agreement with what discussed about the differences between Figure 8.5 (d) and Figure 8.8 (d), since higher shape factor means greater exponential decay.

Comparing Figure 8.6 with Figure 8.3, it can be noted that, as expected, higher exponent according to Jones formulation leads to the computation of a more degraded shaft resistance.

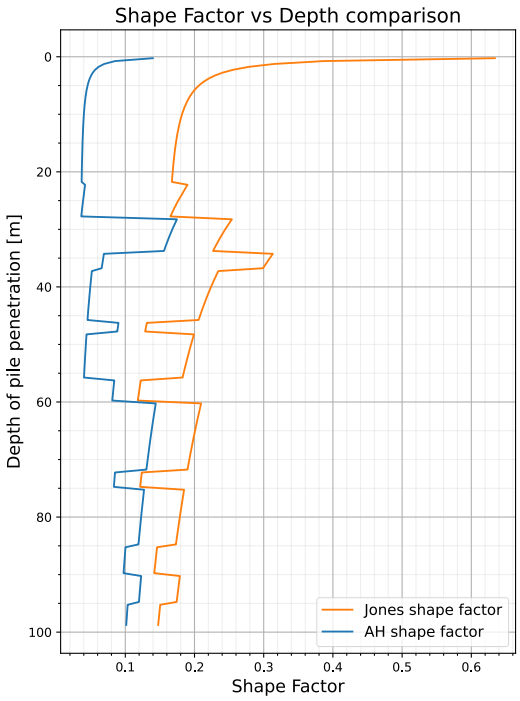

Figure 8.9 : Shape factor profile vs depth for Alm and Hamre (AH) and Jones methods.

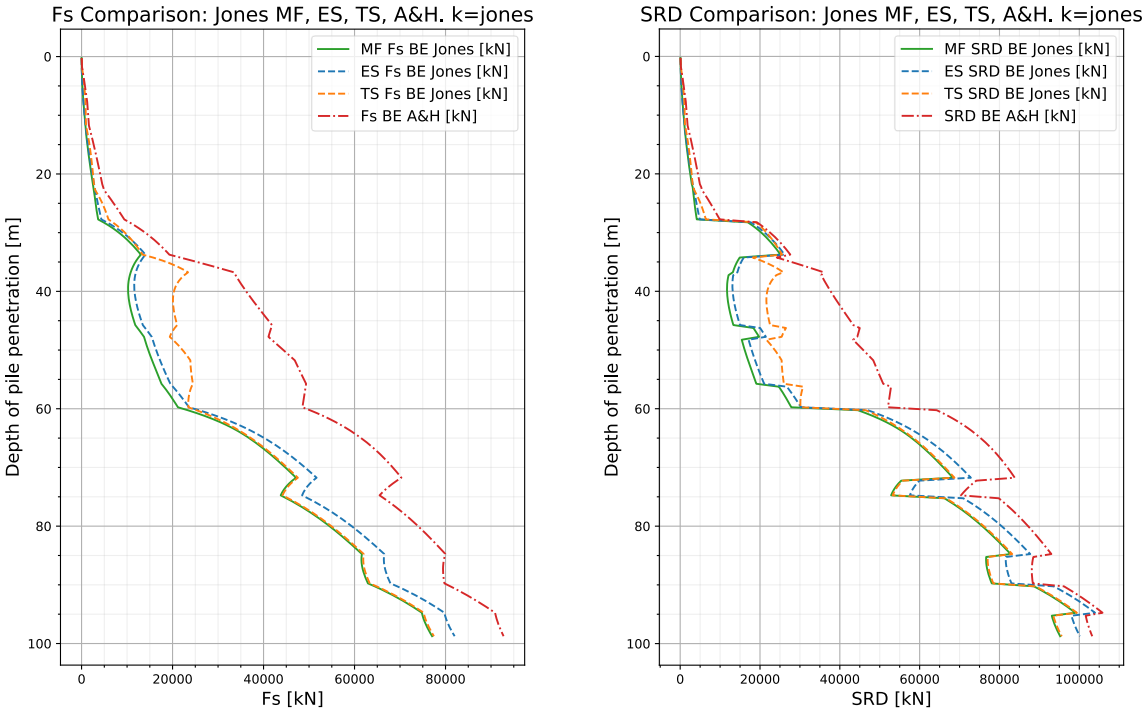

(a) (b)

Figure 8.10: Fs profile (a) and SRD profile (b) comparison of Alm and Hamre (A&H) and Jones implementation, Jones shape factor, MF, TS, ES approach.

To have an idea of the variability between the three approaches, Figure 8.10 compares the obtained results, maintaining the parameters as in the last analyses.

The first thing that can be seen is that the shaft force is in any case smaller than the AH one. This, already mentioned before, is due to the higher shape factor (dependent on the tangent of the interface friction angle at the denominator). Then it is curious to note that beyond 25 metres depth, the ES and MF never coincide anymore, while the TS and MF does. One would expect that, since in the sand the three approaches coincide (actually it exists only one way to compute shaft friction) also the shaft force does. This in reality doesn't happen due to the fact that when only one approach is selected then the same is kept for the whole analysis. Considering Figure 8.8 (d) one can note that at the depth of 25 metres, the behaviour shifts from effective to total stress when the pile penetration overcomes the depth of about 37.5 metres. From that depth on, the shaft resistance considered for that point (at 25 metres depth) is always equal to the TS residual value, that is actually lower than the ES one. For that reason, one can start appreciating a discrepancy between the ES and MF form the depth of about 35 metres on (when the behaviour for the depths above the considered point snaps to the other approach). This higher resistance is then reflected also in the rest of the penetration advancement leading the ES curve to be higher than the MF and TS even when a sandy layer is reached.

Regarding the TS approach this doesn't happen since the approach selected from the beginning for the upper points was already the correct curve (TS) which is associated to the residual value of clays when the behaviour shifts from the ES to TS approach.

To wrap up, in the case of ES approach, the error propagates as the piles penetrates more, whereas in the TS case, the error is concentrated at the point where the pile first reaches that specific depth, but then, when the sandy layer is encountered, the upper resistances are calculated as the analytical formulation suggest being their behaviour already shifted to the TS approach.

It is important to underline that in these examples the behaviour always started from a smaller value of ES initial resistance to a residual TS resistance. But this depends on the input parameters and soil stratigraphy.

To conclude, the main reason addressed to the failure of Milewski's method is the fact that the behaviour of a specific depth shifts from one approach to the other after a certain penetration depth (distance from the pile tip). This is a problem since the software's formulation can accept as input only one set of variables per depth. This not only concerns the limit length, but also the setup factor, which, to accurately describe the resistance of a depth shallower to the one considered at a certain point, should be updated to the second approach in order to be representative of the soil's state.

8.1.2. Possible Upgrade for Jones' Method

As proven in the pervious section, the extension to Jones's method of Milewski's approach for the computation of the limit lengths is not possible, since one single set of input values is not able to reproduce the exact trend of the method, due to the snap from effective to total stress approach after a certain penetration is reached.

One possible way to address this issue is to select one of the two approaches in advance for the entire analysis. However, this requires careful consideration. If the ES initial resistance is lower than the TS resistance, and the ES residual resistance is higher than the TS residual resistance, there will inevitably be a shift in the governing behaviour during the installation process.

Determining the best approach is challenging, as it requires calculating the shaft force for both methods at every depth to identify which one is more conservative. While adopting a conservative approach (resulting in a less degraded resistance) ensures a safer design, it may conflict with recent methods aimed at reducing installation costs by avoiding the overestimation of soil resistance.

Another approach that tries to address the issue is to choose a combination of the initial and residual resistance (ES or TS approach) for every depth. In such a way only one single curve for the degraded resistance is adopted for the whole analysis and, according to the user, different combination can be set.

For example, the less conservative analysis would take, for every depth, the minimum value of residual and initial shaft resistance comparing effective and total stress approaches.

Since these quantities are independent on pile penetration, the curve for the computed degraded shaft resistance is independent on pile advancement as well.

Moreover, choosing the minimum value for both quantities result in lower shaft resistance than what is predicted by Jones' method.

Considering the inputs in Table 8.1, a comparison between the standard formulation and the modification (by using the minimum residual and initial value at every depth) is shown in Figure 8.12, where the yellow curve represents this modification of Jones formulation, the blue line is the analytical formulation and the green line the hand-implemented software formulation, whose *LL* are computed according to Milewski's approach. The difference between the two methods (analytical and modification) is almost negligible. However, it is still interesting to compare the MF approach (analytical formulation) with the proposed method, as illustrated in Figure 8.11.

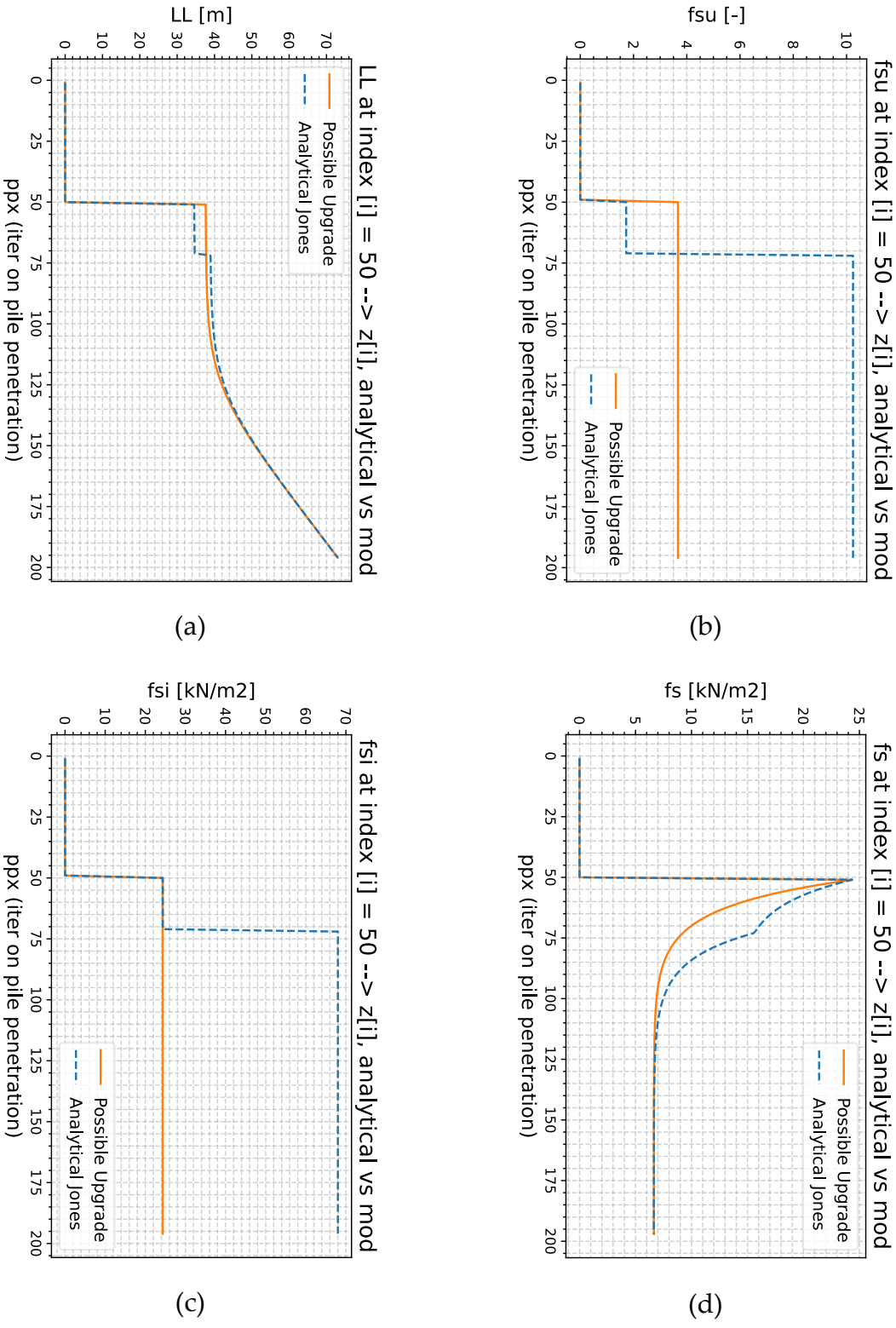

Figure 8.11: LL (a), fsu (b), fsi (c), fs (d) profiles for MF approach, and min fsi and fres method, Jones shape factor. The profiles are obtained for a fixed depth (z=25 m) and increasing pile advancement.

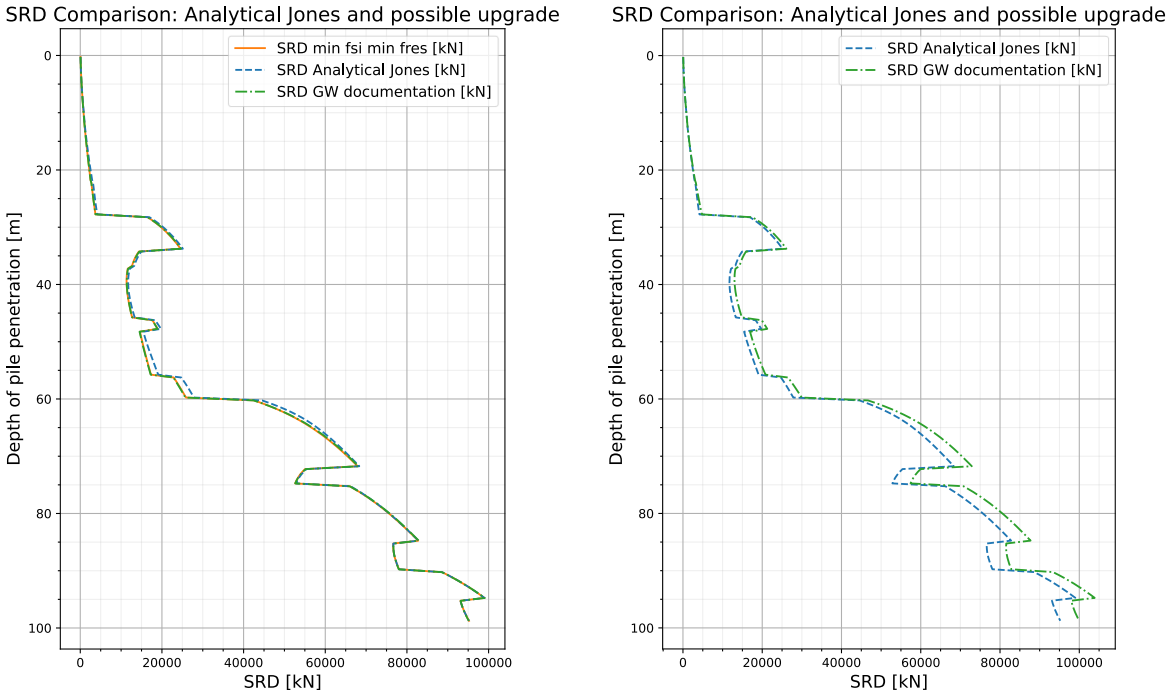

Figure 8.12: SRD profile selecting the minimum residual and initial resistance (a) and standard Jones formulation (b) Jones shape factor.

Limit length appears to have the same trend for most of the pile penetration (Figure 8.11 (a)), as well as shaft resistance which differs only in the top part of the curve (Figure 8.11 (d)).

Moreover, it can be seen that, by applying this modification to the method, the Milewski's formula is again working, due to the fact that no shift in the approach is considered, but only a single shaft degraded resistance curve.

To have more insight of the method's performances, it was applied also to the stratigraphy adopted for the validation in section 7.6. The missing parameters to run Jones analysis have been set as follows.

The friction angle for clay layers has been set to 25 degrees, leading to an interface friction angle of 20 degrees, while the sensitivity has been set to 1 and OCR to 2.

In Figure 8.13 it can be noted first that Jones already predict a remarkably lower SRD profile compared to AH (blue curve), even if this might be due to the choice of non-representative values selected for the unknown parameters mentioned above. Then it can be seen that the two different implementations of Jones method do not differ that much, but, as expected, the one selecting the minimum values (green curve) produces

lower SRD profiles and is perfectly matched by the software documentation (red curve).

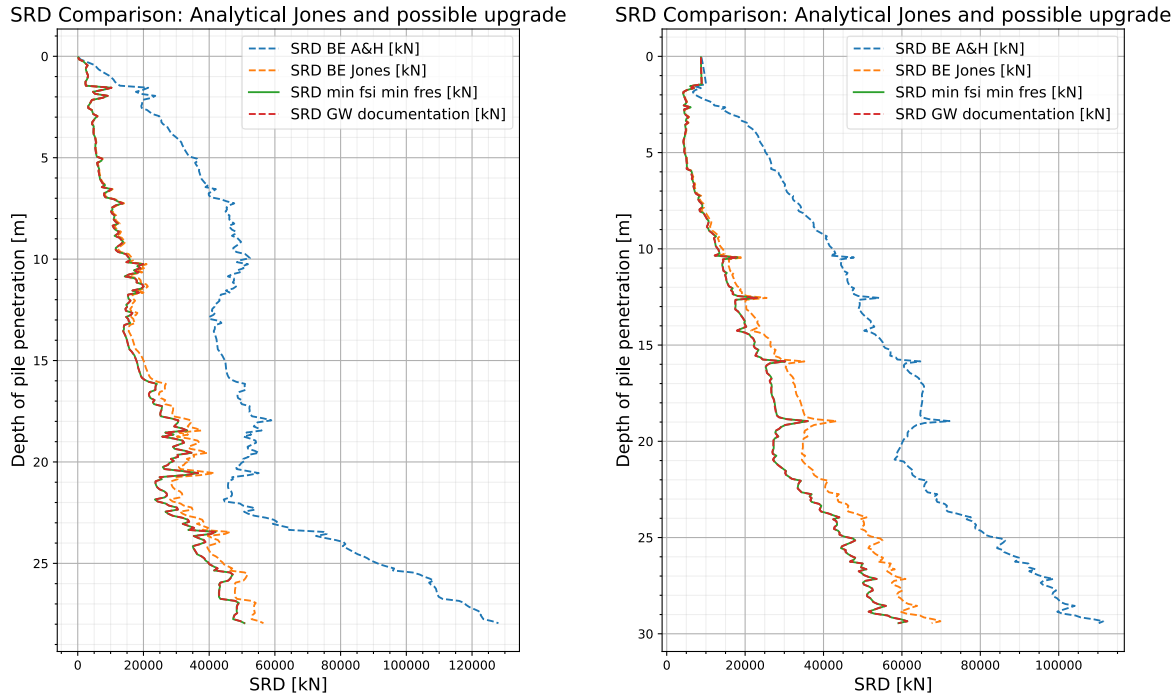

(a) (b)

Figure 8.13: SRD profile selecting the minimum residual and initial resistance vs standard Jones formulation vs Alm and Hamre for location P06 (a) and P03 (b).

8.2. General Numerical Approach

The considerations done in the previous section apply only to methods that employs the Alm and Hamre degradation resistance formula (Eq. 5.11). For any other method an analytical formula, such as Milewski's one, must be derived to establish the limit length based on the specific formulation. This process must be applied every time a new method wants to be implemented in the software.

For that reason, it was decided to develop an optimization routine capable of calculating software inputs regardless of the chosen method.

The routine was designed to operate as follows: first, the analytical model for SRD computation that is to be reproduced needs to be implemented or given. Next, a goal function to be minimized is defined. Finally, the optimization approach must be determined, including whether to focus on specific parts of the stratigraphy and how many parameters are to be involved. This process aims to replicate any analytical model.

A first consideration must be done regarding the concept of the optimization itself. The input parameters needed by GRLWEAP are: f_{si}, q_b, f_{su}, LL_i, f_0.

Among these parameters it has to be decided which one to optimize in order to reproduce the analytical method. Performing an optimization in a 5-dimensional space is extremely computationally expensive. Moreover, another topic to consider is the physical meaning of these variables.

Indeed, boundaries can be set in order to have physically meaningful variables, but this would constrain the optimal result of the optimization process.

Therefore, a choice must be done regarding these two major topics before starting the idealization and implementation of the code.

The aim of the implementation is to be the most lasting and durable as possible, but it is supposed that any analytical method develop in the future will always suggest at least an initial shaft resistance and a base resistance to be considered. Hence, adopting the proposal provided by the analytical formulations, the number of unknowns reduces, decreasing the dimension of the space to 3.

Then, f_0 should be set to a constant value to decrease the number of variables in the optimization.

The final decision to be made concerns the parameter f_{su}, which represent the ratio between the initial and residual unit skin friction. Assuming that all the methods that wants to be optimized in their formulations provide how to compute these two quantities, then the setup factor in not an unknown anymore. However, last sentence is true only theoretically, since in GRLWEAP only one set of values for each depth can be given as input, but, in cases like Jones, where the behaviour changes from total stress to effective stress or vice versa, the setup factor is not a single value for the entire installation process. Therefore, being allowed to input only one set per depth, from a certain depth on, the input setup factor will not be representative of the soil degradation anymore. Same reasoning can be done for the limit length.

Since optimizing the setup factor would lead to nonphysical results, unrelated to either the initial or residual resistance, it was decided to consider it fixed under the assumption of initial and residual resistance computation suggested by any literature method. As a result, the only remaining parameter to be optimized is the limit length.

On the other hand, if the setup factor is also considered in the optimization process, would extend the routine to a larger space of solutions, increasing the degrees of freedom of the optimization. This consideration could be useful in future if new methods will not include the formulation of initial and/or residual resistance or in case the theoretical method is not implemented in the code, so the other input quantities are unknown.

The workflow of the code was decided to be subdivided in 2 main steps:

- Optimization per layer;
- Optimization per blocks.

8.2.1. Optimization per Layer

The first step of the routine consists in computing a preliminary result of the limit lengths by performing an optimization layer per layer. A simple for loop is sufficient to run the optimization function for each layer, which is optimized independently of the others nor considers for errors in other layers or their dependency on the current layer's LL. At the end of the loop a single value of LL is found for each layer. This homogenization allows to reduce considerably the computational cost compared to a process that considers a different limit length for each depth.

8.2.1.1. Optimization function for step 1

For each layer, a scalar objective function is defined to compute the mean squared error (MSE) between the SRD values within that layer computed running the GRLWEAP formulation and the target values of SRD.

The MSE is defined as:

$$MSE = \frac{1}{n}\sum_{i=1}^{n}\left(Y_i - \hat{Y}_i\right)^2, \tag{8.2}$$

where:

- n is the number of data points;
- Y_i is the goal SRD computed according to the target theoretical method;
- $\hat{Y}_i$ is the computed SRD according to GRLWEAP formulation for a given input.

The optimizer tool selected is the "minimize" function provided by "scipy" library. This tool minimizes the goal function for given boundaries and initial guess.

The method used by the optimizer is the "L-BFGS-B", a quasi-Newton method for bounded optimization, based on an iterative gradient algorithm that approximates the Hessian matrix using limited memory, making it efficient for large problems.

The option "finite_diff_rel_step" sets the relative step size for numerical differentiation when estimating gradients and is essentially used when the function does not provide an explicit gradient. The method is remarkably efficient when the function is differentiable or can be approximated using finite differences. Since the

goal function is defined as the difference of discrete points, then the optimizer selected is appropriate.

The initial guess is computed as the mean value of the limit lengths included in a certain interval (in this case each layer) defined in the inputs of the function.

8.2.2. Optimization per Blocks

In the second step, each layer is subdivided into a predefined number of blocks that can be selected by the user. At each block it is assigned an error value and a corresponding weight. The error is calculated as the sum of the errors (difference between target and computed in step 1 SRD) for all points within the block, while the weight is a normalized version of the error, enabling comparisons across layers.

At every iteration, the SRD is updated based on the GRLWEAP formulation, and new error values and weights are recalculated. The block associated to the highest error is then selected for the optimization in order to determine an updated limit length value for that block.

Unlike the first step, the optimization process here is dynamic: due to the prioritization of blocks, updates from early optimizations propagate to subsequent calculations. This is particularly critical for cumulative parameters, such as shaft force, which depend on updates from all preceding layers. As a result, the optimization trajectory for each block in the second step is influenced by updates made to earlier blocks, ensuring that improvements are integrated dynamically throughout the process.

Moreover, if needed, the optimizer tool can explore a different range of LL values compared to the first step, allowing it to better fit the points that previously showed poor agreement.

However, blocks with significantly higher errors compared to others often fail to converge to a better LL value, leading the algorithm to repeatedly attempt optimization on the same blocks. To address this issue, any block that has already been optimized is skipped under the assumption that its current LL value represents the best possible fit.

8.2.2.1. Optimization function for step 2

For the second step a different objective function is considered.

Instead of using MSE which is not related to any physical meaning, it was decided to implement a loss function, $\mathcal{L}$, defined as follows:

$$\mathcal{L} = \sum_{i=1}^{n} w_i \cdot \varepsilon_i, \tag{8.3}$$

where:

- w_i is the weight associated to block i;
- ε_i is the error associated to block i;
- n is the number of blocks along the entire stratigraphy.

The error ε_i is computed at each iteration as:

$$\varepsilon_i = \sum_{j=1}^{p} \epsilon_j, \tag{8.4}$$

where:

- ϵ_j is the error associated to the discretized depth j computed as the difference between the goal SRD and the current computation of SRD according to GRLWEAP formulation;
- p is the total number of discretized depths belonging to a specific block.

The weight w_i is computed as:

$$w_i = \frac{\varepsilon_i}{\max\limits_{i \in \{1,\dots,n\}} \varepsilon_i}, \tag{8.5}$$

which simply is a normalization of the error associated to the block in order to make it comparable with the other blocks error.

One drawback that must be considered is that if the layers are very different in thickness, a predefined number of blocks can lead to very different block's thicknesses. Therefore ε_i could result being much higher than other blocks. For this reason, it was decided to skip the blocks already optimized, since, in case one of this block can't find a solution, the optimizer will be stuck until the maximum number of iterations is reached.

8.3. Validation of the optimization process

Optimization is, by nature, an approximation of the true solution. A function can have multiple local maxima or minima, and the success of an optimization process in finding the global optimum depends on factors such as the initial guess and constraints. For this reason, a certain level of tolerance is generally accepted.

This tolerance is not only defined by the input parameter of the optimization tool (such as scipy.optimize.minimize) but also by the overall loss function used in the second

step of the process. As a result, a small discrepancy may arise between the final computed SRD and the target value.

Defining a clear failure threshold for the optimization is challenging, as the MSE lacks physical significance, and the loss function is influenced by layer thickness. To assess the accuracy of the method, a comparative approach was adopted: the results of a driveability analysis performed in GRLWEAP were evaluated using both the target SRD and the SRD obtained from the optimization process. The selected test case represents the worst-case scenario among all evaluations conducted. If the difference between the two outcomes is negligible, it can be reasonably assumed that the optimization method will yield even more accurate results in other cases.

Using the same stratigraphy as presented in Table 8.1 and maintaining the same pile geometry, the analysis was conducted for Jones's method with a remoulded shear strength equal to the undrained shear strength and a friction angle of 15 degrees for clays. The results are illustrated in Figure 8.14.

The optimization routine required approximately 15 minutes to complete, though the exact duration may vary depending on the processing power of the computer. The number of blocks was set to a maximum of 5 per layer, wherever feasible, and the boundary constraints for both optimization steps were defined within a range of 1 to 200 meters.

Figure 8.14 (a) illustrates the outcomes of the application of Milewski's approach in the case of Jones MF method and the input parameter discussed earlier. As evident from the figure, the approach completely fails. Figure 8.14 (b) shows the results of the optimization routine at the end of the first step, where a good agreement has already been reached. However, as shown in Figure 8.14 (c), the second step further improves the agreement, particularly in the lower part of the curve. Finally, Figure 8.14 (d) compares the value of the limit length obtained at each depth for the three cases.

The limit lengths computed using Milewski's approach are known to be unreliable since the curves in Figure 8.14 (a) do not match. In contrast, the LL values obtained through the optimization provide a more reasonable representation. It can be seen that the refinement applied during the second step in the lower part of the curve where adjustments were made, effectively improves the agreement with the target SRD.

Despite this overall improvement, discrepancies remain in the 50 to 70 metres depth range, where the two curves diverge slightly. This issue arises because the optimizer struggles to converge to an exact solution. Specifically, between 45 and 60 metres, the optimizer fails to find an LL that replicates the target SRD, as it reaches the lower bound of the search space (Figure 8.14 (d)). This suggests that no valid solution exists within the given constraints, implying that the assumed f_{su} may not be appropriate for this depth range.

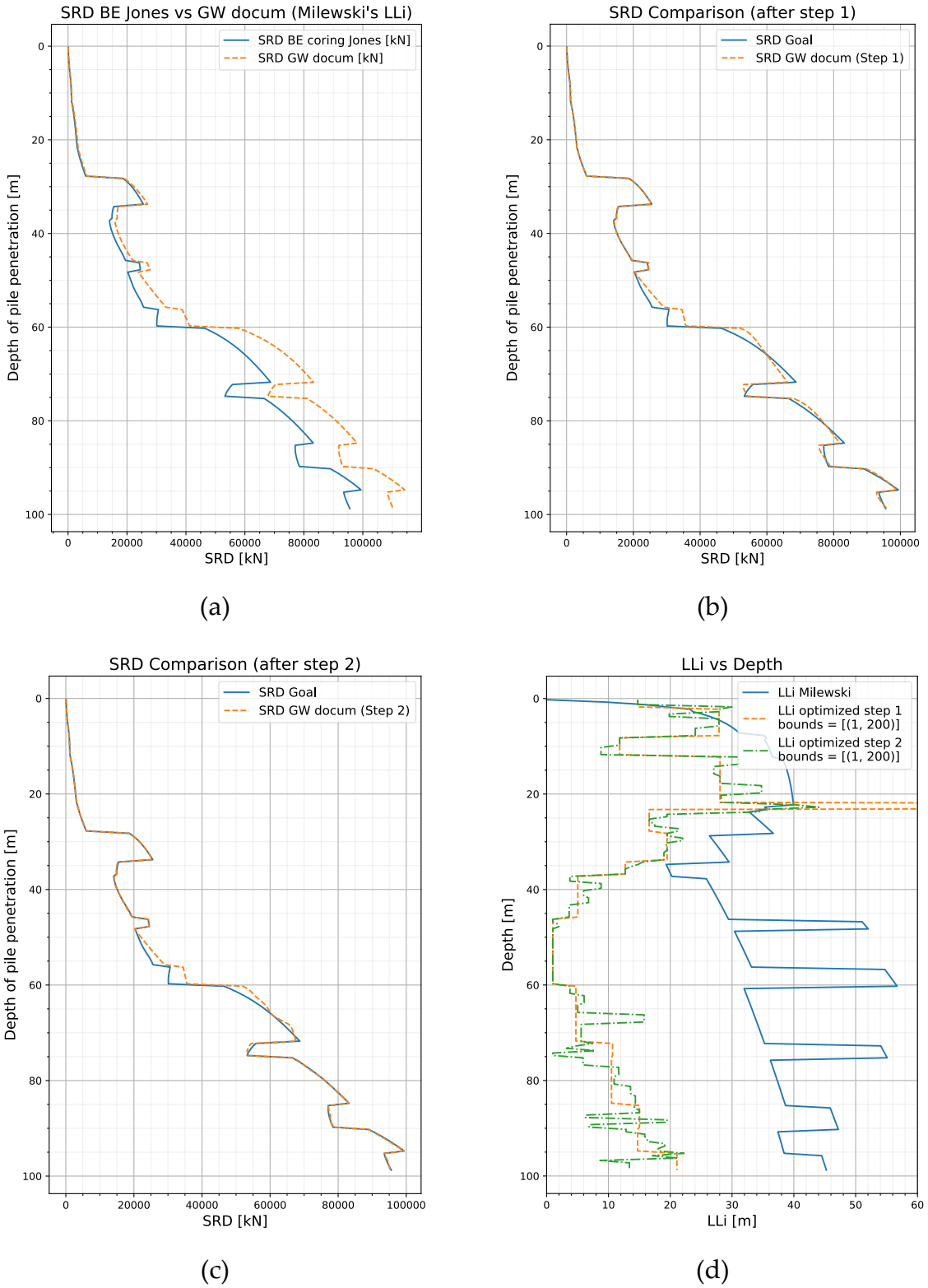

Figure 8.14: Comparison of analytical solution vs: Milewski's formula applied to Jones MF (a), optimized solution after step 1 (b), optimized solution after step 2 (c), and LL for the three cases vs depth (d).

The problem is addressed to the fact that the formulation in GRLWEAP requires as input a single value of both limit length LL and setup factor f_{su} for each depth. Being f_{su} fixed, the degrees of freedom for the solver is only one. Initially, in the upper layers, where the soil is clay, the optimizer works correctly and assign as initial LL and f_{su} values the one computed according to the ES approach. However, at greater depths as the ones under consideration the behaviour has probably already shifted to the TS.

Since the error in step 1 (MSE) in the upper layers is small, the optimizer does not modify the LL values in this region during the refinement in step 2. Consequently, the computed shaft resistance is overestimated in the underlying layers, particularly between 50 and 70 m.

This overestimation occurs because the setup factor f_{su} is assigned based on the ES approach, whereas Figure 8.8 (b) indicates that, as penetration progresses, this assumption is no longer valid. As a result, the underlying layers exhibit higher shaft resistance than expected. This error propagates through the discretized depths, and, even though the value of LL in that region is set to the lower bound, meaning the soil is completely degraded to the residual value as soon as the tip penetrates that specific depth, the optimizer is unable to find an LL value that correctly reproduces the target SRD while keeping f_{su} fixed.

This is proven by the fact that the behaviour in an analysis run by forcing the TS or ES only is perfectly reproduced by the optimizer (already in step 1 for both cases), as illustrated in Figure 8.15.

Anyway, as the optimization proceed downward, the optimizer compensates for the excessive shaft resistance in the middle layers by shortening LL in the bottom sandy layers. This forces the degradation of resistance to occur earlier, counteracting the error from the upper layers. This effect is evident when comparing Figure 8.14 (d) and Figure 8.15 (b) and (d), where the limit lengths for the bottom sandy layer are expected to be the same. Indeed, since for sands only ES approach exists, and f_{su} is the same, one should obtain at least a similar trend to the LL obtained by using Milewski's approach, as it happens for TS and ES approach only.

Since this does not happen, it is assumed that in the optimization process the LL are shorter in order to achieve the degraded resistance sooner and mitigate the errors accumulated from the upper depths.

The effect of the second step successfully reduces the weighted global loss from 102154 to 78903, decreasing the initial error of more than 22%. Nevertheless, despite this improvement, the solver remains unable to fully resolve the discrepancies in the 50–70 metres range.

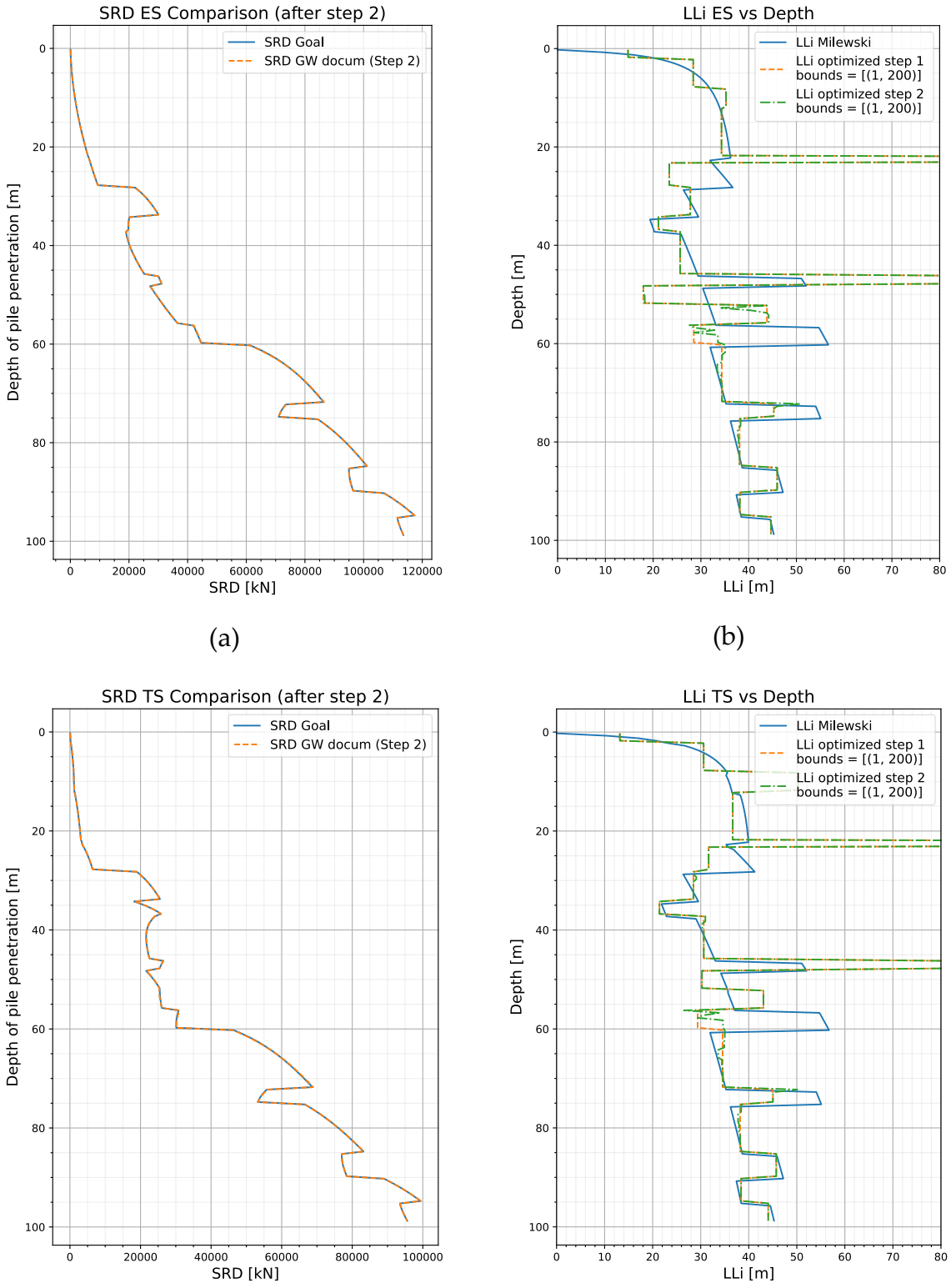

Figure 8.15: SRD profile Jones ES vs optimized (a), optimized ES LL vs depth (b), SRD profile Jones TS vs optimized (c), optimized TS LL vs depth (d).

While the optimization significantly improved the SRD fit, the remaining discrepancy between 50–70 metres raise the question of whether pile driveability predictions (in terms of blow counts) are meaningfully affected. For that reason, the goal of the current analysis is to check whether these small discrepancies affect the final results of the driveability, in terms of blow counts.

Considering the same stratigraphy as in Table 8.1, same additional input parameters as the previous analysis and the same pile geometry, the analysis performed in GRLWEAP used as analytical SRD computed according to Jones, with input data obtained through a two-parameter optimization, where f_{su} was also optimized. Knowing a posteriori the range of the parameters for the specific case, reasonable boundaries had been set: LL was let ranging from 1 to 80 metres and f_{su} from 1 to 10.

Results of the two-parameters analysis are illustrated in Figure 8.16 ((a), (b), (c)). In Figure 8.16 (a) the SRD profile shows an almost perfect agreement, which was considered the analytical solution to be used as input in GRLWEAP to further assess the reliability of the optimization process.

To this end, two Wave Equation Analysis (WEA) were performed using GRLWEAP: one based on the SRD profile obtained from the one-parameter optimization and the other using the SRD profile derived from the two-parameter analysis. The resulting blow counts profiles for both cases are compared in Figure 8.16 (d). The two profiles demonstrate a high level of agreement, with only minor discrepancies corresponding to a negligible difference in the number of blows. This outcome validates the one-parameter optimization method, confirming its accuracy and reliability in reproducing in GRLWEAP Jones's formulations for SRD computation.

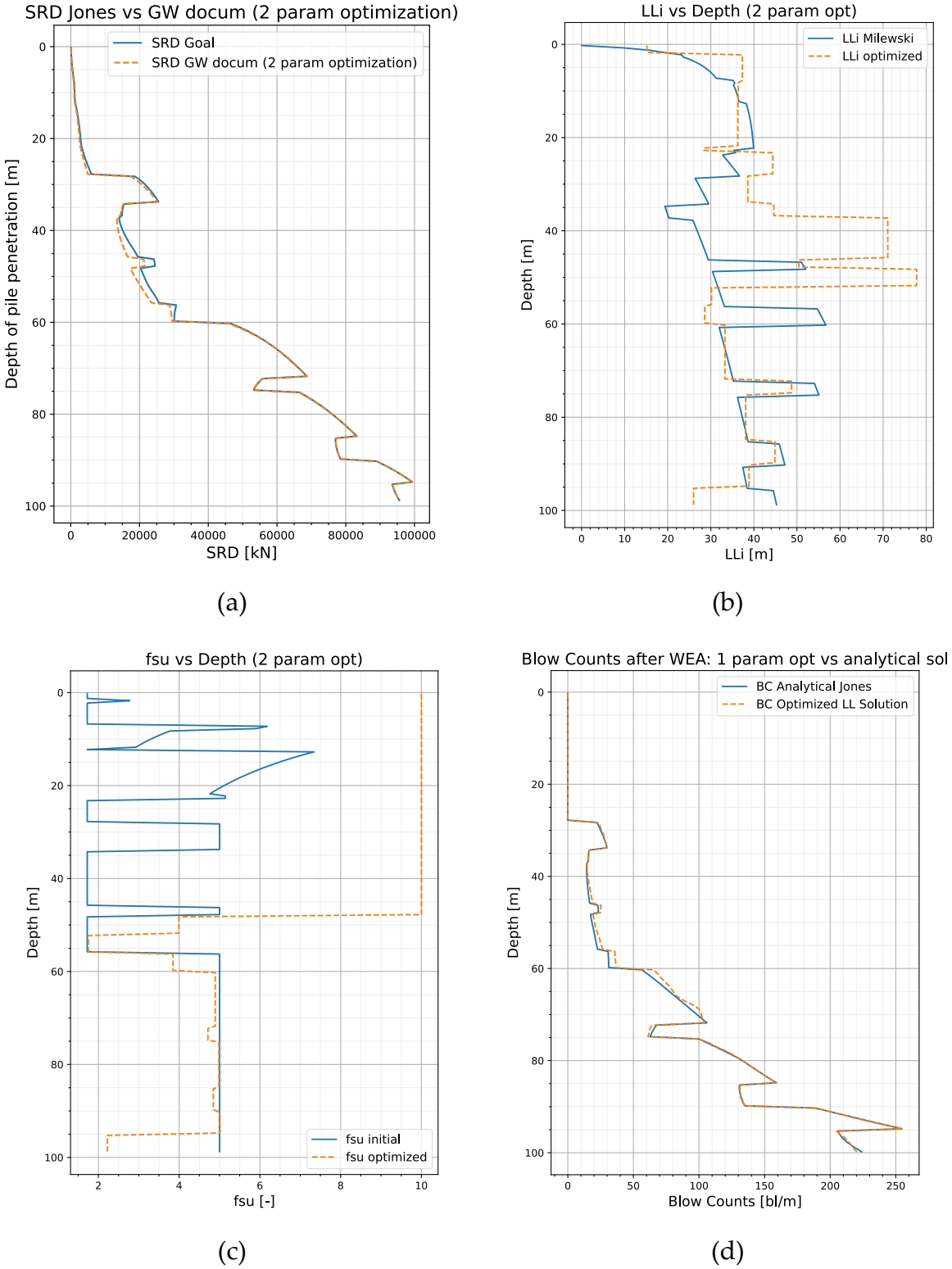

Figure 8.16: Results of the optimization in 2 parameters: SRD profile (a), optimized LL vs depth (b), optimized fsu vs depth (c), comparison of blow counts between the optimized solution and the analytical solution obtained by a two-parameter optimization (d).

8.3.1. Sensibility Analysis on Optimizer Settings

The configuration of the optimizer tool plays a critical role in achieving accurate results that closely replicate the theoretical goal method. The choice of settings directly impacts the optimizer's ability to navigate the solution space effectively and find an optimal or near-optimal solution.

One of the key aspects of this configuration is the definition of boundary ranges, which can be adjusted independently for both steps of the optimization process. Properly setting these boundaries ensures that the optimizer explores a feasible region without being overly constrained or too permissive, both of which could lead to suboptimal results.

In the second step of the optimization, additional parameters can be set to improve convergence and accuracy. Specifically, it is possible to define a maximum number of iterations, which limits how long the optimizer continues searching for a solution before terminating. This parameter is particularly important for balancing accuracy and computational cost, but, in any case, is limited by the number of blocks, as no block is optimized more than once.

Another adjustable setting in the second step is the number of blocks, which influences how the optimization problem is structured and solved. The correct choice of this parameter can enhance the optimizer's ability to find a solution that aligns closely with the theoretical goal, particularly in complex scenarios where multiple local minima or maxima exist.

By carefully tuning these settings, the optimization process can be tailored to yield results that are both precise and computationally efficient, ensuring that the final outcome closely matches the intended target while maintaining practical feasibility.

8.3.1.1. Influence of boundaries constrains

It has been observed that when the boundaries for the limit length optimization are too restrictive, the optimizer tends to assign the highest possible value at certain points, which coincides with the upper bound. This suggests that the optimizer is constrained by the imposed limits rather than selecting the most representative value for that point. On the other hand, when a wider range for *LL* is provided, the optimizer is able to determine values that more accurately reflect the optimal solution.

Naturally, this has a direct impact on the final results. If the upper bound is set too low, the optimization process does not necessarily fail in terms of numerical convergence, but rather in terms of its ability to produce a meaningful and accurate final outcome. The imposed constraint prevents the optimizer from fully exploring the solution space, leading to suboptimal results.

To further investigate this, tests were conducted separately on A&H and Jones using the same *LL* range. When considering a reasonable *LL* range between 1 and 80 meters, the results for Jones showed good agreement with expectations. However, this was not the case for A&H, where the imposed upper boundary was found to be insufficient to achieve satisfactory results (Figure 8.17 (a)). It was necessary to extend the upper bound further to allow the optimization to reach an acceptable solution.

This issue was effectively addressed by increasing the *LL* range up to 200 meters in the second step of the optimization. A direct comparison of A&H limit lengths between the two steps, Figure 8.17 (b), reveals that, for points where the *LL* was initially constrained by the upper bound in the first step, the second step allowed these values to increase. This adjustment resulted in a better-optimized SRD curve, demonstrating that a more flexible boundary setting can significantly improve the accuracy of the final optimization results.

This outcome highlights two key insights. First, it confirms that the range for *LL* must be sufficiently wide to allow the optimizer to find appropriate values without being overly constrained. Second, it demonstrates that the second optimization step effectively adjusts *LL* values within predefined blocks, thereby enhancing the final accuracy and performing as intended.

Based on these observations, it was decided to set the boundaries for both optimization steps within an interval ranging from 1 to 200 meters. This range was determined by analysing all available samples, as it was observed that, in most cases, the optimizer rarely required *LL* values exceeding this threshold. Additionally, this choice aligns well with findings from Milewski's approach, where relatively high *LL* values were identified, yet they resulted in near-perfect matches between the target SRD and the one computed using GRLWEAP as shown in Figure 8.17 (c), where the three curves overlap. Moreover, the limit lengths as well are more accurate.

However, it is important to underline a key consideration: expanding the *LL* range may lead to a deviation from the physical interpretation of this variable. While this has no impact from an optimization point of view since the process is purely mathematical, but it becomes crucial when using the optimized data for other applications. For example, in analyses that involve pauses in pile driving, where setup time and resistance play a role, it is essential to carefully interpret the results. A thorough understanding of the implications of these values ensures that they are used appropriately in contexts where their physical significance is a critical factor.

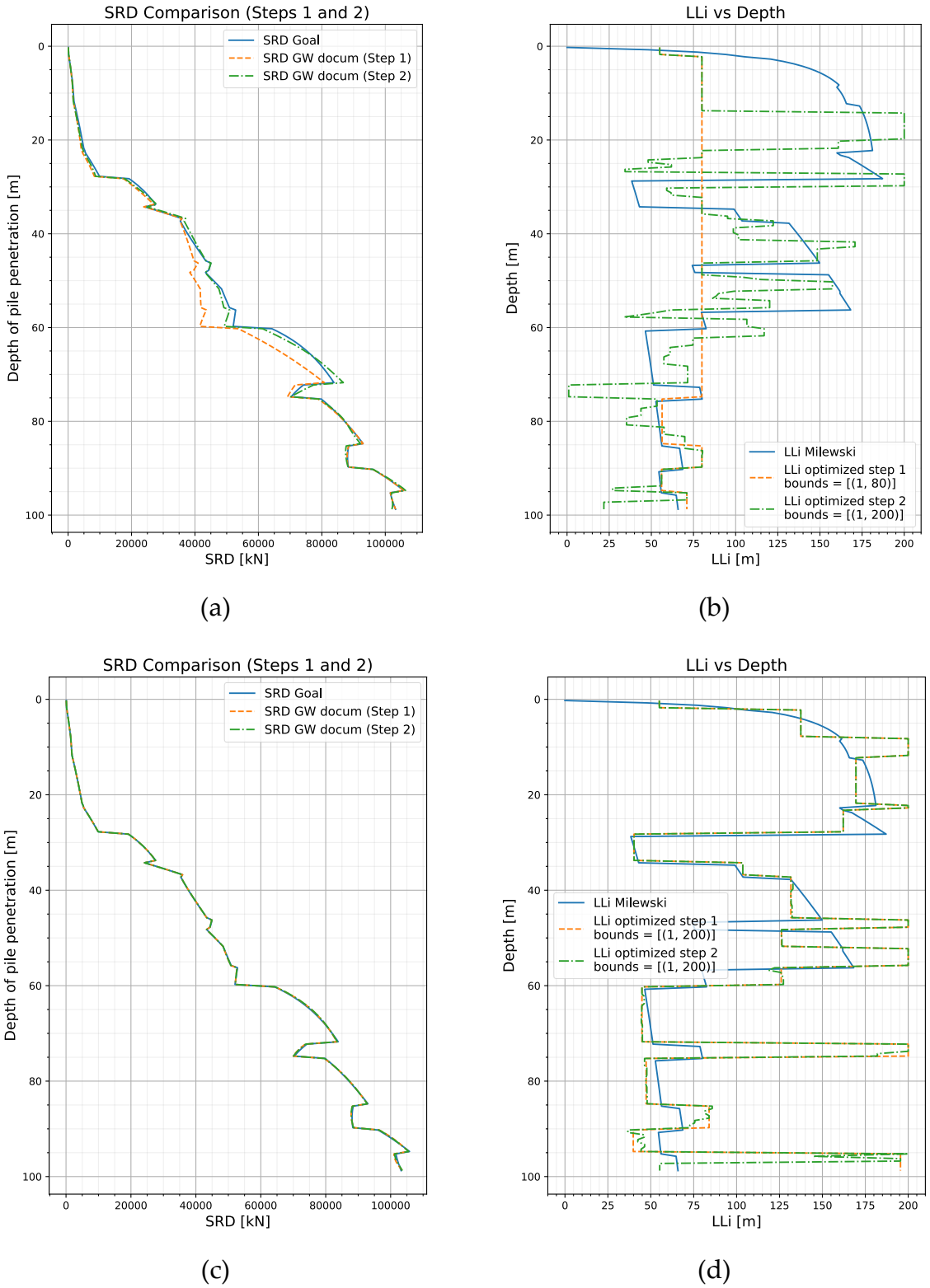

Figure 8.17: Influence of overly constrained boundaries on SRD profile (a), LL (b), and correctly constrained on SRD profile (c), LL (d).

8.3.1.2. Influence of number of blocks

The number of blocks used to subdivide each layer has a significant impact on the optimization. By partitioning the layers into blocks, the optimization process can target specific subsets of depth points, which influence both the efficiency and accuracy of the solution.

Increasing the number of blocks allows for finer adjustments within each layer, potentially leading to a more accurate fit to the goal SRD. However, this comes at the cost of computational efficiency. More blocks mean more parameters to optimize, which can slow down convergence and increase the computational cost. A smaller number of blocks reduces the number of parameters, speeding up the optimization process but potentially sacrificing precision in areas where SRD discrepancies are more pronounced.

With a high number of blocks, the optimization algorithm may overfit to local variations in the SRD values, particularly if the profile is highly heterogeneous. This can result in a model that fits the SRD perfectly at the discretized depth points but fails to generalize well across the entire profile. A smaller number of blocks mitigates this risk by forcing the optimization to focus on broader trends rather than minute details, but this may leave some discrepancies unresolved.

The number of blocks directly affects the global weighted loss, with more blocks leading to a more graded weighting of errors. This allows the algorithm to focus more on regions with larger SRD discrepancies. However, if the number of blocks becomes too large, the optimization might struggle to assess the overall behaviour of the profile, leading to possible inconsistencies in the global model.

For thicker layers, subdividing the layer into a larger number of blocks is generally more beneficial. Thicker layers have more depth points, which often exhibit significant variations in soil properties and SRD. If these layers are treated as a single block, as the case of step one, the optimization might fail to capture the finer variations, leading to inaccuracies in the model. Using more blocks allows for more localized adjustments and better fitting of SRD values at different depths, improving the overall accuracy.

In contrast, subdividing thin layers into too many blocks might not provide significant improvements. In such cases, fewer blocks are often sufficient to achieve a good fit, avoiding unnecessary complexity and computational cost.

Figure 8.18 illustrates the improvement of increasing the number of blocks per layer and all the consideration discussed previously. As shown in Figure 8.18 (a), (b), the use of only two blocks provides a certain level of accuracy, but increasing the number to six, Figure 8.18 (c), (d), especially in the upper part of the curve, allows the optimizer to achieve a more precise estimation of LL.

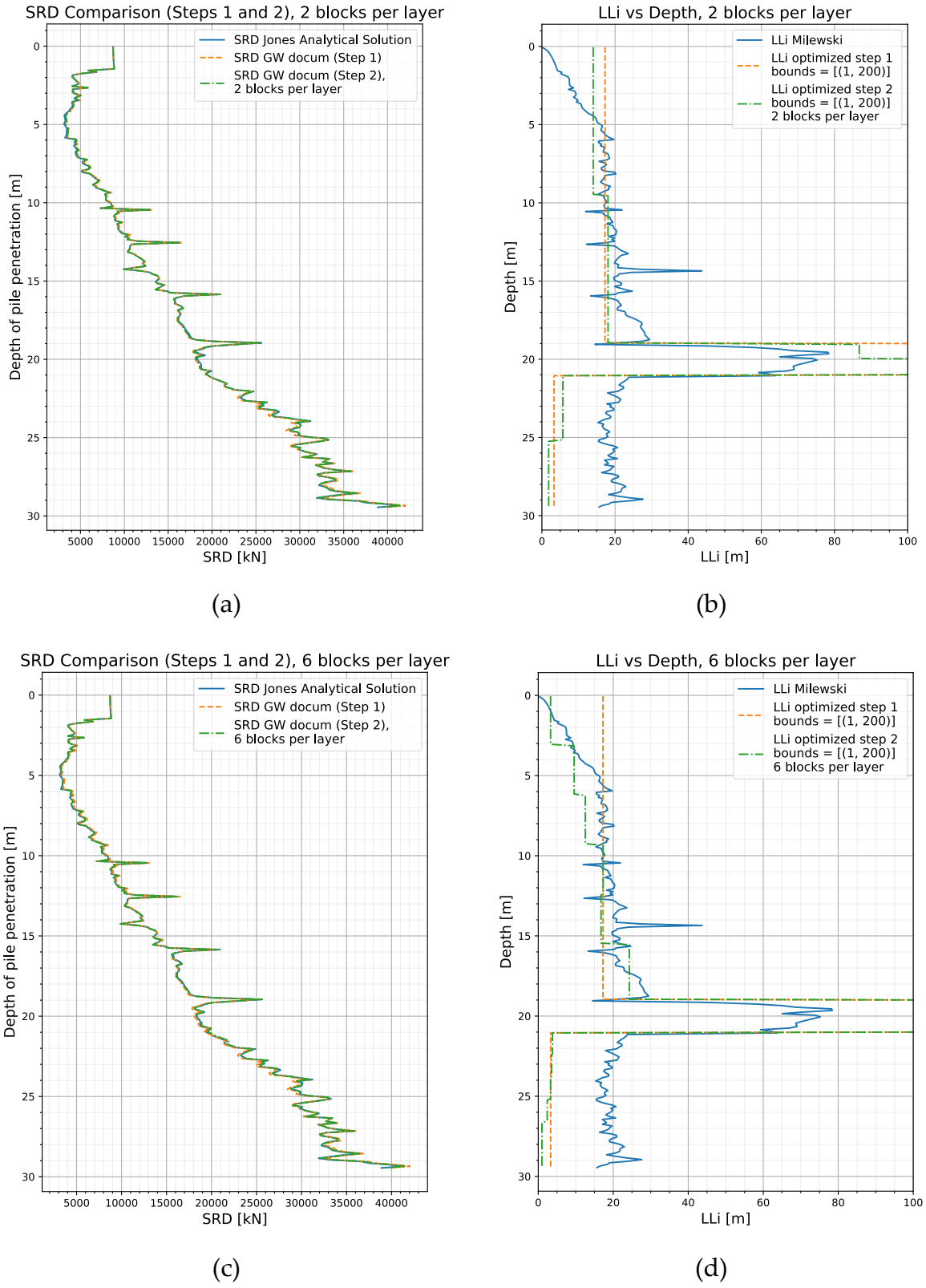

Figure 8.18: Influence of number of blocks: 2 blocks per layer SRD profile (a), LL (b), and 6 blocks per layer SRD profile (c), LL (d). Stratigraphy of loc P03 (see 7.6).

8.3.1.3. Computational time

Increasing computational cost, whether by widening the boundary constraints or increasing the number of blocks, directly impacts the running time of the algorithm. The trade-off between computational efficiency and accuracy must be carefully considered to ensure a balance between precision and practicality.

One of the most significant factors influencing the speed of the algorithm is the number of the model discretized depths. A finer discretization may improve accuracy but also leads to longer computation time. Therefore, it is essential to set a reasonable level of precision to avoid unnecessary computational burden.

For instance, the tests conducted in the previous sections used a discretization step of 0.5 meters for a total stratigraphy depth of 100 meters, resulting in 200 discretized points. The analyses also considered 19 layers, with a maximum of 5 blocks per layer. Under these conditions, the computational time for the algorithm remained within a reasonable range, typically between 5 to 10 minutes per analysis.

If the discretization step is reduced, the computational time increases significantly. The impact of this increase is particularly noticeable in cases where a very fine discretization is chosen, as the number of variables grows considerably, leading to longer processing times and higher computational demands.

For this reason, users must carefully evaluate whether a given discretization step provides sufficient accuracy to capture the SRD profile effectively. It is crucial to find a balance between numerical precision and computational efficiency to ensure that the optimization remains feasible without unnecessarily prolonging the analysis.

8.3.2. Considerations about the method

Performing this kind of analysis somewhat distances one from the physical meaning of the parameters, as the focus is on seeking values that reprice the target curve. It is therefore interesting to analyse the results of the optimisation process, asking whether the results have any meaning.

By comparing the limit lengths obtained using Milewski's method with those derived from optimizing a method where the formula applies correctly, such as A&H (Figure 8.17 (d)) or Jones in TS or ES approach (Figure 8.15 (b), (d)), one can note a similarity.

This suggests that the solution for achieving an exact match with the target curve in this specific approach is likely unique. Since the optimizer can select only a single value of *LL* for each layer, it sets a value that best represent the given range, effectively acting as an average of Milewski's limit length for the block. This approach is the more accurate as the variability of the limiting lengths in the layer is low.

9 Back Analysis of a Real Case

Accurate pile driveability predictions are crucial for installation contractors when selecting a suitable hammer to drive the pile to the required depth. Back-calculations can be essential tools in verifying the reliability of theoretical and empirical prediction methods used in driveability analyses. By analysing pile driving data obtained from pile driving records or monitoring systems, engineers can assess the accuracy of the design, confirm installation feasibility, and refine parameters for future analyses.

Beyond verifying predictions, back-analyses are fundamental for validating design assumptions, like the adopted geotechnical model, and the computed soil resistance. Moreover, since SRD is linked to pile bearing capacity, accurately estimating this parameter through back-analysis provides a crucial confirmation of pile's axial capacity. Given that resistance during driving is always lower than the long-term resistance, this process enhances confidence in the design.

Back-analyses are typically carried out by collecting and analysing in-situ pile driving data, including hammer energy and blow count per penetration depth. These data are recorded using pile driving monitoring (PDM) systems or dynamic testing techniques such as pile driving analyser (PDA). Engineers then compare the recorded values with theoretical predictions from wave equation analyses to assess the accuracy of key parameters in the driveability analysis, including the geotechnical model and the damping. The SRD is back-estimated by separating the total measured resistance into its static and dynamic components using signal-matching techniques.

This section aims to perform a back-analysis of a real case study, with a primary focus on obtaining an SRD profile that reproduces the recorded blow counts. It was chosen to focus on SRD modelling since it is the most influential factor in driveability analysis and of particular importance since it provides important highlights on bearing capacity.

For the case in hand, 4 piles have been considered. A single CPTu is provided and considered as representative of the entire site where the pile has been installed. The CPTu was particularly useful as input data for the Alm and Hamre method, while not necessary if Stevens was considered. Nevertheless, CPT data are fundamental for soil geotechnical modelling, which is required as input for Stevens's method as well.

Moreover, the driving data available, represented in Figure 9.1, included the number of blows, the hammer energy and the stroke required for each advancement step.

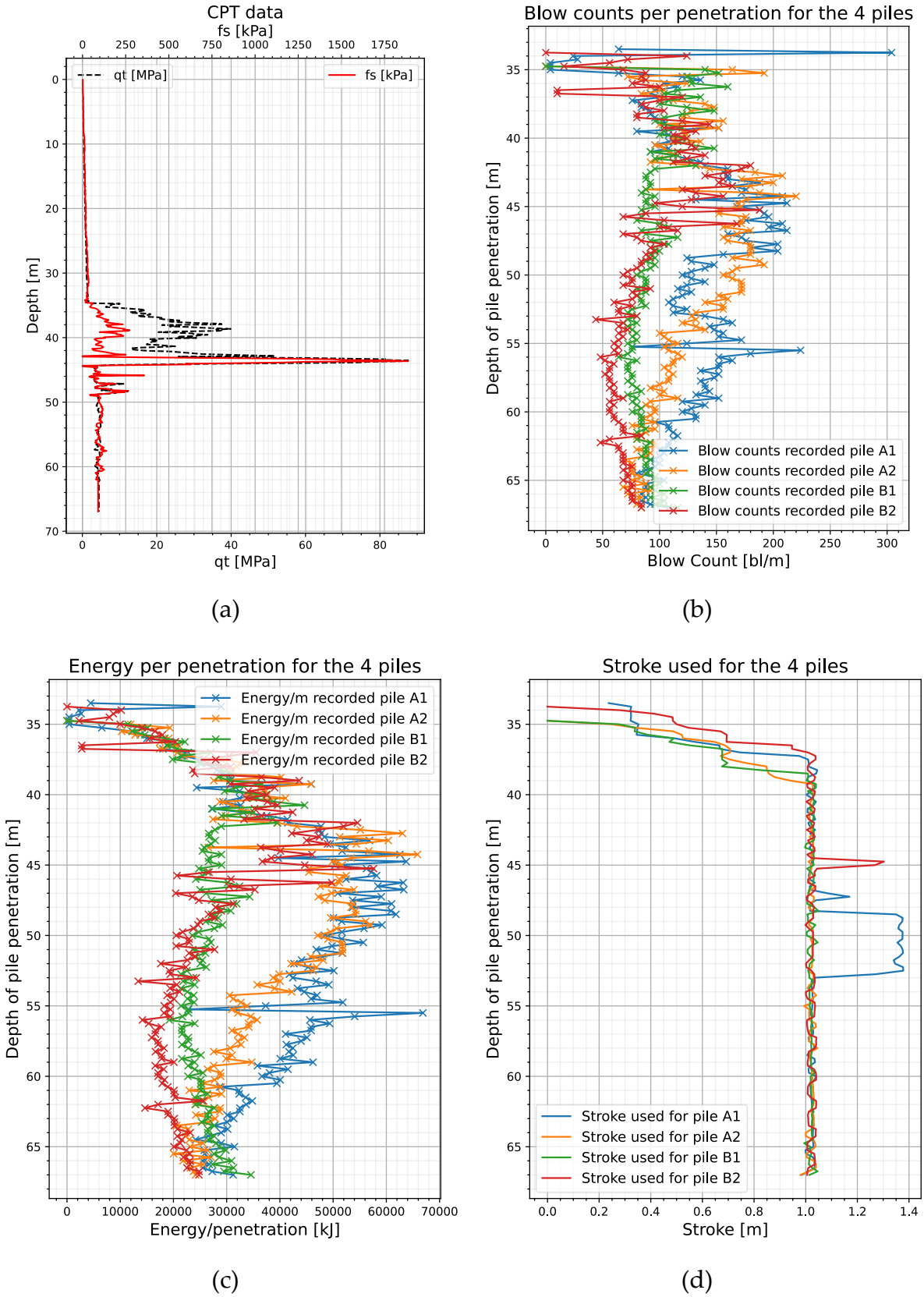

Figure 9.1: CPT data (a), blow counts recorded (b), energy per penetration (c), stoke (d) for the four piles.

Finally, pile geometry, target penetration and hammer model were also provided and reported in Table 9.1.

Table 9.1: Pile data for the back analysis.

Pile Name	Length $[m]$	Thickness $[mm]$	Diameter $[mm]$	Target Penetration $[m]$	Self-Penetration $[m]$	Hammer Model
A1	101	50.8	1828.8	67	33.50	MHU-600B
A2	101	50.8	1828.8	67	34.75	MHU-600B
B1	101	50.8	1828.8	67	34.75	MHU-600B
B2	101	50.8	1828.8	67	33.75	MHU-600B

It must be underlined that the CPT data from the in-situ test provided recorded values only up to a depth of 62 metres, while the piles were driven up to 67. For that reason, the values of sleeve friction and base resistance in the 5 remaining metres were assumed constant and equal to their corresponding last recorded value.

The aim of the back analysis is to determine a SRD such that, when used in driveability analyses, could be able to reproduce the blow counts recorded.

If the recorded and predicted blow count profiles align, then the assumed SRD is probably the one that actually reproduce soil behaviour observed during driving at the tip of the pile and the other factors affecting the response are not far from the real ones. In case not, the input SRD (as well as the other parameters that contribute to its computation) must be adjusted in order to achieve better agreement.

Before detailing the procedure undertaken, a clarification regarding the interpretation of the CPT at hand is necessary. According to Robertson's SBT classification, [15], the stratigraphy consists of the layers outlined in Table 9.2:

Table 9.2: CPT interpretation according to Robertson SBT.

SBT_n zone	SBT description	$z\ start\ [m]$	z end [m]
2	Clay – organic soil	0	8.8
3	Clays: clay to silty clay	8.8	34.1
6	Sands: clean sands to silty sands	34.1	44
5	Sand mixtures: silty sand to sandy silt	44	50
5	Sand mixtures: silty sand to sandy silt	50	67

Analytical methods for computing SRD provide different formulations to model the resistance depending on whether the soil behaves in a cohesive or granular way. In the case of the lower part of the stratigraphy, beyond 44 metres, the behaviour is not univocally defined, as silty soils can exhibit cohesion under certain conditions.

However, as a first step, it was decided to adopt the geotechnical model included in the original project data, which is summarised in Table 9.3.

Table 9.3: Original geotechnical model adopted initially for the back analysis.

Geological Unit	Behaviour Type	$\gamma' \left[\frac{kN}{m^3}\right]$	$z\ start\ [m]$	z end [m]	$\varphi'[deg]$
Very soft clay	Cohesive	6.5	0	8.8	-
Very soft clay	Cohesive	5.5	8.8	34.1	-
Medium to very dense silica sand	Granular	10.5	34.1	44	35
Stiff to hard clay	Cohesive	8	44	50	-
Hard clay	Cohesive	7	50	67	-

For the first trial of the back analysis, the Alm and Hamre method for the computation of SRD was employed, utilising the Milewski approach to analytically determine correct values of limit lengths, which were then given as input in GRLWEAP to perform the driveability analysis. Quake and damping factors were set as their typical standard values: 2.5 mm for shaft and toe quake, 0.25 s/m for shaft damping and 0.5 s/m for tip damping, for all soil types. The procedure adopted to run the analysis in GRLWEAP is the same methodology described in section 7.6.

The results obtained are illustrated in Figure 9.2. In this trial case, the results show a significant discrepancy with the recorded data. Specifically, in the lower part of the curve, the trial SRD, after the wave analysis, is not able to provide a blow counts profile that reproduce the recorded data.

For piles A1 (Figure 9.2 (a)) and A2 (Figure 9.2 (b)), the recorded blow counts continuously decrease below 50 meters, while for piles B1 (Figure 9.2 (c)) and B2 (Figure 9.2 (d)), the profile initially decreases before rising again. This observed pattern is not accurately captured by the results of any trial analysis conducted.

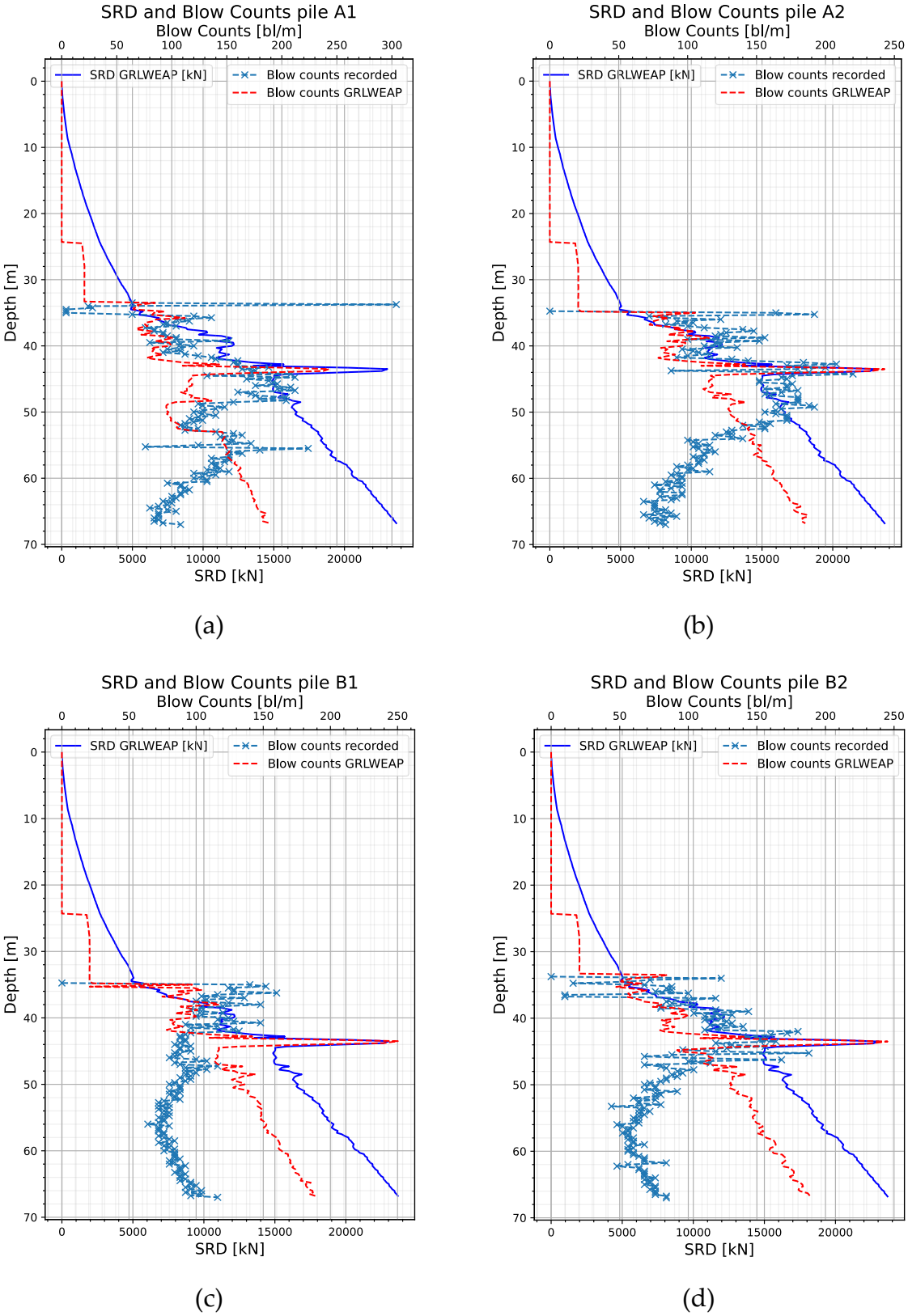

Figure 9.2: SRD using A&H method, blow counts obtained by wave analysis and recorded during installation for the 4 piles, initial stratigraphy considering cohesive soils (44–67 m).

To address this inconsistency, a revised analysis was conducted by updating the geotechnical model. As previously mentioned, the *SBT* classification for that region identifies the material as silty sand. Given that in the first trial the worst results occurred within this region, a different soil behaviour was assumed for the second analysis. In the revised approach, soil layers below 44 metres were considered to behave as granular material, unlike the previous step. The friction angle was assumed to be the same as the clean sandy layer immediately above. The updated geotechnical model is summarised in Table 9.4.

Table 9.4: Geotechnical model adopted for the back analysis.

Geological Unit	Behaviour Type	$\gamma' \left[\frac{kN}{m^3}\right]$	$z\ start\ [m]$	z end [m]	$\varphi'[deg]$
Clay	Cohesive	6.5	0	8.8	-
Clay	Cohesive	5.5	8.8	34.1	-
Sand	Granular	10.5	34.1	44	35
Sand	Granular	8	44	50	35
Sand	Granular	7	50	67	35

Following the same procedure described for the first attempt, the Alm and Hamre method was once again used to compute a new estimate of SRD which, given as input to GRLWEAP, produced the results shown in Figure 9.3 for the four locations.

The second analysis carried out better results than the previous one. Notably, in the final part of the profile, the predicted blow counts now exhibit a decreasing trend, aligning more closely the recorded data. However, a discrepancy remains, particularly for piles A1 and A2. To further improve accuracy, it was decided to develop a new approach aimed at obtaining more precise estimates.

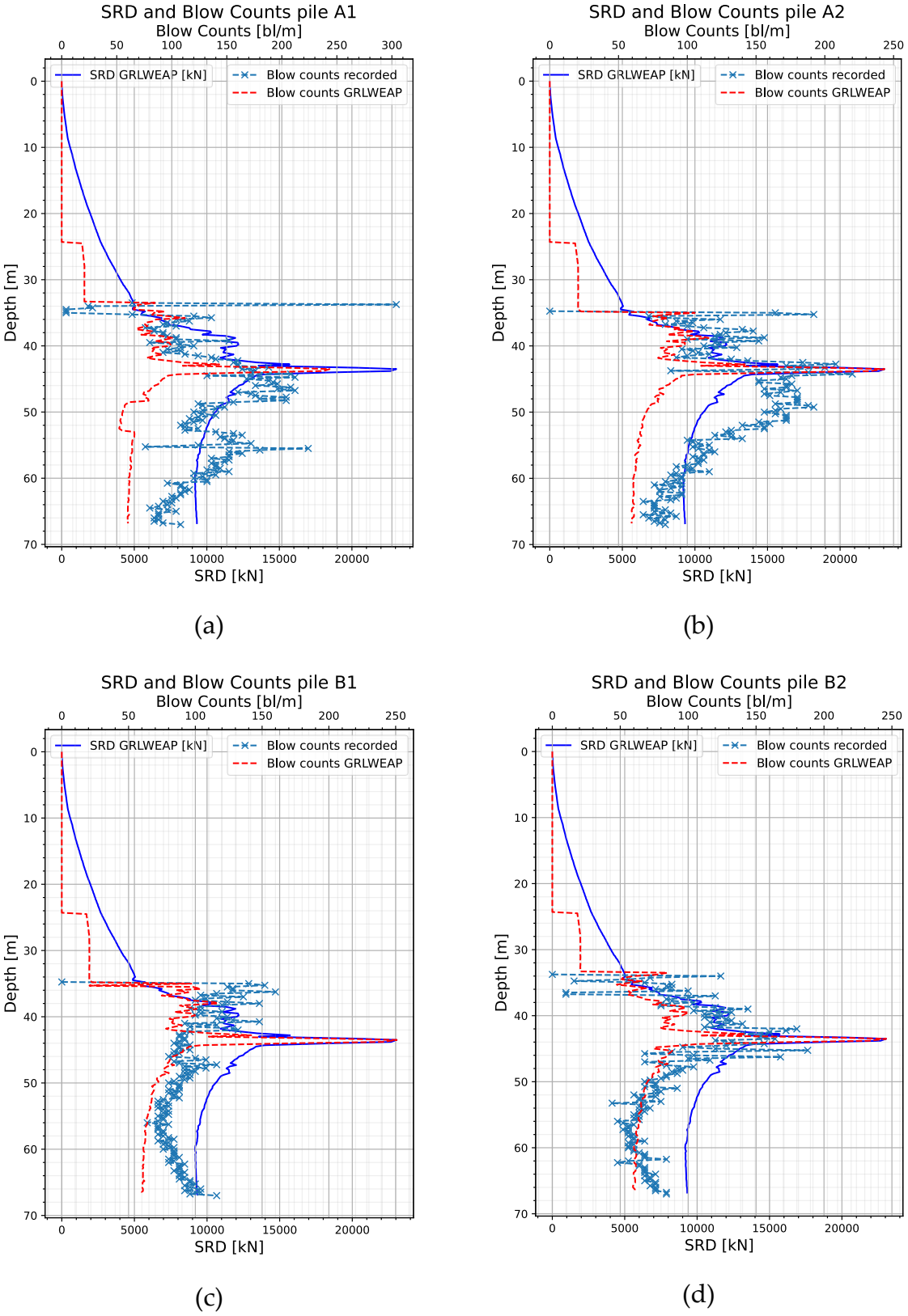

Figure 9.3: SRD using A&H method, blow counts obtained by wave analysis and recorded in installation for the 4 piles, updated stratigraphy considering granular soils (44–67 m).

9.1. Formulation of a new procedure for SRD back estimation.

Since the results in Figure 9.3 were not satisfactory, it was essential to investigate the possible causes.

One potential reason is the choice of the method used to describe soil resistance, which may not accurately capture the actual behaviour of the soil. Another explanation concerns the limitations of CPT data in representing soil characteristics, as a single test cannot account for local variations that differ from site to site. Additionally, incorrect assumptions regarding damping values could have affected the results, as damping influences the amount of energy dissipated and effectively transferred to drive the pile. Finally, another possible cause is the inherent limitations of Smith's wave equation theory, which may not be fully adequate for modelling a problem as complex as the pile driving.

The primary reason for the discrepancy between the recorded and predicted blow count profiles was attributed to the method used for calculating SRD. Thus, a new approach was developed to obtain a more representative SRD value.

As detailed in section 7.4, the input required in the "S window" for the customized parameters (Figure 7.2) are: f_{si}, q_b, f_{su}, LL_i, f_l, f_0 and the quake and damping coefficients for each discretized depth. The new method aims to achieve an estimate of SRD so to replicate the recorded blow count profile in the most accurate may. To accomplish this, all the previously mentioned parameters must be optimized. This is because, while the procedure implemented in chapter 8.2 aimed to reproduce an analytical method, where explicit formulas were provided for the computation of initial and residual friction as well as base resistance, in this case instead the goal is to replicate an unknown method, meaning that f_{si} and q_b are also unknown.

On this basis, attempting to optimize a six-parameter process, in which the parameters interact through highly non-linear equations, such as those in the GRLWEAP formulation (Eq. 6.9 and Eq. 6.10), poses a significant challenge. The complexity is further amplified by the fact that these parameters continuously change with each iteration, corresponding to the advancement of the pile tip, making a direct optimization approach virtually unfeasible.

It was therefore necessary to think of a procedure that would simplify this process, in particular by reducing the number of unknowns in the various stages, by making use of methods that had been considered previously and found to be effective.

The method comprises 6 steps, and GRLWEAP analysis is involved twice to elaborate SRD inputted and provide the corresponding blow counts profile.

One fundamental achievement is that the method starts directly from CPT data (shaft friction and base resistance) and produces a final result in terms of SRD profile of the

stratigraphy. The process begins by computing an initial tentative value of SRD, which is then used in the software to generate a blow count profile. These two quantities are analysed to establish a relationship that defines a target SRD. Based on this target SRD the input parameters required by GRLWEAP are optimized so that, in the subsequent wave equation analysis, the resulting blow count profile better aligns with the recorded data.

The steps of the procedure can be summarized as follows:

- Step 1: preprocessing of CPT data;
- Step 2: GRLWEAP analysis to obtain the blow count profile;
- Step 3: unified bearing graph computation;
- Step 4: estimate of target SRD;
- Step 5: reproduction of target SRD through optimization;
- Step 6: GRLWEAP run to check the final results in terms of blow counts profile.

In the following paragraphs the core steps of the process will be deepened and explained in detail.

9.1.1. Pre-processing of CPT data

The first step of the process involves the computation of f_{si} and q_b. It was determined that the most effective approach for preprocessing these data was to relate them to an established method for the computation of SRD. Since Alm and Hamre provides a sufficiently accurate SRD profile for a wide range of conditions, adopting it as initial estimate ensures reliable values for both the initial shaft friction and base resistance.

With Alm and Hamre chosen for preliminary SRD computation, it is natural to assume f_0 = 0.001 for all depths, as suggested by Milewski's method. Additionally, it is assumed that soil degradation begins as soon as the tip advances, leading to f_L being zero. However, this assumption can be adjusted as needed.

This preprocessing phase leads to the computation of all the initial quantities required by GRLWEAP to perform the driveability analysis, which, among other outputs, provides the tentative blow count profile.

From the analysis results (Figure 9.3) it is evident that a reasonable agreement, though not entirely satisfactory, is already achieved simply using Alm and Hamre's and Milewski's input values. However, this initial alignment cannot be assumed to hold universally. Therefore, the remaining steps of the procedure aim to further refine the results, ensuring improved accuracy in the final outcome.

9.1.2. Unified bearing graph computation

This phase begins with the observation that the blow counts obtained using Alm and Hamre's method do not perfectly match the recorded values. This discrepancy indicates that the SRD computed by the method does not fully represent the actual soil conditions.

Analysing the relationship between blow counts and the influencing factors, it becomes clear that the number of blows depends on several key variables. First and foremost, it is a function of SRD, as higher soil resistance requires more blows to advance the pile. Secondly, it depends on penetration depth, since increased penetration leads to grater energy dissipation, necessitating more energy for the same resistance. Then, they depend on the amount of energy given as input to the system.

Blow counts are also influenced by pile length, as a longer pile implies a propagation of the wave at greater distances along the pile, though higher dissipation. The axial stiffness of the pile also plays an important role, as it contributes to the elastic deformation during driving. Finally, soil damping also impacts blow count, as it influences the dissipation of energy during installation. It can be therefore written the following relationship:

$$bc = f(SRD, p, L, EA, E, D), \tag{9.1}$$

Where bc is the number of blows, p is the pile penetration, L the pile length, EA the axial stiffness, E the hammer energy and D the damping.

The most straightforward approximation of this relation is to correlate the number of blow counts directly to the SRD value, assuming that the inverse relation also exists.

Eq. 9.1 reduces then to $bc \cong g(SRD)$ and $\exists\ g^{-1}(bc) \cong SRD$.

The goal is then to find the $g^{-1}(bc)$ function, which describes the soil resistance in terms of blow counts.

What is known is that blow counts and energy are related by some function, h, such that: $bc = h(E) \mid E = h^{-1}(bc)$.

Before the development of wave equation theory, engineers assessed pile capacity using empirical formulas relating the hammer's energy to the dynamic resistance of the pile. These formulas, known as dynamic formulas, include examples such as the Gates formula and the Engineering News Record (ENR) formula (see [17]).

The relation introduced by these formulas can be written as: $F_D = m(E)$, where m is a function that correlates the dynamic force sustained by the soil F_D. This dynamic force, assuming negligible the dynamic contribution of the total soil resistance, can be assumed to behave as the SRD, leading to the following relation:

$$SRD \cong m\left(h^{-1}(bc)\right) \cong\ g^{-1}(bc) \tag{9.2}$$

Therefore, a relation that links soil resistance and blow counts must exist.

Given the results obtained in Figure 9.3, a relationship between the computed SRD and the blow count profile obtained, enabling the identification of the g or g^{-1} function mentioned earlier. This relationship can be determined by plotting the number of blows against the SRD, directly linking the blow count to a corresponding soil resistance value. This makes it a useful tool for the following stages of the back analysis. Such plots remind the concept of bearing graph, with the key difference that they are not specific to depth or energy levels. Instead, they represent a single relationship applicable to the entire driveability analysis.

A bearing graph is a graphical representation that illustrates the relationship between the pile driving resistance and the blow count per unit of penetration. The curve depicts how the blow count varies with changes in the pile's SRD. To generate a bearing graph, an iterative process is followed in which different assumed bearing capacities are tested in a driveability model for different depths. The corresponding blow counts are calculated for each assumed capacity, forming a relationship between these two variables. Basically, for every assumed capacity, a wave equation analysis is performed for a defined hammer energy and damping coefficient set. The result is a series of curves that relates the soil resistance to the number of blows per set. An example is provided in Figure 9.4.

Before installation, bearing graphs help determine whether a pile can be driven to the required depth using the available hammer without causing damage to the pile or surrounding structures. They also aid in selecting the right pile driving equipment by illustrating the energy needed to achieve the desired penetration for a given soil resistance.

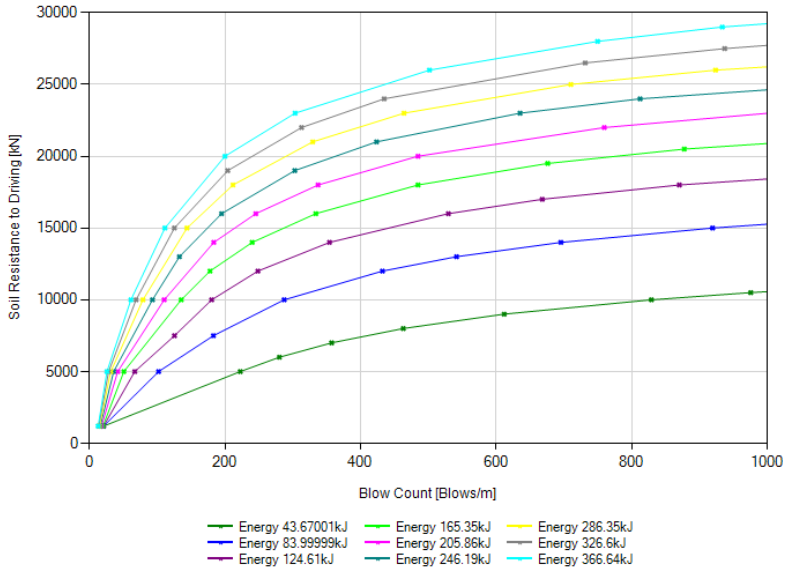

Figure 9.4 : Example of bearing graph. Source [24].

For each investigated location, a specific relation, referred to as the bearing graph, is established, assuming it holds for the entire driveability analysis. This relationship is generated based on data from the corresponding pile, being the hammer energy already known. The SRD values are derived using the Alm and Hamre method, while the blow counts are obtained from the wave analysis conducted in GRLWEAP. Upon analysing the bearing graphs for different locations, a linear relationship was found to provide a sufficiently accurate fit. However, a bi-linear function was adopted to account for self-penetration observed in the software, which occurred earlier than in the actual installation. This discrepancy suggest that the A&H method overestimated soil resistance in that region. The results in terms of bearing graphs are presented in Figure 9.5.

For each case, a linear regression was performed on the data points excluding those corresponding to self-penetration (where blow count is zero). From this, a scaling factor represented by the slope of the curve was derived. This parameter establishes a linear relationship between the input SRD in GRLWEAP and the resulting blow count profile.

This scaling factor remains consistent across all cases as the predicted SRD values for the four sites is the same (Alm and Hamre method based on the same CPT input data). What changes is the number of blows given as output by the wave equation analysis. This is because the number of blows depends on the energy per blow provided to the hammer which exhibit to be slightly different in the four cases, as it can be observed in Figure 9.1 (d). As a result, the four bearing graphs exhibit a comparable trend in each case.

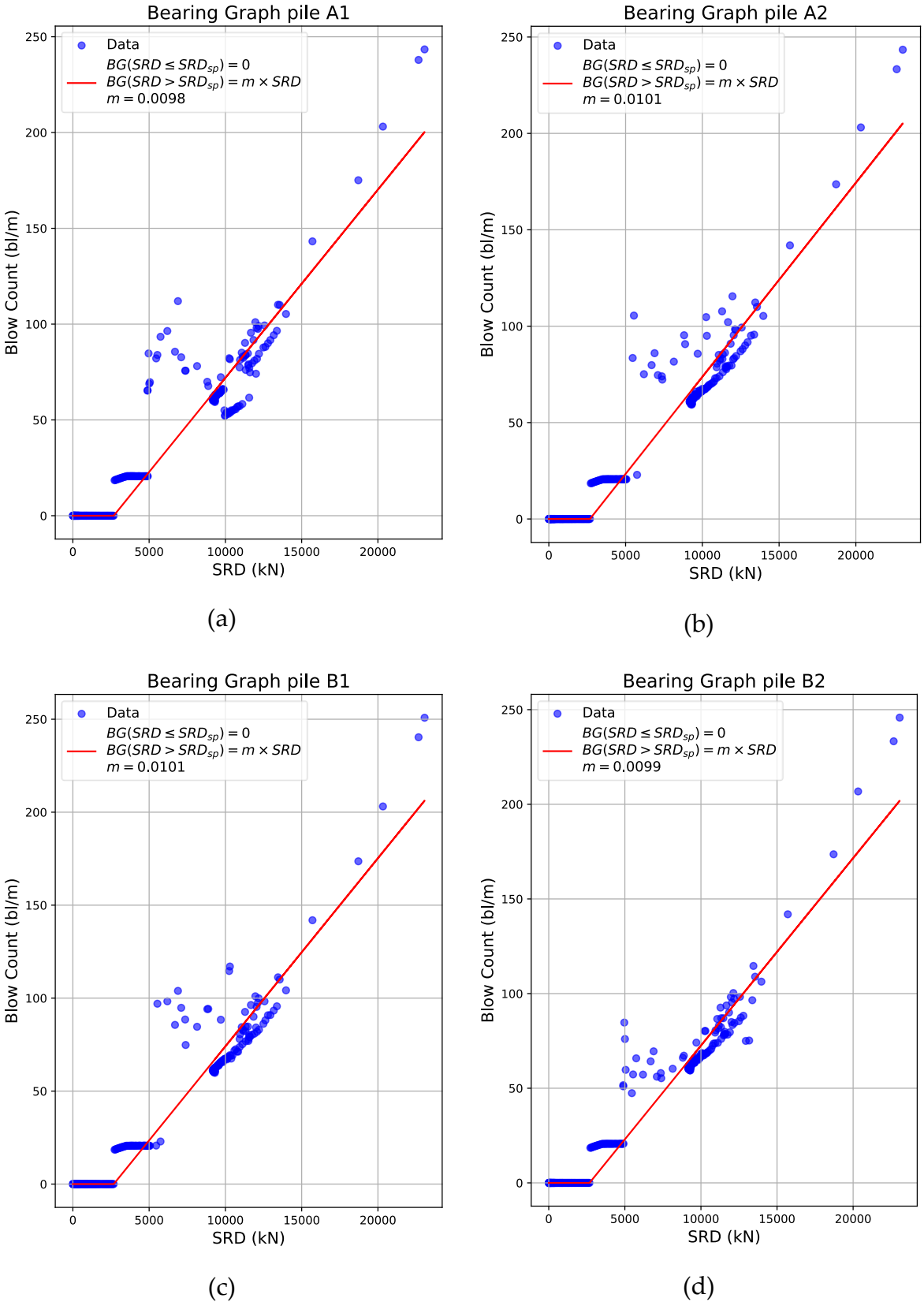

Figure 9.5: Bearing graphs obtained for the 4 cases by means of bi-linear regression.

9.1.3. Definition of target SRD

Once the relationship between SRD and number of blows is determined, the target SRD that best represents the actual soil resistance can be estimated, knowing the recorded blow counts. The same bearing graphs obtained in the previous section are used, but in this case, the SRD is derived directly from the actual number of blows.

Recalling the notation in Eq. 9.2, the function used to compute the target SRD is $m\left(h^{-1}(bc)\right) = g^{-1}(bc)$, which is the inverse of the one plotted in Figure 9.5: $bc \cong g(SRD)$. As an example, for pile A1 the relation used to find the target SRD is the following:

$$SRD \cong g^{-1}(bc) = \frac{bc}{0.0098} + SRD_{sp}, \tag{9.3}$$

where SRD_{sp} is the value of SRD corresponding to the weight of the pile and the hammer, so where the self-penetration stops and to proceed with penetration the hammer starts to work

This process yields a target SRD, which, compared to the initial profile obtained using Alm and Hamre method, provides the results presented in Figure 9.6 (green and blue curves).

9.1.4. Optimization of SRD profile

At this stage of the procedure, a target SRD is obtained, representing the estimated soil resistance for the specific location. However, to verify its accuracy, an additional analysis in GRLWEAP is required to compare the predicted blow counts with the recorded data. Since GRLWEAP does not allow to directly input SRD values but instead requires the f_{si}, q_b, f_{su}, LL_i, f_l, f_0 that reproduce it, an optimization process is necessary to determine these values.

To achieve this, the standard numerical approach presented in section 8.2 had to be updated and improved. A new class was developed in order to generate an SRD profile in cases where no predefined analytical method is selected. This posed a challenge, as the analytical approaches provided some fundamental input quantities, namely f_{si}, q_b and f_{su}, which are required not only by GRLWEAP but also by the algorithm in the standard optimization procedure.

To address the issue of missing inputs, it was decided to use the pre-processed data from the initial step of the procedure. By doing so, only two parameters remained unknown, reducing the complexity of the optimization process.

The newly developed optimization class, referred to as "custom," takes as input the pre-processed data (f_{si}, q_b) and the target SRD profile. It then performs an optimization in two parameters for each layer of the input stratigraphy, identifying the optimal values of f_{su} and LL_i representative of the considered depths, that best

reproduce the target SRD. This approach ensures that the missing input values are determined, providing a complete set of parameters required for GRLWEAP.

The final step of the process involves running the wave equation analysis using the optimized values. This allows for a final validation of the procedure by comparing the computed blow count profile with the recorded data, ensuring that the estimated SRD accurately represents the actual soil resistance conditions.

The decision to use f_{si} and q_b from the Alm and Hamre method is based on their effectiveness in better reproducing SRD. However, by optimizing only two parameters instead of four, imposing f_{si} and q_b fixed, the degrees of freedom in the solution decrease, thereby reducing the size solution space.

If values too far from the actual solution were imposed, the optimizer might be unable to find a valid combination for the remaining two parameters (f_{su} and LL_i). In such cases, no feasible solution would exist because the fixed values of f_{si} and q_b would exert excessive influence on the final result, preventing the optimizer from accurately reproducing the target SRD. Nevertheless, it was observed that enlarging the boundaries for the two parameters improved the accuracy of the results, as a narrow constraint interval limited the optimizer's ability to adjust a custom SRD based on two fixed parameters.

Moreover, it is more coherent to use the same inputs employed for the computation of the first tentative SRD used also to obtain the bearing graph, ensuring a structured optimization process of all the four parameters in 2 steps (the first two parameters in the preprocessing and the last two in the optimization routine).

Despite the pre-processed values have a significant impact on optimization performance, an increase in SRD accuracy is achieved by the end of the routine. The results of the custom optimization based on the target SRD, obtained through a manually computed bearing graph for the four piles, are shown in Figure 9.6.

It is also important to emphasize that the initial SRD (blue dashed line in Figure 9.6) is the same for all four cases, as it is derived from a single available CPT. However, the target SRD is specific to each pile, as it is back calculated from the recorded number of blows for that particular location.

Once the optimization is completed, all the required parameters are determined, allowing the GRLWEAP analysis to be conducted. The improved results in terms of blow counts are presented in Figure 9.7.

The results show an increase in accuracy in the blow counts, proving that the method is efficient and able to improve back analysis quality.

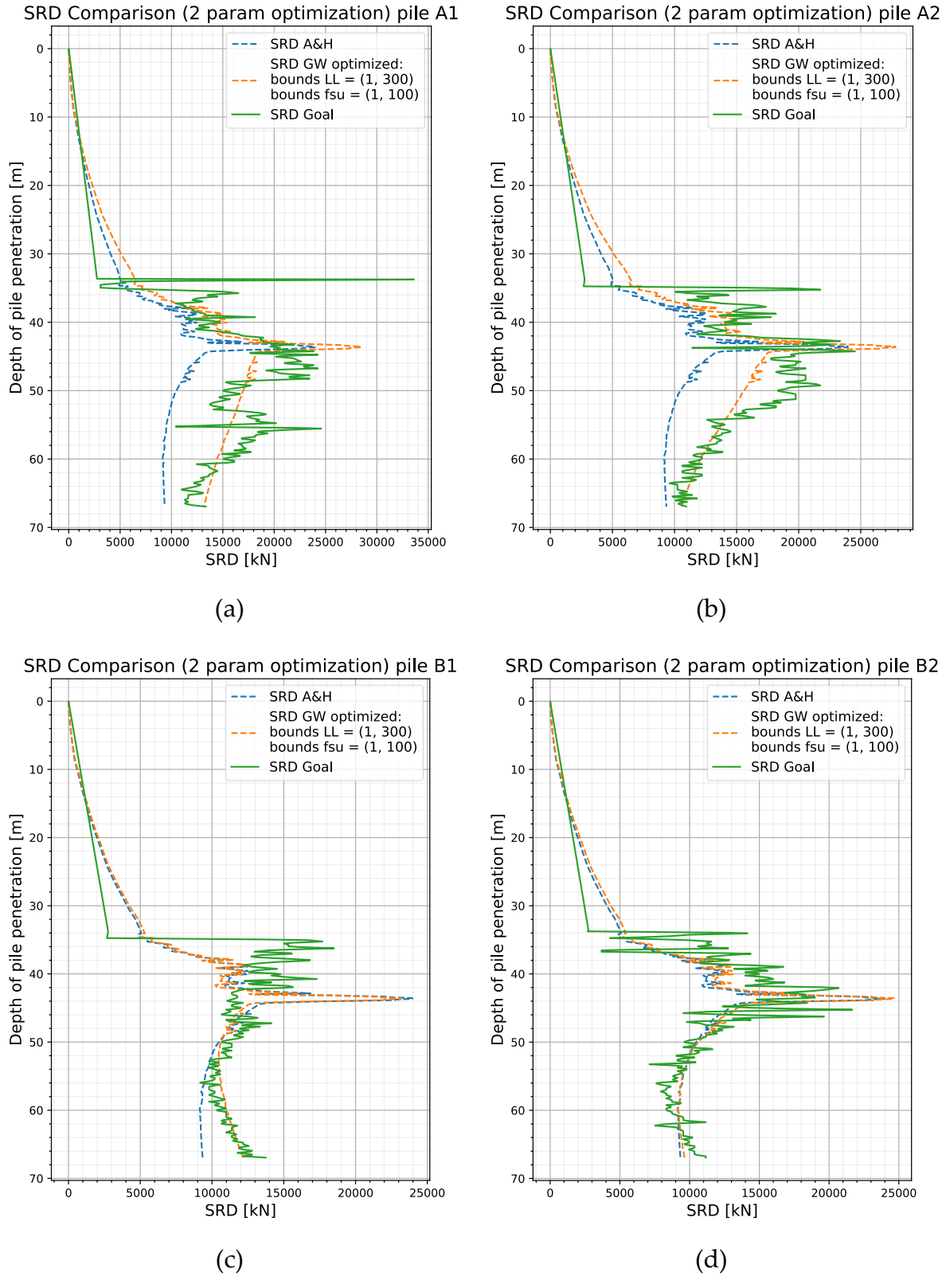

Figure 9.6: Comparison of SRD computed by A&H, target SRD obtained by bearing graph and optimized based on the target SRD.

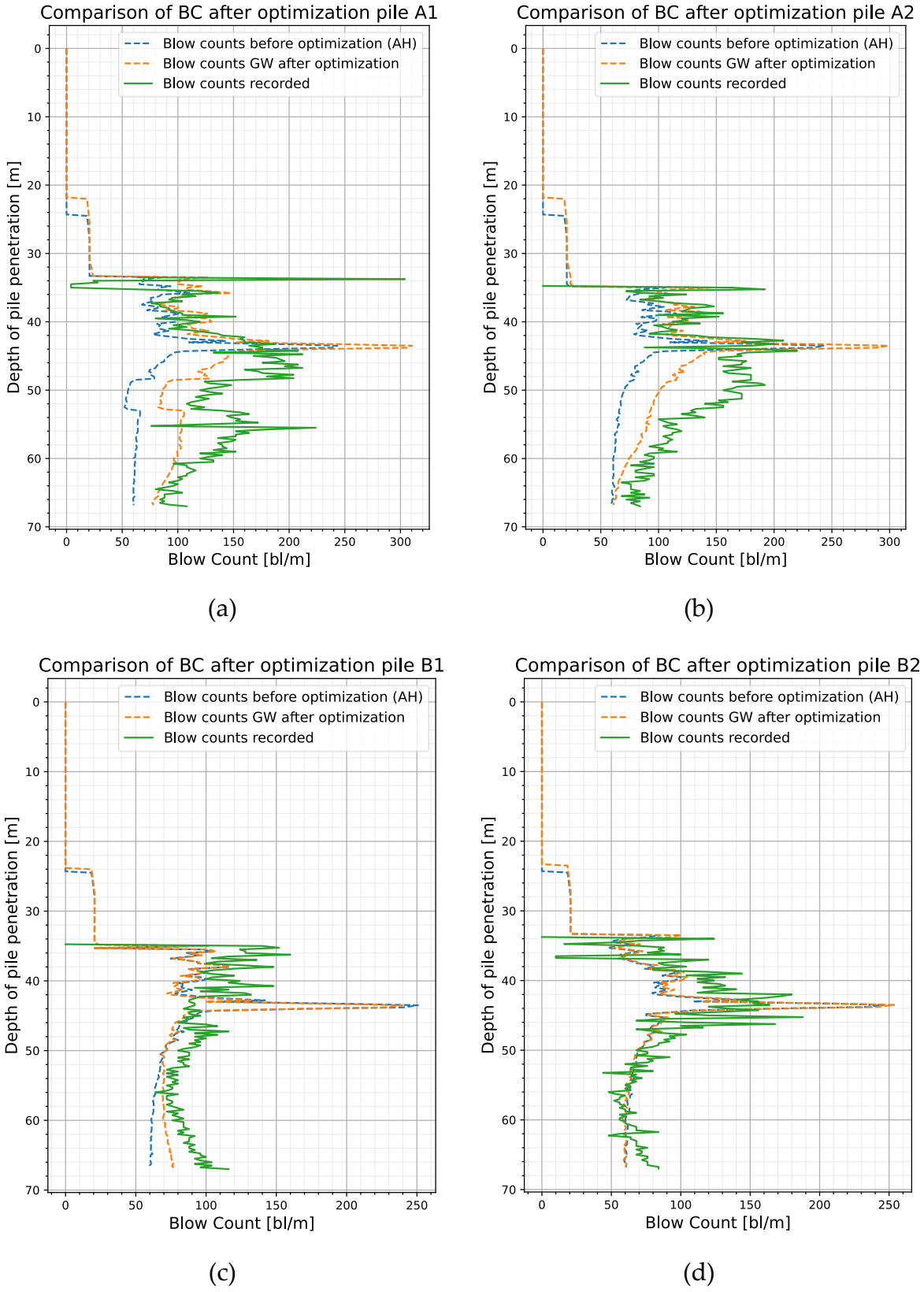

Figure 9.7: Comparison of Blow counts obtained by A&H SRD, optimized SRD and recorded data.

9.2. Limitations of the method

While for the case of piles B1 and B2, the results were extremely satisfactory, for piles A1 and A2, the predictions were less accurate.

Analysing the results in Figure 9.6, it appears that the optimizer struggles to find an optimal combination of f_{su} and LL to match the target SRD. This makes it worthwhile to examine the obtained values for each depth, choosing as example the pile A1, illustrated in Figure 9.8.

Notably, in the upper part of the stratigraphy, the LL values reach the upper bound of the constraints, while the f_{su} values are at the lower bound. These results have physical significance, indicating that the resistance in the upper stratigraphy is insufficient to replicate the target SRD. Specifically, the high LL value attempts to delay degradation as much as possible, while a very high value of f_{su} = 1 suggests that no degradation must occur in the upper part of the stratigraphy in order to increase the cumulative shaft resistance when computed at deeper depths. However, this alone is insufficient to achieve the required resistance in the lower part of the SRD profile, where the optimized value is too low and the optimizer cannot find any solution to further increase the accuracy of the result, setting the setup factor to the upper bound.

The core issue appears to be that the f_{si} and q_b values do not adequately represent the target SRD. This could be due to one of two reasons:

1. The preprocessing phase is not functioning correctly and requires revision or replacement.
2. The input data do not accurately reflect the local soil conditions.

The latter issue was already mentioned at the beginning of this chapter and may explain the discrepancy between expected and obtained results. In fact, for pile B2, where the CPT is assumed to provide a better representation of soil conditions, the predictions were satisfactory.

A potential solution is to manually adjust the CPT input data to better capture the actual local conditions, even if this was not carried out in the work.

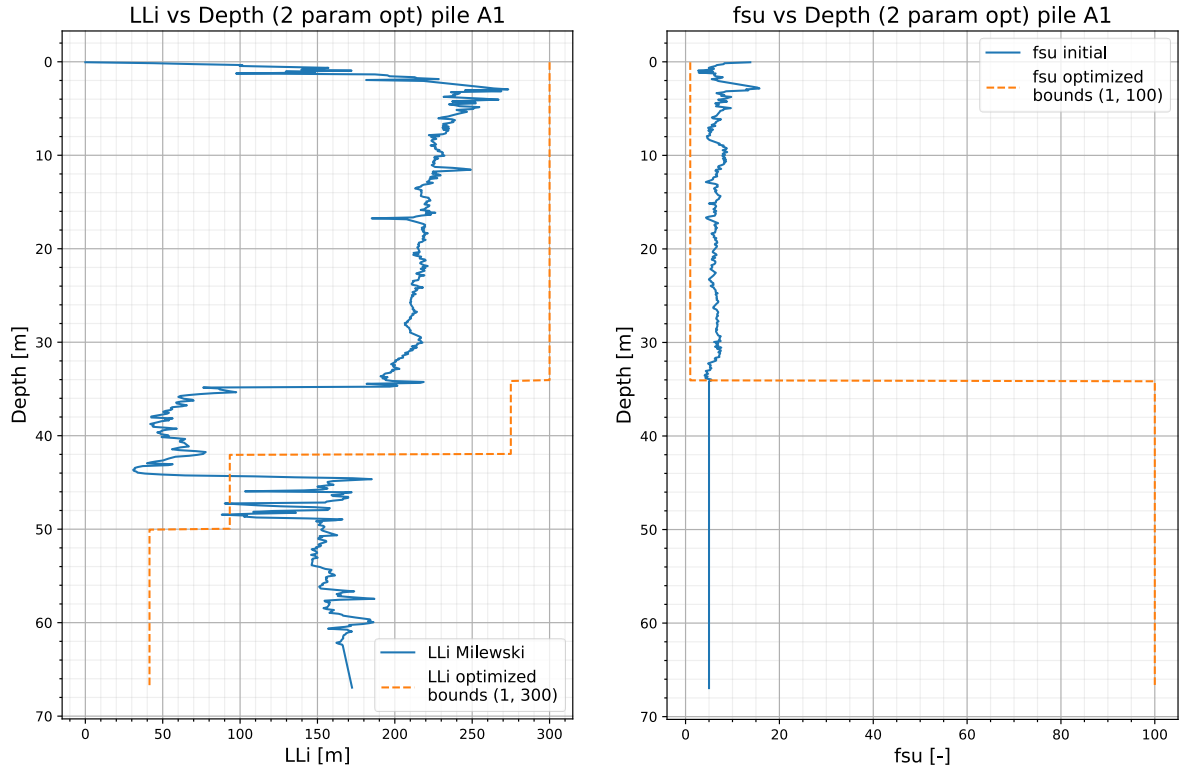

(a) (b)

Figure 9.8: Comparison of LL (a) and fsu (b) values plotted against depth before and after optimization for pile A1.

10 Conclusions and Perspectives

The study presented in this thesis has focused on the development of a generalised approach for integrating friction fatigue-based Soil Resistance to Driving (SRD) models within the GRLWEAP software. By addressing a key limitation in current driveability analysis methodologies, this study introduces a systematic procedure for translating analytical SRD models into a format that can be effectively implemented within widely used numerical tools. By aligning theoretical models with numerical simulation capabilities, this study enhances the reliability and applicability of offshore pile foundation design.

A comprehensive review of existing SRD models incorporating friction fatigue has been conducted. Additionally, the internal structure of the GRLWEAP software was analysed in detail to assess how it currently implements SRD calculations. A key achievement of this study is the development of an optimisation-based methodology to calibrate GRLWEAP input parameters so that they align with external SRD models. This approach provides engineers with a tool, that allows greater control over the design assumptions. By enabling the implementation of any analytical method, rather than relying solely on predefined numerical tools from a software provider, the suggested method developed in the study contributes to having a more conscious idea of the assumptions undertaken during the design.

Another key practical outcome of this work is the development of a systematic procedure for back-estimating SRD from driving records. This method enables the validation of design assumptions by analysing real-world pile driving data. Through the application of this technique to a real case study, it was demonstrated that this approach enhances the understanding of soil behaviour during installation and refine predictive models for future projects. A major advantage of this method is its independence from external software, relying solely on GRLWEAP for the solution of the wave equation, thing which could be hopefully substituted in future. In standard practice, back analysis typically requires numerical tools for signal processing or specialized software to analyse large sets of bearing graphs. However, the proposed procedure offers a more efficient and straightforward alternative, delivering accurate SRD estimates with greater simplicity.

While the findings of this research contribute significantly to offshore geotechnical engineering, it is not without limitations. First, the proposed optimisation methodology calibrates GRLWEAP input parameters solely based on finding the

optimal solution that better reproduces the target SRD. However, if the optimized parameters exceed their physically meaningful range, they may lose practical applicability, making them unsuitable for further analysis. This issue is particularly relevant in the context of the setup phenomenon, where soil strength recovers after a pause in driving. When driving resumes, if the limit length lacks physical significance, it becomes uncertain whether friction fatigue is correctly accounted for.

Another notable limitation, as previously discussed, is the strong dependence of the back-analysis method on pre-processed data. The preprocessing phase significantly influences the solution space, potentially constraining the optimization. While exploring an alternative preprocessing phase or optimizing directly in a four-dimensional space could improve the approach, the complexity introduced by the nonlinear interactions among input parameters (updated repeatedly throughout the optimization routine) made this impractical within the scope of this research.

The research opens several promising directions for future development. One potential improvement is the application of the methodology to different SRD models allowing for broader validation of the optimizer tool.

Another further development is to consider a more sophisticated functional form of $g(bc)$, which may better represent the relationship between SRD and blow counts. The assumption of a linear relationship is not always ideal, as higher SRD values should correspond to a rapid increase in blow counts, eventually reaching an asymptote at refusal. Polynomial or exponential interpolation functions may more accurately represent this behaviour. However, since the number of blows in the case study remained well below refusal, the linear regression was deemed sufficiently accurate for this analysis.

In conclusion, this contributes to offshore geotechnical engineering by developing a systematic approach for integrating different SRD models into GRLWEAP through an optimisation framework. The research provides practical tools for improving the accuracy of driveability and back analyses and offers insights into soil resistance estimation methods. Moreover, by bridging analytical models and numerical simulations, this work enhances the reliability of offshore pile design.

Bibliography

[1] Alm, T., & Hamre, L. (2001). Soil model for pile driveability predictions based on CPT interpretations. In *International Conference on soil mechanics and geotechnical engineering* (pp. 1297-1302).

[2] American Petroleum Institute, *Recommended Practice for Planning, Designing and Constructing Offshore Platforms*, API RP 2A, 12th Edition, (1981).

[3] Anusic, I., Eiksund, G. R., & Liingaard, M. A. (2016, May). Comparison of pile driveability methods based on a case study from an offshore wind farm in North Sea. In *Proceedings of the 17th Nordic Geotechnical Meeting Challenges in Nordic Geotechnic, Reykjavik, Iceland* (pp. 25-28).

[4] Chow, F. C., Jardine, R. J., Brucy, F., & Nauroy, J. F. (1998). Effects of time on capacity of pipe piles in dense marine sand. *Journal of Geotechnical and Geoenvironmental Engineering*, 124(3), 254-264.

[5] Fenske, C.W. and Hirsch, T.J. (1986) Pile driveability analysis. Planning and design of fixed steel offshore platforms. New York: Springer.

[6] Heerema, E. P. (1978, October). Predicting pile driveability: Heather as an illustration of the" friction fatigue" theory. In SPE Europec featured at EAGE Conference and Exhibition (pp. SPE-8084). SPE.

[7] Jardine, R. J., Chow, F. C., Overy, R. and Standing, J. (2005). ICP Design Method for Driven Piles in Sands and Clays. London: Thomas Telford.

[8] Jiang, Z. (2021). Installation of offshore wind turbines: A technical review. *Renewable and Sustainable Energy Reviews*, *139*, 110576.

[9] Jones, L., Rattley, M., & Manceau, S. (2021). A CPT-Based Soil Resistance to Driving (SRD) Method for Offshore Pile Driveability Analyses. In *Piling 2020*: Proceedings of the Piling 2020 Conference (pp. 207-216). ICE Publishing.

[10] Kikuchi, R. (2010). Risk formulation for the sonic effects of offshore wind farms on fish in the EU region. Marine Pollution Bulletin, 60(2), 172-177.

[11] Milewski, H., & Kennedy, J. (2019, June). Application of Friction Fatigue Pile Driving Models in GRLWEAP. In *International Conference on Offshore Mechanics and Arctic Engineering* (Vol. 58769, p. V001T10A012). American Society of Mechanical Engineers.

[12] Pile Buck International. *Introduction to pile driving: Hammers and techniques*. Volume 36, Issue 1.

[13] PDI, Wave Equation Analysis of Pile Driving, Pile Dynamics Inc., Cleveland, Ohio, 2010.

[14] Randolph, M., & Gourvenec, S. (2017). *Offshore geotechnical engineering*. CRC press.

[15] Robertson, P. K., & Wride, C. E. (1998). Evaluating cyclic liquefaction potential using the cone penetration test. *Canadian geotechnical journal*, *35*(3), 442-459.

[16] Roussel Jr, H. J. (1979). Pile Driving Analysis of Large Diameter High Capacity Offshore Pipe Piles. Tulane University.

[17] Salgado, R., Zhang, Y., Abou-Jaoude, G., Loukidis, D., & Bisht, V. (2017). Pile driving formulas based on pile wave equation analyses. *Computers and Geotechnics*, *81*, 307-321.

[18] Schneider, J. A., & Harmon, I. A. (2010). Analyzing drivability of open ended piles in very dense sands. *DFI Journal-The Journal of the Deep Foundations Institute*, 4(1), 32-44.

[19] Semple, R. M., & Gemeinhardt, J. P. (1981, May). Stress history approach to analysis of soil resistance to pile driving. In *Offshore Technology Conference* (pp. OTC-3969). OTC.

[20] Smith, E. A. L. (1960). Pile-driving analysis by the wave equation. *Journal of the soil mechanics and foundations division*, 86(4), 35-61.

[21] Stevens, R. S., Wiltsie, E. A., & Turton, T. H. (1982, May). Evaluating drivability for hard clay, very dense sand, and rock. In *Offshore Technology Conference* (pp. OTC-4205). OTC.

[22] Tsetas, A., Tsouvalas, A., Gómez, S. S., Pisanò, F., Kementzetzidis, E., Molenkamp, T., ... & Metrikine, A. V. (2023). Gentle driving of piles (GDP) at a sandy site combining axial and torsional vibrations: Part I-installation tests. *Ocean Engineering*, *270*, 113453.

[23] White, D. J., & Lehane, B. M. (2004). Friction fatigue on displacement piles in sand. Géotechnique, 54(10), 645-658.

[24] https://cathiegroup.com/OPILE/Website

Acknowledgments

This thesis was developed as part of a collaboration between Politecnico di Milano and Soil Engineering s.r.l. through an internal internship. Soil Engineering is a company specializing in geotechnical and foundation engineering, offering advanced solutions for offshore and onshore projects. I would like to express my sincere gratitude to all those who contributed to making this opportunity possible, their guidance and shared knowledge have greatly enriched this journey, making it an invaluable learning experience. In this regard, I would like to thank Ing. Luigi Albert for his priceless advice and expertise.

First and foremost, I would like to express my deepest appreciation to Prof.ssa Donatella Valeria Sterpi, advisor of this thesis, for her precious guidance, continuous availability and suggestions, which greatly improved this research.

I am also profoundly grateful to Davide Spinelli, project director, for his willingness to assist me, always providing his unique expertise and constructive feedback.

A special mention goes to Giovanni Piunno, co-advisor and direct supervisor during my internship, whose mentorship has been fundamental throughout the entire project. His guidance and stimulating discussions not only enhanced the quality of this research but have also contributed significantly to my personal and professional growth. I am truly grateful for his patience, dedication, and willingness to exchange ideas, which have challenged me to think critically and continuously improve. His passion for the field and commitment to knowledge-sharing have been a true inspiration.

Lastly, I extend my gratitude to all my colleagues who have, in various ways, provided support along this journey. This experience has been deeply enriching, and I sincerely appreciate the opportunity to have worked alongside such dedicated and knowledgeable professionals.